IDEALIZED SIMULATIONS OF SUPERCELL THUNDERSTORMS INTERACTING WITH STATIONARY BOUNDARIES

by

Jasen Greco

A thesis submitted to the faculty of
The University of North Carolina at Charlotte
in partial fulfillment of the requirements
for the degree of Master of Science in
Earth Science

Charlotte

2024

Approved by:

____
Dr. Casey Davenport

____
Dr. Matthew Eastin

____
Terry Shirley

ABSTRACT

JASEN GRECO. Idealized Simulations of Supercell Thunderstorms Interacting with Stationary Boundaries (Under the direction of DR. CASEY DAVENPORT)

Stationary frontal boundaries have a considerable impact on the weather within their vicinity. The enhanced horizontal vorticity seen at these boundaries can aid in the development and intensification of severe weather, especially supercell thunderstorms. A supercell's mesocyclone is known to be enhanced near boundaries, as proximity helps to strengthen the storm and increase the changes for tornado production. However, stationary boundaries are also associated with strong spatial gradients in environmental quantities (e.g., instability, vertical wind shear, and helicity) that are known to influence storm intensity and longevity; thus, these temporal and spatial variations in the environment can also significantly influence supercell evolution. It is unclear which is more influential on supercell intensity and evolution: the attendant boundary circulation or the rapid changes in the near-storm environment. Thus, the research presented herein aims to explore the impact of rapidly changing background environments in idealized simulations without an accompanying boundary circulation.

The base-state environment tested in the model was based on a real-world supercell-stationary boundary interaction event from 29 May 2011. Representative environments were generated from RUC model analyses at near-storm inflow locations on the warm-side of the boundary, on the cold-side of the boundary, and at the boundary itself. Idealized model experiments in CM1 tested each of these environments either fixed over time (control simulations) or varying over time via base-state substitution (BSS). In the BSS experiments, the background environment either transitioned from warm-to-cold or cold-to-warm environments; the amount of time spent in either the warm-side, cold-side, or boundary environment was varied

in 15 min increments to mimic different angles of approach for a supercell to interact with a boundary, impacting the “dwell time” on the boundary itself. While the results from the transition from the warm-to-cold environment were not informative about the study goal due to the generation of widespread convection, the results from the transition from the cold-to-warm environment revealed that, contrary to observational studies, longer dwell time in the boundary environment led to less organization and dissipation of the supercell. Dissipation is suspected to have occurred due to the increasingly warm and dry mid-level in the boundary environment, which likely enhanced entrainment and supported eventual dissipation of the supercell. However, the generalizability of this result should be explored with additional research. Future work includes a deeper analysis of the main aspects of this study, such as including more representative supercell/boundary interaction events, analyzing the metrics of the supercells themselves, and addressing the development of widespread convection in the warm-to-cold simulations.

ACKNOWLEDGEMENTS

I would first like to thank Dr. Casey Davenport for being so gracious and helpful to me during the process of developing my thesis. She has been such a great advisor, mentor, and support system as we conducted this research. I couldn’t have gone through this process without her constant support and great suggestions! I want to also thank the other faculty members in the meteorology department for providing extra support to me and being overall great people. Another group of people that helped me so much with this process are the other meteorology/atmospheric science graduate students. From helping me edit/write Python scripts to providing useful feedback on my research, they have been a constant help to me these past two years. Lastly, I want to thank my family and friends for keeping my spirits up and making me laugh during particularly difficult times. I couldn’t have done any of this without any of these people!

TABLE OF CONTENTS

LIST OF TABLES

LIST OF FIGURES

CHAPTER 1: INTRODUCTION AND MOTIVATION

1.1 Introduction

Supercell thunderstorms are characterized by a deep, persistently rotating mesocyclone, and are well-known for their production of severe weather, including large hail, gusty winds, and/or tornadoes. The interaction of supercell thunderstorms with their surrounding environment is crucial for understanding and predicting their evolution. An environment with high vertical wind shear (> 20 m/s) and high buoyancy (> 1000 J/kg) can help create and sustain a supercell thunderstorm (Rasmussen and Blanchard 1998). Furthermore, the evolution in buoyancy and wind shear is known to heavily influence the intensity of multiple aspects of these storms including structure, severe weather production, and longevity (e.g., Klemp et al. 1981; Atkins et al. 1999; Ziegler et al. 2010; Davenport and Parker 2015; Klees et al. 2016; Gropp and Davenport 2018; Hartigan et al. 2021; Davenport 2021).

One such source of environmental variability known to influence supercell intensity and severe weather production is a physical synoptic-scale boundary (e.g., warm front, stationary front, outflow boundary), which typically contain sharp spatial gradients in temperature, wind, and/or moisture. Prior observational and early idealized modeling work demonstrated that as a supercell approaches and interacts with a spatial gradient (e.g., a synoptic boundary), its intensity noticeably increases. These spatial gradients are typically associated with ample horizontal vorticity, which can be tilted into vertical vorticity and intensify a supercell thunderstorm (e.g., Maddox et al. 1980; Markowski et al. 1998a; Atkins et al. 1999; Rasmussen et al. 2000). This enhanced vertical wind shear can lead to an increase in severe weather production, leading to a higher chance of tornadogenesis (Rasmussen et al. 2000). These spatial gradients, or boundaries, can provide a supercell thunderstorm with the necessary instability and/or wind shear to extend its lifecycle and intensify its overall morphology.

Investigation of the interaction of supercells and boundaries has been ongoing for decades, exploring, via a combination of case studies and model simulations, many types of boundaries, including: warm fronts, cold fronts, stationary fronts, sea-breeze fronts, and outflow boundaries (e.g., Maddox et al. 1980; Markowski et al. 1998a; Atkins et al. 1999; Fierro et al. 2006; Scott 2017; Magee and Davenport 2020; Hartigan et al. 2021; Axon 2022). One clear theme is the enhancement of supercell intensity along with severe weather production during the interaction (e.g., Markowski et al. 1998a; Atkins et al. 1999; Magee and Davenport 2020). Notably, however, is the finding that boundary strength does not play a major role in severe weather enhancement in supercell thunderstorms (Atkins et al. 1999). Instead, the position and intensity of severe weather production in supercell thunderstorms is sensitive to boundary type, as well as the angle of storm-boundary interaction (Magee and Davenport 2020). From these results, it is clear that the boundary circulation plays an important role in strengthening the supercell mesocyclone (e.g., Maddox et al. 1980; Markowski et al. 1998a; Atkins et al. 1999). Even so, boundaries represent sharp gradients in temperature, moisture, and/or wind, with concomitant variations in key forecasting parameters such as storm-relative helicity (e.g., Markowski et al. 1998b); such variations (outside of their presence near boundaries) are known to influence supercell evolution and severe weather production (e.g., Gropp and Davenport 2018; Davenport 2021). Thus, it would be useful to determine the relative contribution of the environmental gradients versus the boundary circulation itself, which can help provide a more fundamental understanding of supercell-boundary interactions. Importantly, these two factors have historically been difficult to disentangle, due to the boundary circulation being intrinsically tied to the spatial gradients in the environment. However, as will be discussed, the application of an idealized modeling technique known as base-state substitution (BSS; Letkewicz et al. 2013) allows for experiments to test the sensitivity of environmental variability without a boundary circulation.

1.2 Motivation and Goals

This study will focus on idealized simulations of supercell thunderstorms interacting with stationary boundaries due to their evident temperature gradients and wind shear, as well as these gradients being relatively fixed over time (Blanchard 2008). The primary goal of this research is to improve our understanding of supercell-boundary interactions through idealized simulations. In particular, given prior work highlighting the role of boundary circulations in enhancing supercell intensity, this study will focus on the role of spatial gradients in the environment and those contributions to supercell evolution. These models will build off of previous research that has focused on supercells crossing boundaries with varying temporal scales (Scott 2017), but also leveraging recent observational work (Magee and Davenport 2020). The use of numerical modeling in studying supercell/boundary interactions is an effective method that allows systematic experimentation to determine the influence of environmental variability on the evolution of a mature supercell.

CHAPTER 2: LITERATURE REVIEW

2.1 Introduction

This section provides an overview of key findings from previous studies involving supercell thunderstorms and their interactions with their background environment. This chapter has been split into six sub-sections. Section 2.2 discusses prior studies that have focused on supercell development/evolution in a fixed base-state environment. Section 2.3 continues this discussion, but instead focuses on prior studies that have examined supercell development/evolution with a varying base-state environment. Section 2.4 begins to narrow down the focus of supercell morphology with an emphasis on a changing background environment due to an air mass boundary. Prior observational-based studies that focus on supercell/boundary interactions are discussed in detail. Section 2.5 continues with the theme of supercell/boundary interactions, but with an emphasis on previous idealized modeling studies. Section 2.6 provides a summary of the literature review, talks about the key research gaps in previous studies, and how the current work plans to fill those gaps.

2.2 Supercell Morphology in Fixed Environments

Several foundational studies provide information regarding the fundamental physical processes that occur in a supercell thunderstorm within a fixed background environment. These studies provide observation-based context for the dynamics that occur in a supercell within a relatively consistent base environment. The results from these previous works will help us to formulate an understanding of how a supercell's evolution, intensity, and tendency to generate severe weather is affected by preexisting conditions. The information from these studies will provide a basis for how supercells should behave within a simulation with a fixed background environment.

A supercell thunderstorm begins as an isolated, buoyant cumulus cloud with access to sufficient thermal energy (e.g., Klemp 1987). This thermal energy will cause the air around the cloud to rise, eventually becoming a powerful updraft seen in supercells. If this cumulus cloud is located in an environment with high wind vertical shear, it will begin to rotate around a vertical axis. This rotation, combined with the powerful updraft, will cause a pair of counter-rotating vortices to form (e.g., Wilhelmson 1974; Schlesinger 1975; Kropfli and Miller 1976; Wilhelmson and Klemp 1978). This propagation is assumed for an environment with unidirectional wind shear and constant buoyancy (Fig. 2.1).

A phenomenon commonly referred to as storm-splitting occurs when the powerful updraft separates the counter-rotating vortices into two distinct supercells (Fig. 2.2). This updraft is enhanced by a vertical pressure gradient that is present in a supercell. This pressure gradient arises from the downdrafts within the storm. The downdrafts, which contain colder, denser air, reach the surface and create an isolated area of high pressure. This causes a pressure gradient force to form, moving air from the surface to the upper levels of the atmosphere (Klemp 1987). The cold air from these downdrafts could potentially cut off the storm from its supply of warm air and cause the storms to weaken. However, if there is ample low-level inflow from the east, it will prevent the cold air from cutting off the heat supply of the supercell (e.g., Wilhelmson and Klemp 1978; Thorpe and Miller 1978). With high wind shear and a powerful updraft, the two distinct storms will continue to split and develop. One storm will rotate anti-cyclonically and move to the left of the mean wind, and the other storm will rotate cyclonically and move to the right of the mean wind.

Prior observations have found that the cyclonic, right-moving supercell tends to outlive the anticyclonic, left-moving supercell. A study by Davies-Jones (1985) sampled the radar data of 143 storms that had strong, mid-level rotation. Out of these storms, only 3 had anticyclonic rotation. One might think the preferential enhancement of the cyclonic storm is due to the effects of Coriolis force, but scale analysis suggests that supercells are too small-scale to be affected by planetary vorticity (Morton 1966). This suggests that planetary vorticity has little to no effect on strengthening the cyclonic storm or weakening the anticyclonic storm. Instead, cyclonic turning with height of the environmental wind-shear vector is what creates preferential enhancement of the right-moving storm (e.g., Klemp and Wilhelmson 1978). A cyclonically-turning environmental wind-shear vector creates a favorable pressure gradient in the right-moving storm and an unfavorable pressure gradient in the left-moving storm. This pressure gradient, combined with the main updraft, creates a right-moving storm that will continue to strengthen (Fig. 2.3). There are rare instances where the left-moving, anticyclonic supercell will enhance in an environment with anticyclonic wind shear. However, these anticyclonic supercells only account for approximately 2% of all strong supercells (Klemp 1987).

Once storm splitting has finished occurring, the right-moving storm will continue to propagate in sufficiently supportive environmental conditions. At this point of the supercell's life cycle, there is a strong, rotating updraft along with a clear forward-flank downdraft. Environmental wind shear has caused the storm to tilt, separating the updraft and downdraft. One extraordinary feature of a supercell thunderstorm is its ability to remain in a quasi-steady state for multiple hours. With the updraft and downdraft being separate from one another, the supercell can remain in its mature stage for much longer than an ordinary thunderstorm. The strong rotation in a supercell, combined with its longevity, creates an ideal environment for a low-level mesocyclone (Burgess 1976).

The low-level vorticity generated in supercell thunderstorms creates an environment primed for tornado production. Although not all supercells produce tornadoes, a majority of significant tornadoes are generated within supercells. In a study by Burgess (1976), 37 storms were analyzed between 1971-1975. Out of these 37 storms, 62% that exhibited strong storm-scale rotation ended up developing tornadoes. Storms that did not have any storm-scale rotation produced no tornadoes. Supercell thunderstorms may last for many hours, but the tornadogenesis process can be as short as 10 minutes (Klemp 1987). Barnes (1978) and Lemon and Doswell (1979) found through their research that the most likely source of the transition into the tornadic phase is the rear-flank downdraft. This downdraft forms at the mid-levels of a supercell, descends to the surface, and intensifies low-level rotation by either producing strong wind shear (Barnes) or a strong thermal gradient (Lemon and Doswell). A strong tornado forms as a result of the sharp intensification of the low-level wind shear. Recent studies have expounded on this research by observing more specific dynamical processes associated with tornadogenesis. The cold pool generated by a supercell's downdrafts aids in the process of tornadogenesis, as long as the negative buoyancy associated with it is not too strong. It has also been found that tornadogenesis chances increase when the environmental boundary-layer relative-humidity is higher (Markowski and Richardson 2009). This creation of a rotating, steady-state storm and significant tornado is a result of an idealized, fixed background environment. Strong vertical wind shear combined with ample thermal buoyancy allows for the creation and persistence of a supercell thunderstorm.

Introducing a pressure gradient to the background environment of a supercell thunderstorm allows for many dynamical processes to occur. The most important process that is introduced is preferential enhancement of the cyclonic vortex within a supercell. In the study by Rotunno and Klemp (1982), a veering wind shear vector was introduced into the environment of a supercell thunderstorm to see what kind of effects it would have. The main effect that was noted was the initially symmetric updraft growing preferentially toward the right of the storm. From this, it was believed that a perturbation pressure gradient was formed on the right side of the storm that created favorable conditions for enhancement of the cyclonic updraft. This study builds off of the foundational information that was available for supercell dynamics because it shows how a perturbation pressure gradient can cause rotation in an updraft without any initial background rotation. In most supercell environments, there is some sort of directional wind shear present (Klemp 1987). Knowing how this directional wind shear can create a perturbation pressure gradient, enhance the right side of the updraft, and enhance cyclonic rotation is important for understanding how a changing background environment affects supercell propagation.

2.3 Supercell Morphology in Varying Environments

In an idealized setting with horizontally-homogeneous conditions fixed over time, it is possible to study a supercell thunderstorm's development and interaction with its background environment in a more straightforward, predictable manner. However, real-world environments are much more complex, with temporal and spatial variations in temperature, moisture, and winds. When taking into account different kinds of gradients that can be present in the background environment of a supercell, subsequent behaviors can be more challenging to predict.

One of the first fundamental studies that focused on idealized simulations of supercell thunderstorms used a three-dimensional cloud model to examine the rotation and propagation of convection (Rotunno and Klemp 1985). This study was key in understanding the base dynamics of a supercell thunderstorm, and was an important step forward for the idealized modeling of severe convection. What was found in this study showed that a cool, rainy downdraft is necessary to produce the circulation needed for a tornado (Fig. 2.4). These results are crucial for future idealized modeling studies of supercell thunderstorms, where researchers need to have this base knowledge of tornadogenesis to be able to analyze the severe convection within a storm. Knowing how a supercell thunderstorm interacts with a fixed background environment in an idealized simulation opens the way for researchers to change the background environment.

On 9 June 2009, the second Verification of the Origins of Rotation in Tornadoes Experiment (VORTEX2) generated a unique set of observations throughout the lifetime of an isolated supercell. These observations included the propagation and eventual demise of the supercell, summarized in Davenport and Parker (2015a). This storm developed on the cool side of a quasi-stationary boundary, and continued to move into the cool side. As it moved further into the cool side of the boundary, it rapidly dissipated while encountering increasing near-surface CIN, though the elevated environment remained favorable (Fig. 2.5). This cooling in the low-levels resulted in a weaker temperature along the rear-flank outflow, making it more difficult to lift a low-level parcel up to the level of free convection due to the increasing CIN. At the same time, bulk shear and storm-relative helicity decreased. The relative contributions of the weakening shear and helicity versus the increasing near-surface CIN was difficult to determine with just the observations, however.

Davenport and Parker (2015b) continued the research into this dissipating supercell by systematically testing the independent effects of the varying thermodynamic and kinematic environments on its morphology. Idealized simulations were utilized in conjunction with the base-state substitution technique (Letkewicz et al. 2013) to evolve the base-state environment in a manner consistent with the observations. While the increasing low-level CIN played a dominant role in dissipating the supercell, the experiments also revealed that changes to the wind profile resulted in the storm ingesting drier and more stable parcels into the updraft from higher altitudes, which also contributed to the weakening and dissipation of the supercell (Fig. 2.6).

While near-surface stabilization can result in supercell dissipation, as in the 9 June 2009 case, Gropp and Davenport (2018) explored multiple evolutionary pathways that supercells can undergo as a result of the nocturnal transition, which is associated with enhanced low-level CIN as well as stronger low-level shear. A total of 157 Great Plains supercells were categorized based on their behavior post-sunsets: maintained, dissipating, growing upscale, or merging. Each of these storm classifications contained unique evolutions in the near-storm environment; this distinction was most evident when comparing the maintained and dissipated categories, particularly for parameters such as most unstable convective inhibition (MUCIN), storm-relative helicity, and a CIN-scaled supercell composite parameter. Most notably, the maintained supercells had significant increases in storm-relative helicity and much smaller increases in MUCIN during the nocturnal transition compared to dissipating supercells, likely supporting their longevity (Fig. 2.7). Indeed, other studies have found that increases in shear and SRH over time in the near-storm environment can lead to longer-lived supercells (e.g., Davenport et al. 2019; Davenport 2021).

Axon (2020) explored the effects of an pre-existing airmass boundary on a tornadic supercell that occurred on 28 May 2019 in north-central Kansas. Observations from this event, including data from mobile mesonets, environmental soundings, and mobile radars, revealed that the cool side of the boundary had a higher equivalent potential temperature. A higher equivalent potential temperature means that the cool air mass had higher instability compared to the warm air mass. The cool side also had a lower lifted condensation level (LCL), so there was more of a potential for convection to form. The northeasterly winds present on the cool side of the boundary were much stronger than on the warm side, creating enhanced wind shear in the cool air mass. The main idea to draw from this study is that a tornadic supercell thunderstorm will generally see more enhancement on the cool side of a boundary because of the higher instability and greater wind shear present.

Knowing how a varying background environment is key to understanding the development and propagation of supercell thunderstorms. Knowing the prior research and science involved in the physics and dynamics of a supercell's interaction with its background can provide the foundation for future research into actual storms. Looking at real-life examples of supercells interacting with a changing environment is another crucial step in understanding supercell/boundary interactions as a whole.

2.4 Observational Studies of Supercell/Boundary Interactions

Thus far, the focus of this literature review has been on the effects of the background environment on the initiation and propagation of supercell thunderstorms. This section will examine studies that focus specifically on supercell interactions with any type of air mass boundary. We will begin by going over the first major study on supercell interactions with frontal boundaries (Maddox et al. 1980). Next we will look at a case study which focuses on the storms in VORTEX-95 and how their proximity to a boundary enhanced tornado production (Markowski et. al. 1998). We will then continue by looking at an observational study of the effects of a baroclinic boundary on tornadogenesis (Rasmussen et al. 2000). Lightning production and how it is affected by such a boundary will also be discussed for the same storm (Fierro et al. 2006). Finally, we will look at two more case studies that broadly focus on multiple types of boundaries and how those can affect supercell convection and severe weather production (Magee and Davenport 2020; Hartigan et al. 2021).

Maddox et al. (1980) is considered the seminal study of supercell thunderstorm interactions with frontal boundaries. In this study, Storm Data reports of tornadoes from NOAA were used in conjunction with 3-hour surface charts to identify supercells that were near stationary boundaries. The findings in this observational analysis showed that supercell thunderstorms experienced a clear increase in intensity when crossing a thermal boundary. It was found that the sharp temperature gradient, along with the strong wind shear that a boundary brings can cause a supercell to strengthen near a boundary. It was speculated that the reason for this strengthening was due to increased moisture convergence and cyclonic vorticity along a boundary.

Markowski et al. (1998) examined a large number of tornadoes that were observed during the VORTEX-95 field campaign. Out of 47 strong (F2 or higher) tornadoes, 31 of them were associated with some type of pre-existing mesoscale boundary. Notably, most of the tornadoes produced were within 10-30 km of a boundary, the majority of which were located on the cold side of the boundary (Fig. 2.8). They theorized that the baroclinic horizontal vorticity produced by boundaries, located on the cool side, could be ingested by supercells and support tornado production (Fig. 2.9).

Rasmussen et al. (2000) continues to focus on the effects of a baroclinic boundary on tornado production by carrying on with observing the VORTEX-95 data. In this study, supercell evolution is observed as it interacts with and crosses a boundary. One specific storm, the Friona tornado supercell, was a topic of interest because of the apparent changes that occurred in its morphology when it crossed a pre-existing mesoscale boundary. When this storm crossed its respective boundary, a noticeable increase in intensity of the mid-level rotation was observed (Fig. 2.10). It was speculated that this was due to the boundary enhancing the low-level updraft seen in the Markowski (1998) conceptual model, causing the mid-level mesocyclone to increase in intensity via the twisting term. Rasmussen et al. (2000) made note that this result was not initially expected, and that they believed the presence of a boundary would enhance the low-level rotation the most. They believed this due to previous results in Maddox et al. (1980) which found that vorticity and convergence show a significant increase at the lower levels of a boundary. This would lead one to believe that the lower levels would be enhanced the most, but this is not the case according to the results in Rasmussen et al. (2000). These results found that the mid-levels were actually enhanced the most compared to the lower and upper levels.

Magee and Davenport (2020) expands upon Markowski et al. (1998) by systematically exploring the sensitivity of severe weather production near boundaries by quantifying the distance at which severe weather occurs relative to the boundary, and also categorizing the differences among various boundary types (outflow boundaries, stationary fronts, and warm fronts). While supercells typically initiate on the warm side of a boundary, they move into the cool side over time; a majority of severe weather reports occurred with smaller interaction angles (i.e., supercells traveling more parallel to the boundary), supporting the idea that supercells benefit from baroclinically-generated horizontal vorticity present near thermal boundaries. Additionally, there were unique distances at which severe weather occurred based on the type of boundary (Fig. 2.11), indicating that perhaps the specific environmental conditions on either side of a boundary may be important contributors to severe weather production. The observational studies discussed within this section provide key insights as to how supercells have interacted with boundaries in past events. Knowing what has occurred in the past can guide future research in understanding the complex processes. Having access to this data and knowledge provides a good foundation for further knowledge of these processes. One key way this observational data can be used is by inputting it into numerical model simulations to test different boundary types and initial conditions. Being able to simulate this data with numerical models can provide a lot of information that cannot be obtained through observational studies.

2.5 Simulating Supercell/Boundary Interactions

Idealized modeling studies of supercell thunderstorms is a common method used to conduct controlled experiments of storm dynamics and how they interact with various components of their environments. Studies involving idealized modeling focus on many unique aspects of the surrounding environment such as terrain, thermodynamics, etc. More recently, modeling studies have started to focus on supercell thunderstorm interactions with a pre-existing air mass in the background environment (Atkins 1999; Laflin and Houston 2012; Scott 2017; Hartigan et al. 2021; Axon 2022). The main findings of these studies are discussed in the following paragraphs. The beginning focuses on idealized simulations of any air mass boundary, and then stationary boundaries become the specific point of interest.

Atkins et al. (1999) is one of the first idealized modeling studies that explored the evolution of supercell thunderstorms near a thermal boundary. Overall, it was found that the presence of a boundary in the background environment of a supercell thunderstorm caused the low-level mesocyclone to form much earlier, grow stronger, and be more persistent. A more persistent mesocyclone directly affects the intensity of a supercell, creating a higher chance for severe weather production. Additionally, supercells with a storm motion component oriented more toward the cold side of a boundary had weaker mesocyclones, while those with a storm motion component oriented toward the warm side of the boundary had stronger mesocyclones. Yet, the strongest supercell was produced when its motion was oriented parallel to the boundary, allowing it to access the enhanced horizontal vorticity. This direct interaction resulted in faster storm motion (4-5 ms^{-1}) compared to storms in a homogeneous environment, which would enhance storm-relative winds and further intensify the storm.

Supercell-boundary interactions not only affect storm intensity and tornado production, but other characteristics as well, including rain intensity, hail production, and lightning frequency. Fierro et al. (2006) simulated the same supercell thunderstorm as in Rasmussen et al. (2000), but also built upon previous work (Gilmore and Wicker 1998; Gilmore et al. 2002) through more sophisticated microphysics, electrification, and lightning parameterization (Mansell et al. 2002; Mansell et al. 2005; Straka and Mansell 2005). Within their simulations, Fierror et al. (2006) found that the supercell thunderstorm underwent rapid intensification as it moved into the cold side of the boundary, in line with the observations. The updraft speed and low-level mesocyclone rotation speed increased after crossing the boundary. The intensification of the updraft caused graupel and hail sizes to be larger on the cold side of the boundary. More water vapor was able to be lifted into the atmosphere, leading to a much higher cloud water content. The stronger updraft also lofted particles further up in altitude, causing intracloud lightning to be more frequent at higher levels. It was found that enhancement of the environment via the cold pool allowed for the enhancement of graupel and hail. The increased frequency of graupel and hail led to a higher charge rate, meaning more frequent cloud-to-ground lightning strikes.

Laflin and Houston (2012) continued upon the research of Atkins et al. (1999) and used idealized models to simulate supercell thunderstorm *development* near an air mass boundary. Convective initiation was simulated within the warm sector environment, cool sector environment, or along the boundary itself. It was found that a long-lived, steady-state supercell formed only in the simulation where convection was initiated along the boundary. This result further proved that a boundary enhances the dynamical processes of a supercell and can strengthen it greatly. Specifically, the boundary was found to enhance the low-level mesocyclone of the supercell, along with enhancing the gust front. The strength of the updraft was also increased within the boundary, which is key for a strong and consistent supercell thunderstorm (Fig. 2.12).

Scott (2017) continued the research on supercell/boundary interactions, but focuses solely on supercells crossing from the warm sector to the cool sector of a boundary. This study is important to the foundation of supercell/boundary research because it simulates a supercell crossing a boundary with a pre-existing cold pool. The results of this study show that as a supercell crosses a boundary, the low-level mesocyclone is cut off. This means that the updraft in the supercell must reorganize on the cold side of the boundary, where conditions have been notably more favorable for supercell enhancement (Maddox et al. 1980; Atkins et al. 1999). It was found that the low-level rotation was increased on the cold side of the boundary, but the strong capping inversion present may alter the vorticity. The enhancement of a supercell on the cool side of a boundary is due to the cool side having higher CAPE, boundary-layer moisture, and low-level vertical wind shear than the warm side. Scott (2017) found that the vertical vorticity was cut off when the supercell reached the boundary and was reorganized as horizontal vorticity after crossing the boundary. This horizontal vorticity was stretched for a longer period of time before entering the mesocyclone, priming the environment for tornadogenesis. The results of this study are important in understanding the dynamics of supercell development as it crosses a thermal boundary.

Hartigan et al. (2021) shifts the primary focus from a single boundary to multiple types of boundaries. This study observes supercell interactions with drylines and cold fronts due to the supercell of interest, which produced an F5 tornado. This supercell, which occurred in Jarrell, Texas on May 27, 1997, was responsible for the production of 12 tornadoes. In the post-storm analysis, it was noted that there was a dryline and cold front that interacted with the supercell during its lifecycle. The focus of this study was to simulate this storm with a dryline and cold front to see how it interacted with each. It was found that when the supercell interacted with both of the boundaries during the simulations, the updraft was kept steady for a longer period of time. When only the dryline was present, it was found that backbuilding of the supercell was increased, which refers to storm propagation occurring opposite to the mean flow (Bluestein and Jain 1985). These results further support the idea that boundaries represent important inflection points that can change supercell intensity and evolution.

Through idealized simulations, it is clear that air mass boundaries have a profound effect on the propagation and strengthening of supercell thunderstorms. The enhanced horizontal vorticity and lift at an air mass boundary allows for a more convective environment. The thermal and wind gradients observed within a boundary can greatly enhance the dynamical aspects of a supercell thunderstorm. Atkins et al. (1999) found that the low-level mesocyclone became much stronger when a supercell interacted with a pre-existing boundary. It was also discovered that storm motion is greatly influenced by a boundary in that a storm can increase in speed by up to 5 ms^{-1} when crossing a boundary. Laflin and Houston (2012) found that convection initiated in an environment primed for supercell development created stronger, longer-lasting supercells when initiated directly on a boundary. Scott (2017) furthered this research by showing how a supercell crossing an air mass boundary can enhance the low-level mesocyclone and create a stronger updraft. A stronger updraft with higher vorticity leads to a higher chance for tornadogenesis.

A temperature and moisture gradient being present in the background environment of a supercell thunderstorm can influence the vorticity, instability, and wind shear of the storm. In Hartigan et al. (2021), sea-breeze air masses are studied to observe their interactions with supercell thunderstorms. Sea-breeze air masses are known to have cooler, moister air than the surrounding environment. This cool, moist air provides extra lifting and horizontal vorticity to a supercell thunderstorm, which can be tilted to vertical vorticity and intensify the mesocyclone. It was found that storms became more organized when moving into a sea-breeze air mass environment. This is due to the strong shear present in these air masses, which keeps the low and mid-level circulation of the supercell alive for a longer period of time (Fig. 2.13). Having a moisture and temperature gradient present near a supercell is key for increasing its longevity and important for severe weather production (Hartigan et al. 2021).

2.6 Summary

The aforementioned studies provide the basis of our current understanding of boundary influences on supercell structure and intensity. Initial research on the dynamics of supercell thunderstorms has given a foundational knowledge of what processes are expected within a fixed background environment (e.g. Wilhelmson 1974; Schlesinger 1975; Kropfli and Miller 1976; Thorpe and Miller 1978; Wilhelmson and Klemp 1978; Lemon and Doswell 1979; Rotunno and Klemp 1982; Davies-Jones 1985; Klemp 1987). However, it is clear from a variety of observation-based studies (e.g., Davenport and Parker 2015a; Klees et al. 2016; Gropp and Davenport 2018; Davenport 2021; Lyza et al. 2022) and idealized modeling-based studies (e.g., Ziegler et al. 2010; Letkewicz et al. 2013; Davenport and Parker 2015b; Davenport et al. 2019) that supercell intensity, longevity, and severe weather production are sensitive to variations in the inflow environment. Supercell interactions with surface boundaries are no exception to this. Observed case studies have highlighted the complexities of supercell/boundary interactions in a real-world setting (e.g., Markowski et al. 1998; Rasmussen et al. 2000; Houston and Wilhelmson 2012; Magee and Davenport 2020), but emphasize that supercells tend to intensify near boundaries and produce more severe weather. Modeling studies have largely supported these findings (e.g., Atkins et al. 1999; Fierro et al. 2006; Scott 2017), indicating that approach angle and ingestion of baroclinically-generated vorticity along the boundary is key.

The research-focused goals of this study are related to idealized modeling techniques and their relationship to the advancement of supercell/boundary interactions. It is known that air mass boundaries provide the necessary thermodynamics for supercell enhancement and severe weather production, such as stronger thermal gradients and enhanced vertical motion (e.g., Maddox et al. 1980, Atkins et al. 1999). Prior studies have investigated how the differing environments of the warm and cool sector of a boundary can affect severe weather parameters such as storm-relative helicity (SRH) and vertical wind shear, with Markowski et al. (1998b) noting that SRH was enhanced on the cool side of a boundary. Thus, while many studies demonstrate that proximity to the boundary and its horizontal vorticity is important, it is unclear what the relative contributions are of storm enhancement through the intrinsic circulation associated with the boundary versus the favorable kinematics (such as enhanced SRH or vertical wind shear) that are present on the cool side of the boundary. This study aims to differentiate between these two types of enhancements within stationary boundaries. The effects of stationary boundaries on supercell development will be isolated to provide insight to the specific processes that occur in this environment. Using simulations with an idealized, but also realistic, stationary boundary will provide the best data output for real-world applications.

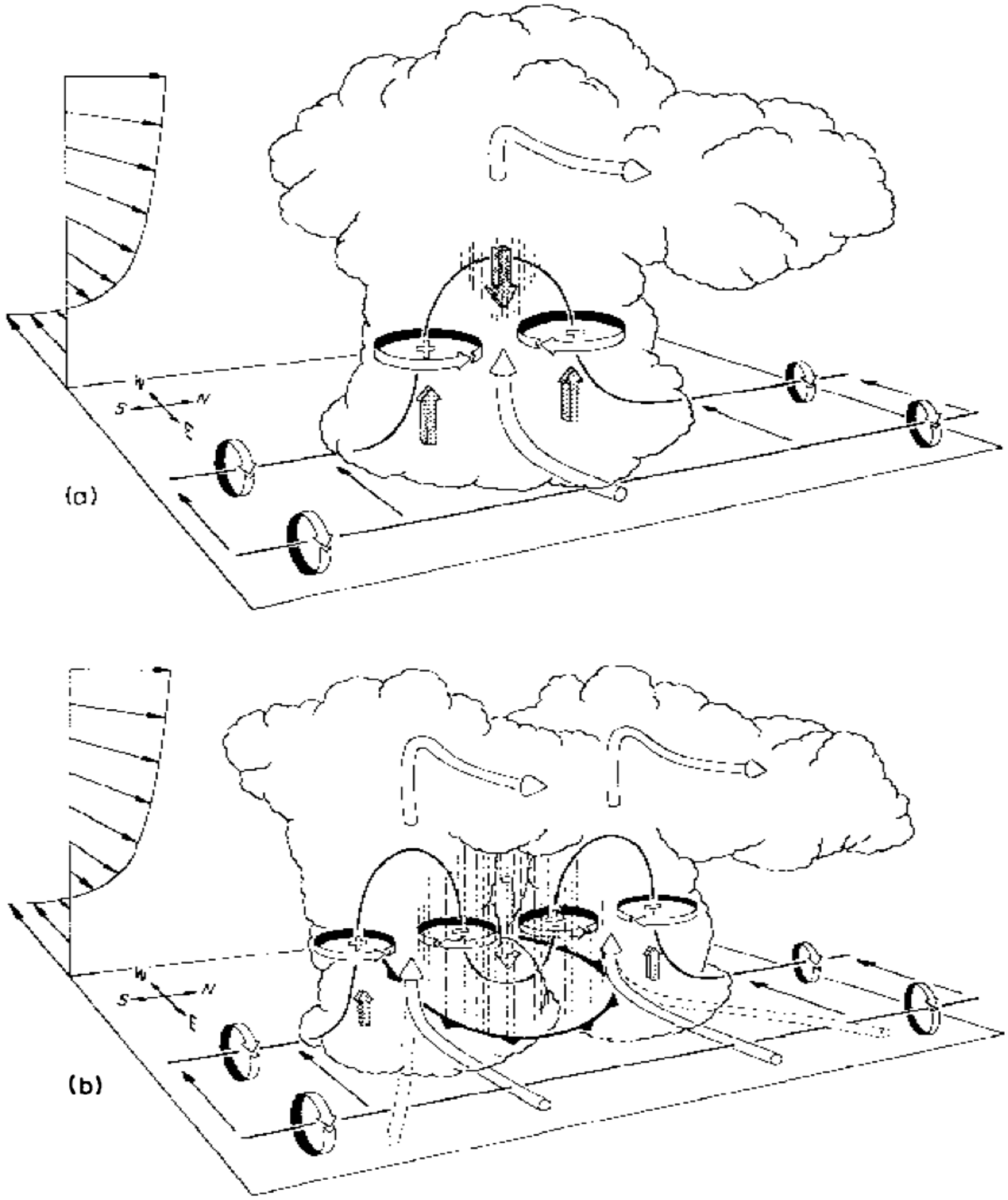

Figure 2.1: Schematic depicting how a typical vortex tube contained within (westerly) environmental shear is deformed as it interacts with a convective cell (viewed from the southeast). Cylindrical arrows show the direction of cloud-relative airflow, and heavy solid lines represent vortex lines with the sense of rotation indicated by circular arrows. Shaded arrows represent the forcing influences that promote new updraft and downdraft growth. Vertical dashed lines denote regions of precipitation. (a) Initial stage : Vortex tube loops into the vertical as it is swept into the updraft. (b) Splitting stage: Downdraft forming between the splitting updraft cells tilts vortex tubes downward, producing two vortex pairs. The barbed line at the surface marks the boundary of the cold air spreading out beneath the storm. (Adapted from Rotunno 1981.)

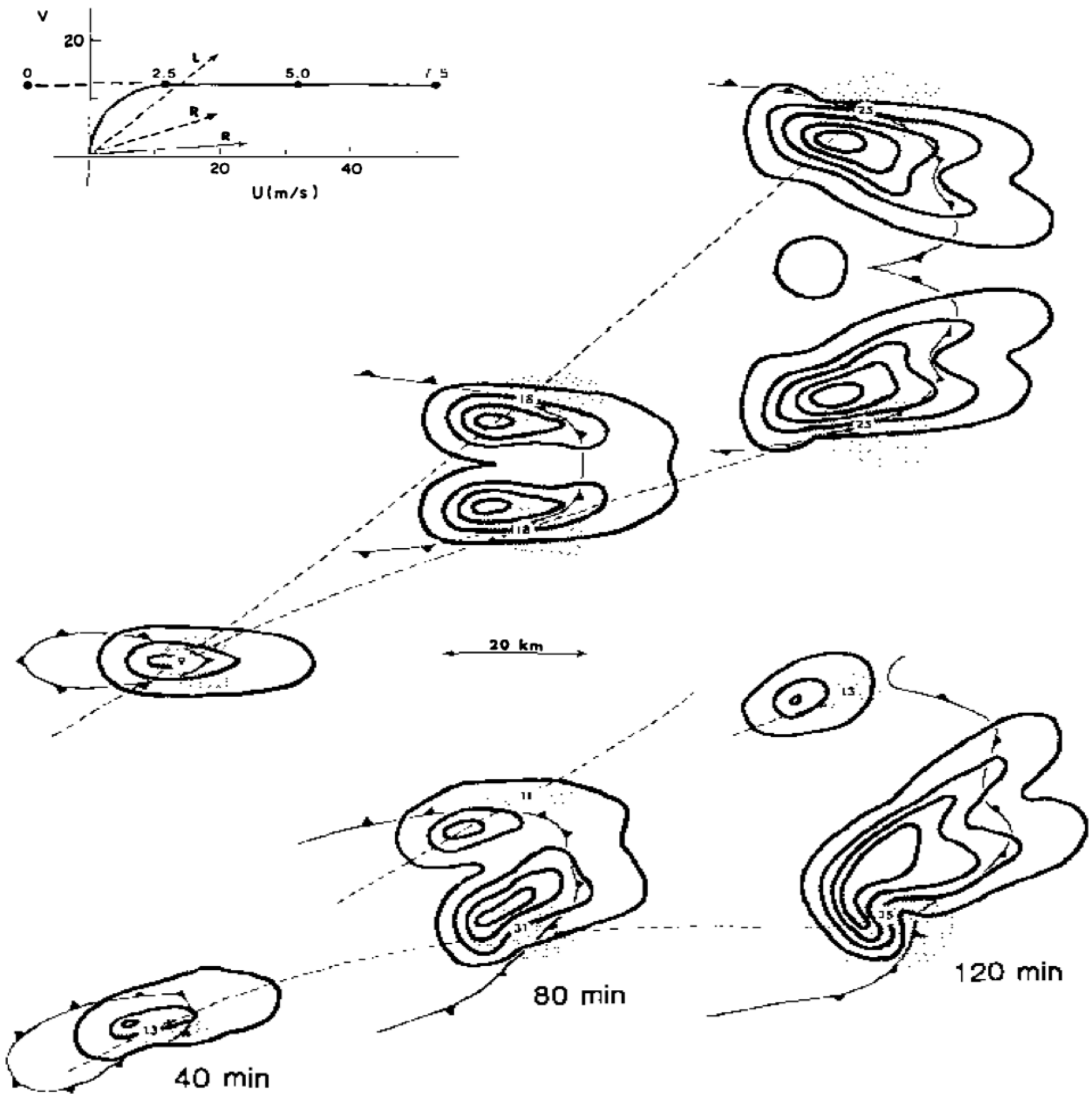

Figure 2.2: Plan views of numerically simulated thunderstorm structures at 40. 80, and 120 min for two environmental wind profiles (displayed at upper left) having wind shear between the surface and 7.5 km. The storm system in the lower portion of the figure evolves in response to the wind profile, in which S turns clockwise with height between the ground and 2.5 km (heavy solid line in wind plot), while the upper system develops when S is unidi-rectional (same wind profile except following the heavy dashed line below 2.5 km). The plan views depict the low-level (1.8 Ian) rainwater field (similar to radar reflectivity) contoured at 2 g kg-1 intervals, the midlevel (4.6 km) updraft (shaded regions), and the location of the surface cold-air outflow boundary (barbed lines). The maximum updraft velocity is labeled (in m S-I) within each updraft at each time. The dashed lines track the path of each updraft center. Arrows in the wind plot indicate the supercell propagation velocities for the unidirectional (dashed) and turning (solid) wind-shear profiles. (Adapted from Klemp & Weisman 1983.)

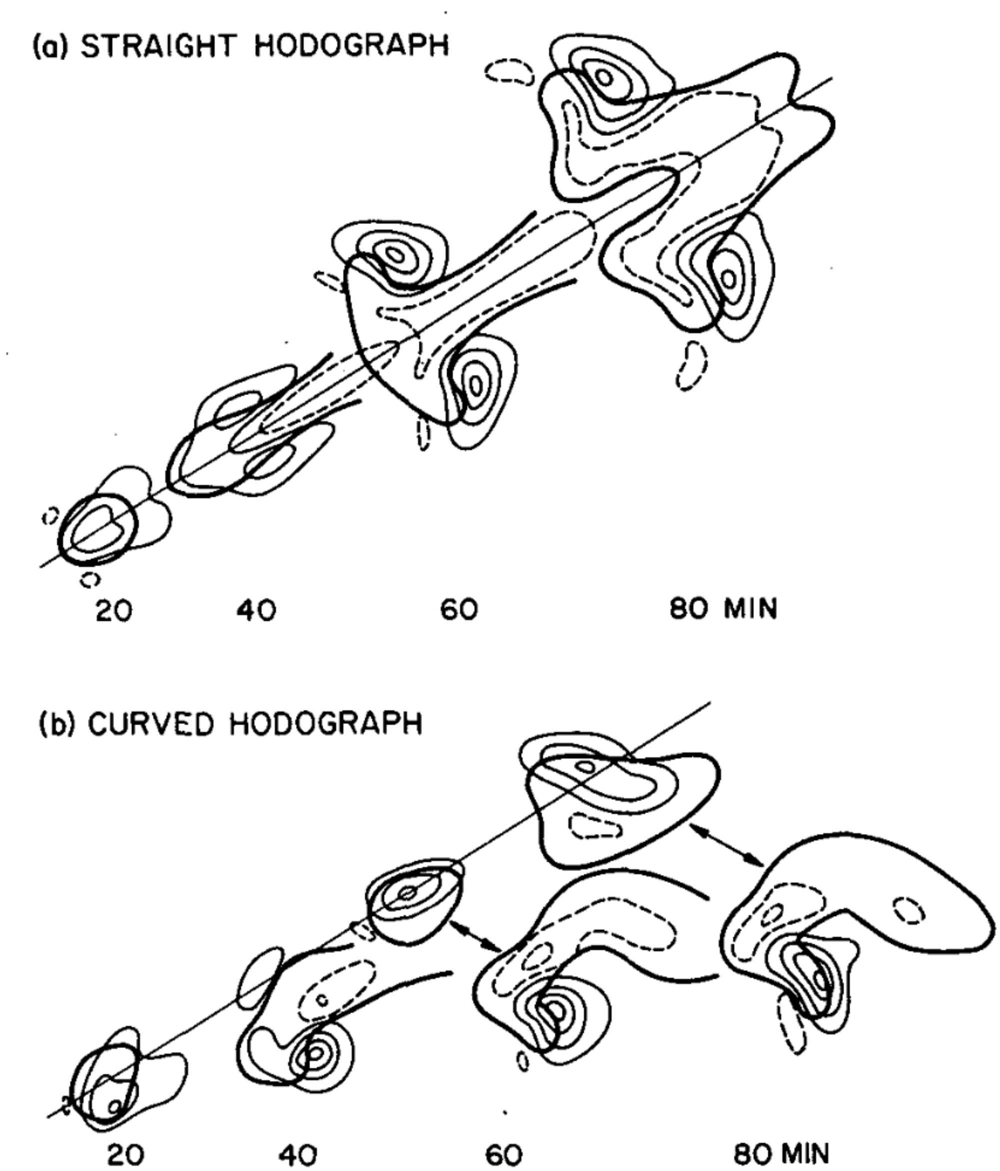

Figure 2.3: Horizontal contour plots of vertical velocity at 2.25 km AGL at t = 20, 40, 60, and 80 min from the three-dimensional numerical cloud model developed by Klemp and Wilhelmson (1978a) for (a) the straight line hodograph of Fig. 1 and (b) the 20 May sounding also contained in Fig. 1. Updrafts (solid lines) and downdrafts (dashed lines) are contoured at 4 m s^{-1} increments, beginning at ±2 m s^{-1}. The heavy line is the outline of the 0.5 g kg^{-1} rainwater field predicted by the model. Note that in (a) the development is completely symmetric with respect to the diagonal line which represents the direction of the shear vector. The diagonal line in (b) is the same as in (a) and also corresponds to the direction of the shear vector at 2.25 km. Here the development is skewed so that the right member is enhanced over the left. (Adapted from Klemp 1987.)

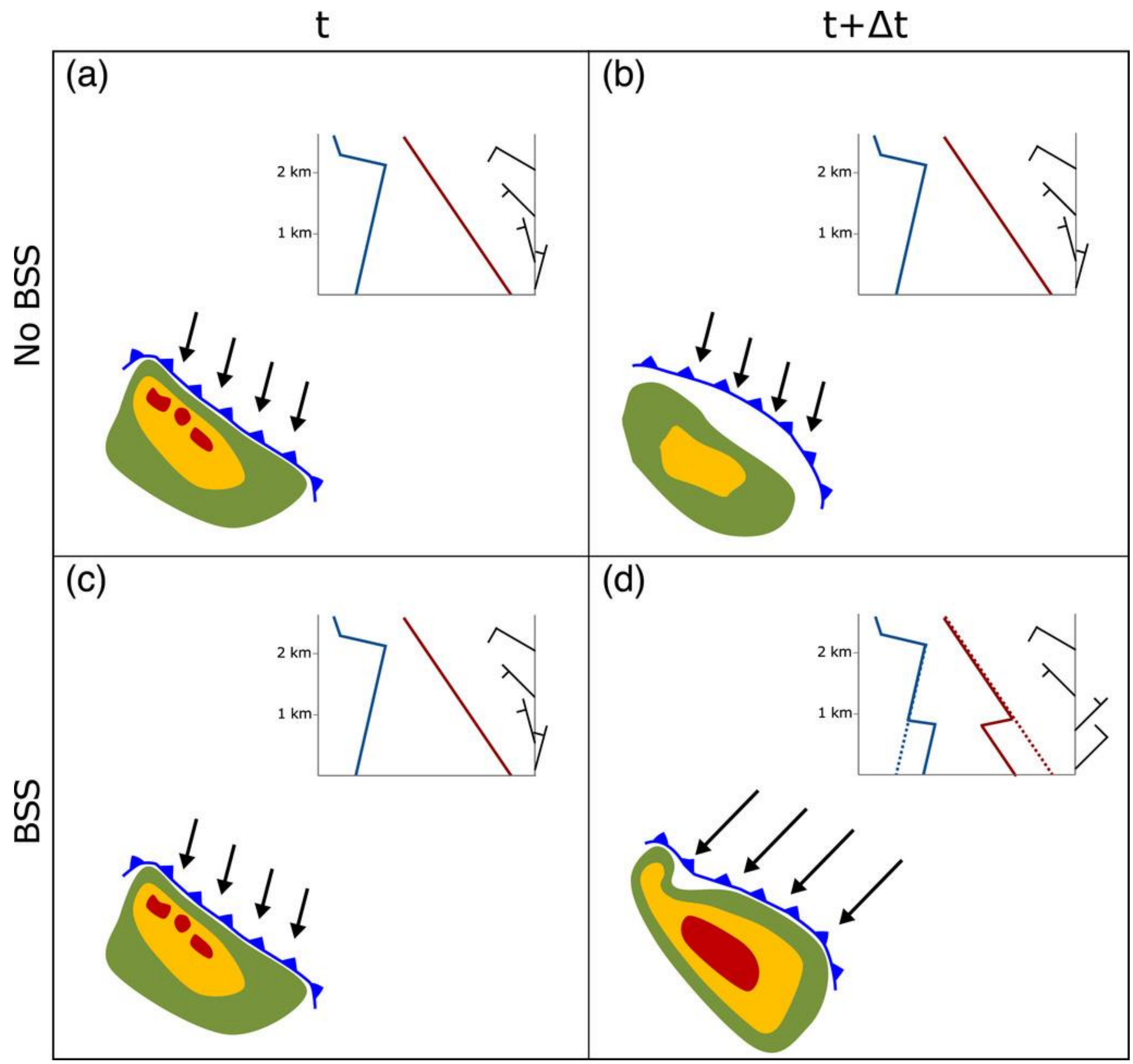

Figure 2.4: Summary of the modeling results of the change in storm morphology upon encountering an SB air mass: (a),(c) a mature multicell storm; (b) the multicell storm decaying as it remains in an environment characterized by weak-to-moderate 0–6-km bulk wind difference; and (d) the multicell storm increasing in organization and displaying supercell characteristics after moving into an SB air mass. Storm reflectivity is depicted by the green (weak), yellow (moderate), and red (heavy) filled contours; the storm gust front is depicted by the blue line with triangles; and black arrows depict surface winds ahead of the storm. Idealized boundary layer thermodynamic and wind profiles are provided for the continental air mass in (a)–(c) and the SB air mass in (d). Thick solid lines show the environmental temperature (red) and dewpoint temperature (blue); wind barbs are shown on the right, with short barbs indicating speeds of 5 kt (1 kt ≈ 0.51 m s^{-1}) and long barbs indicating speeds of 10 kt. The dotted lines in the SB sounding depict the continental air mass in which the storm originally resided. (Adapted from Hartigan et al. 2021.)

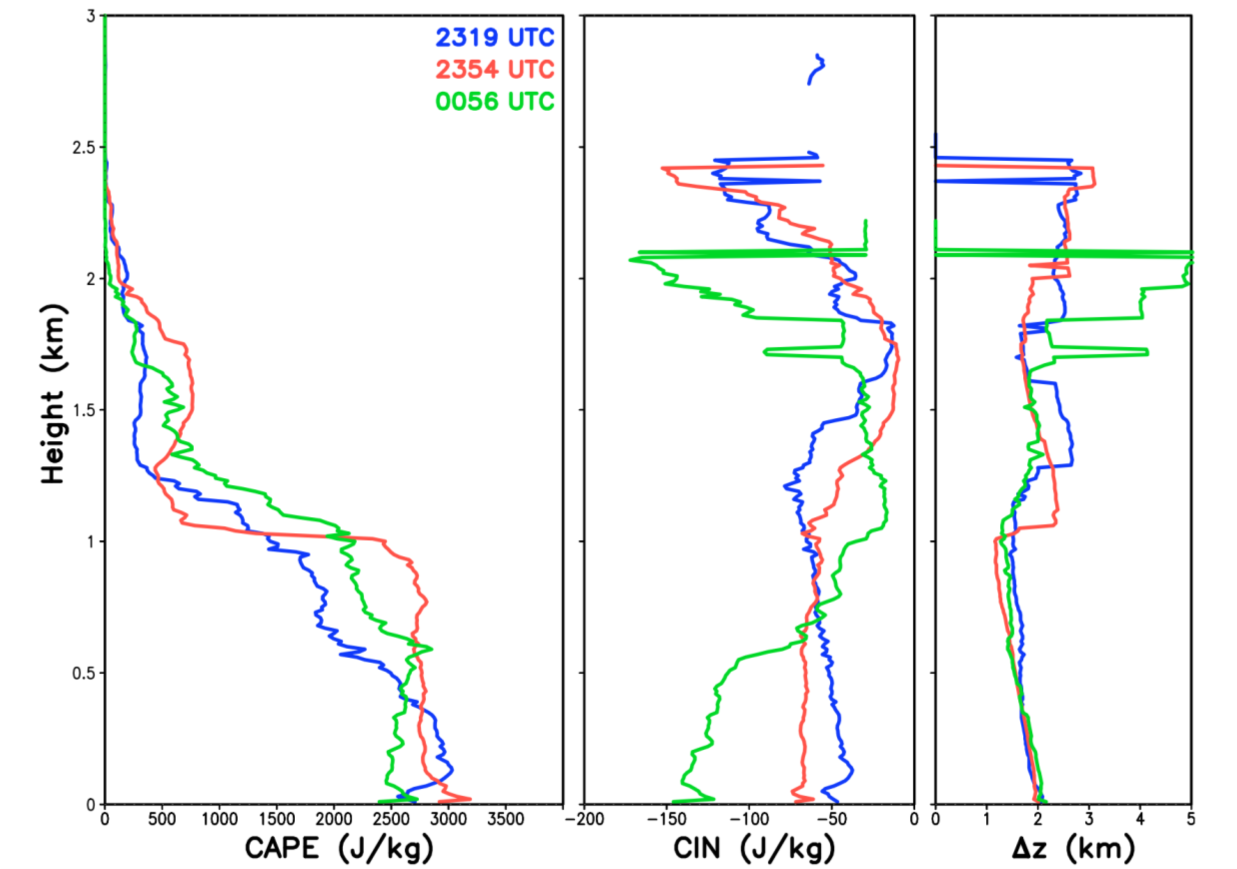

Figure 2.5: Vertical profiles of CAPE (J kg^{-1}), CIN (J kg^{-1}), and Dz (km AGL) over time from the near-inflow soundings on 9 Jun 2009. (Adapted from Davenport & Parker 2015a.)

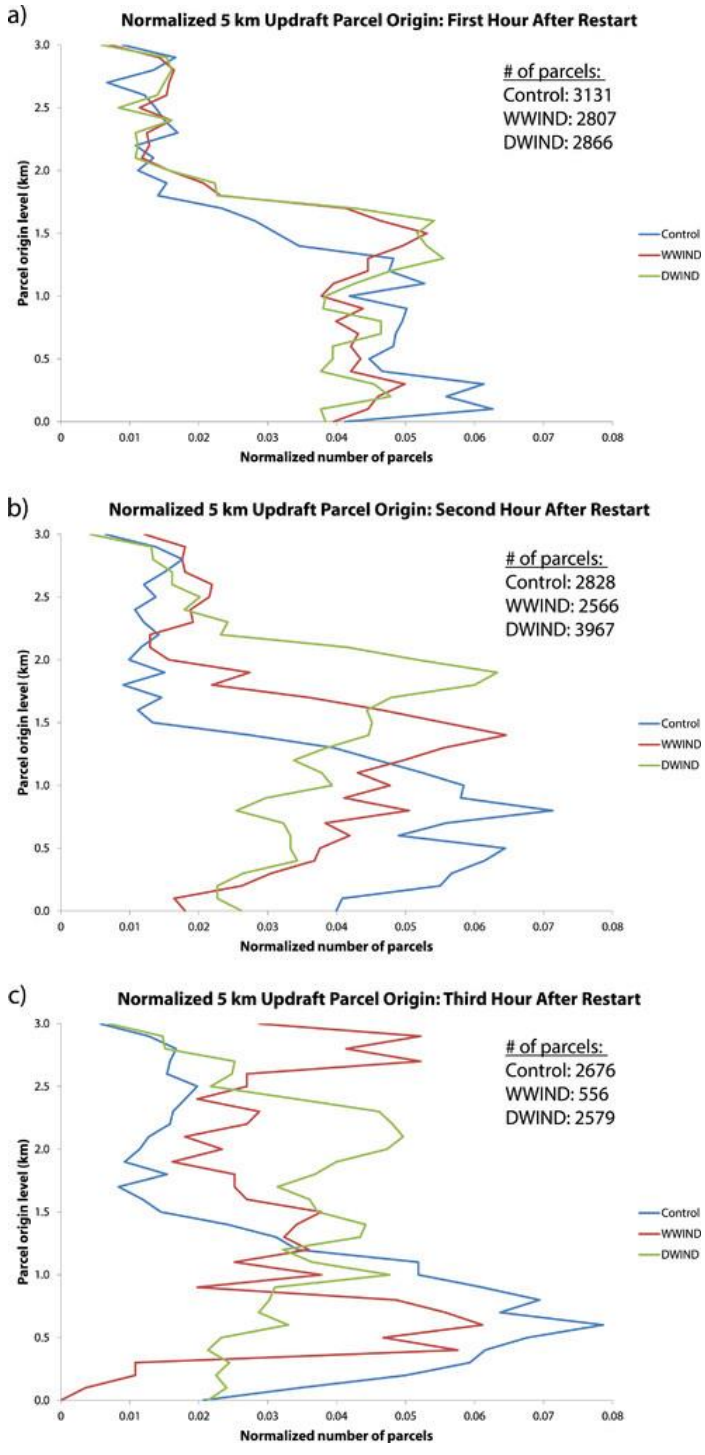

Figure 2.6: Histograms of the number of updraft ($w \geq 10$ m s^{-1}) parcels at 5 km, normalized by the number of parcels at each origin level, binned by parcel origin level for the WIND simulations during the (a) first, (b) second, and (c) third hour after the initial model restart. The number of updraft parcels for each simulation is also listed on each panel. (Adapted from Davenport & Parker 2015b.)

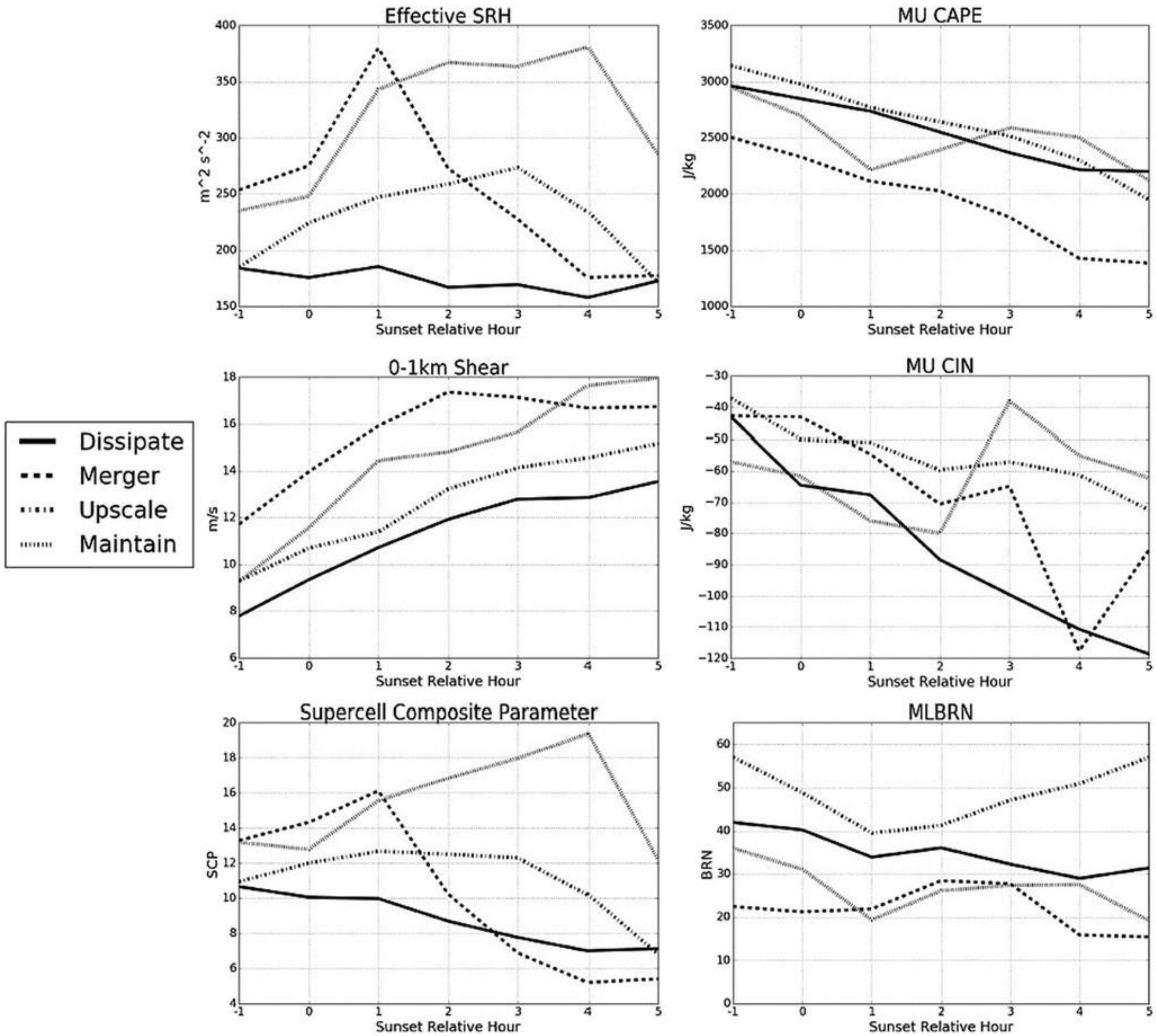

Figure 2.7: Time series of mean parameter values (as labeled) at every hour between SS −1 and SS +5 for each evolution category (as labeled). (Adapted from Gropp & Davenport 2018.)

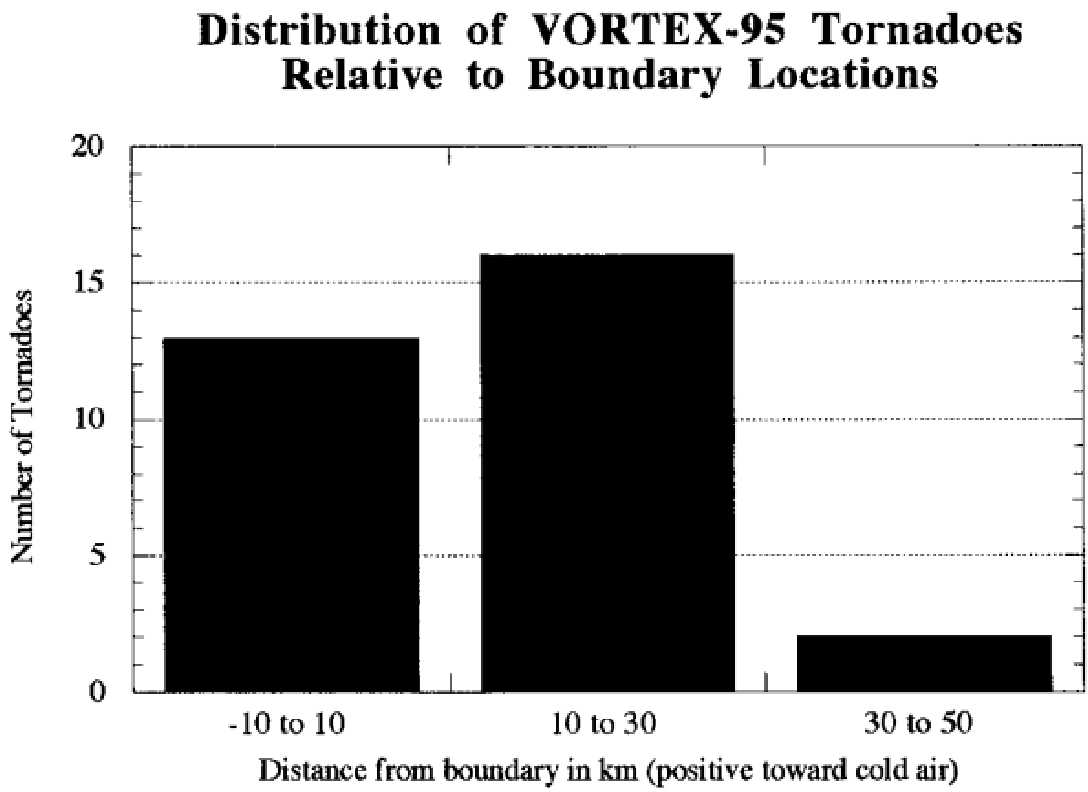

Figure 2.8: Frequency distribution of tornado occurrences relative to boundary locations (distances from boundaries were known to within 610 km) in cases where tornadoes occurred near detected boundaries. (Adapted from Markowski et al. 1998.)

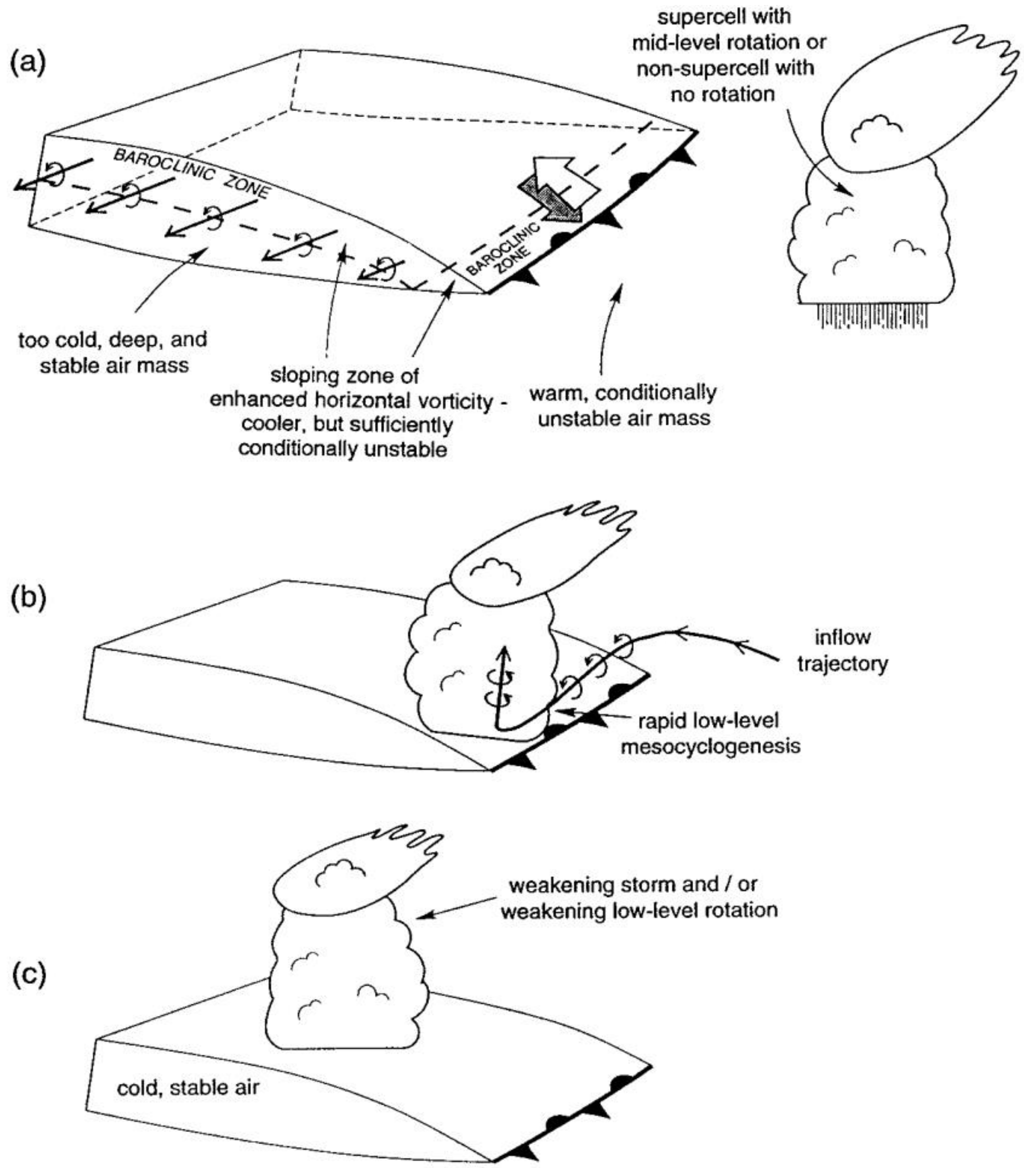

Figure 2.9: A conceptual model for how an updraft-boundary interaction may lead to low-level mesocyclogenesis. (Adapted from Markowski et al. 1998.)

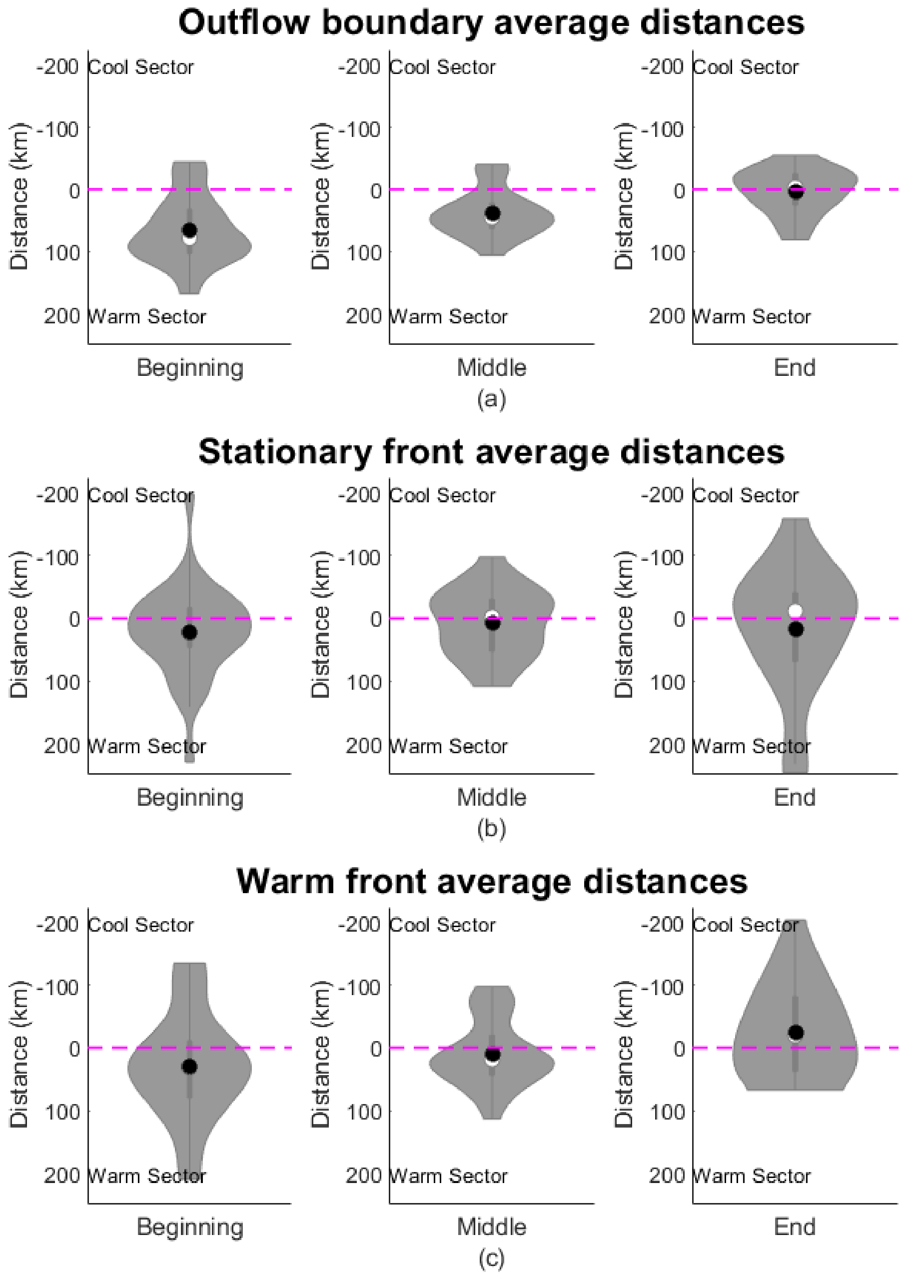

Figure 2.10: Violin plots with the mean distances of supercells interacting with an outflow boundary (top), stationary front (middle), or warm front (bottom) at the beginning, middle, and end of their lifetimes. Boundary location denoted by the magenta dashed line. The central dot marks the median, the thick gray line marks the inter-quartile range of the 25th and 75th percentiles, and the thin gray line is the range containing 95% of all data. The edges are a kernel density function of the distribution of data points, thus showing the distribution and frequency of reports rather than a traditional box plot. The black dot denotes the distribution mean. Analyzed distances +/– 10 km. (Adapted from Magee & Davenport 2020.)

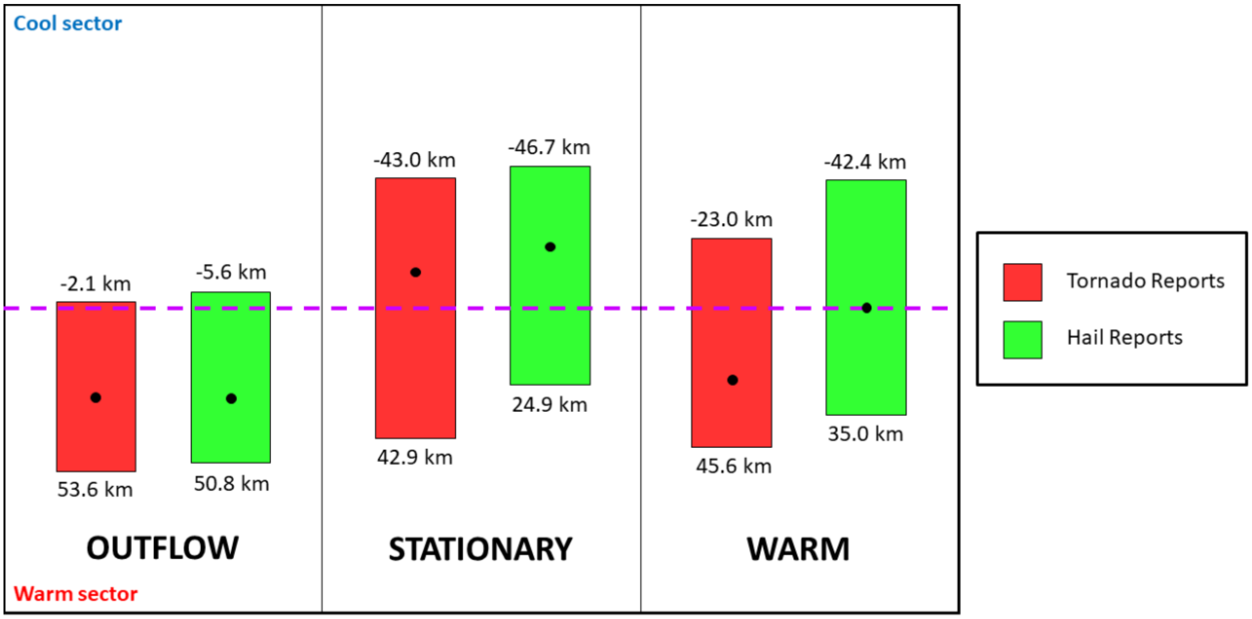

Figure 2.11: Visual representation of the distances that contain one standard deviation around the mean distance from the boundary (dashed magenta line) for each storm report type per boundary type (+/– 10 km). Negative distances indicate distance is in the cool sector, positive distances are the warm sector. Black dot represents median of the distribution. (Adapted from Magee & Davenport 2020.)

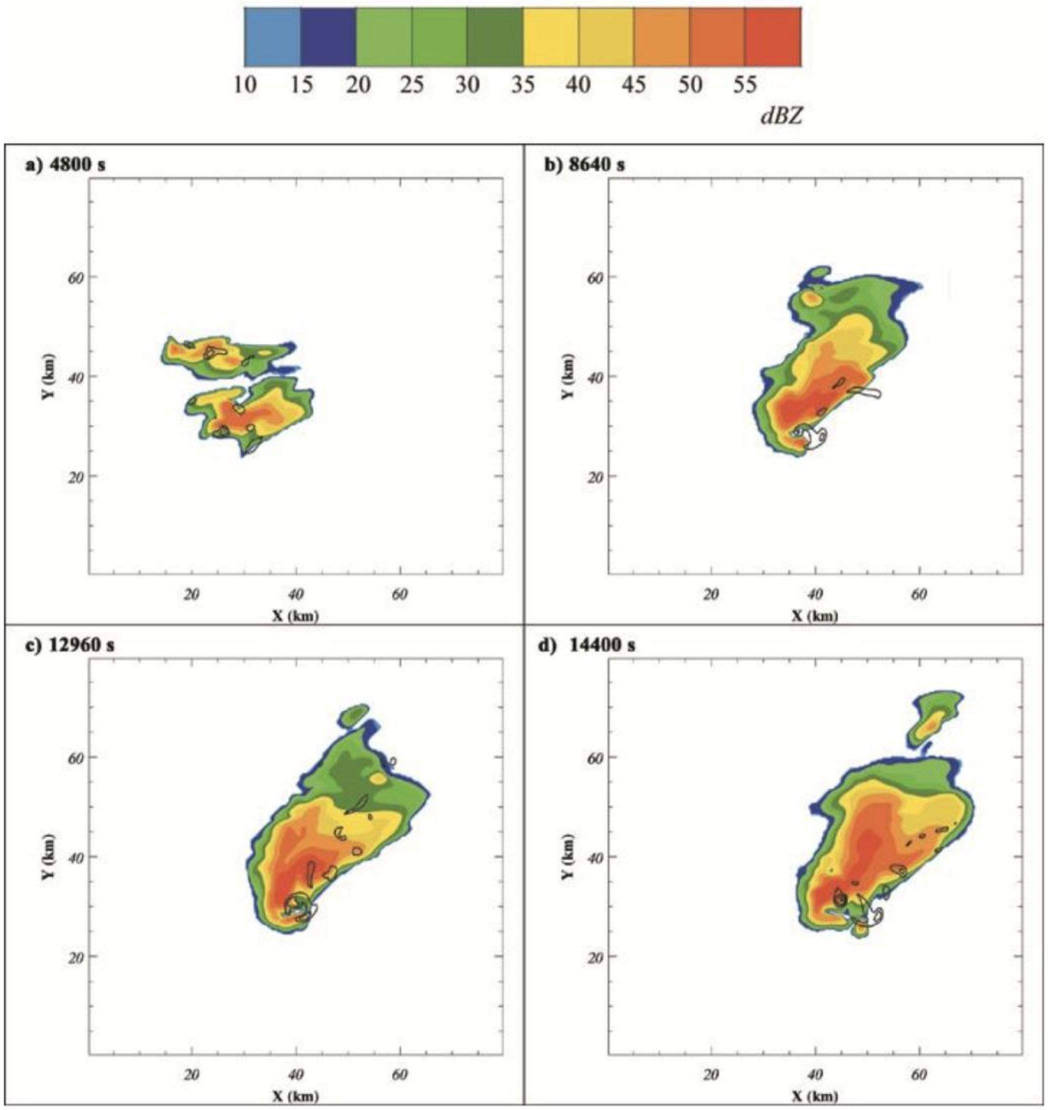

Figure 2.12: Surface simulated radar reflectivity (shaded, following the legend above) and vertical vorticity at 5 km AGL (contoured at 0.01 s–1 intervals; dashed contours indicate negative vorticity) for the boundary simulation at a) 1980 s, b) 2340 s, c) 2700 s, and d) 3060 s. (Adapted from Laflin & Houston 2012.)

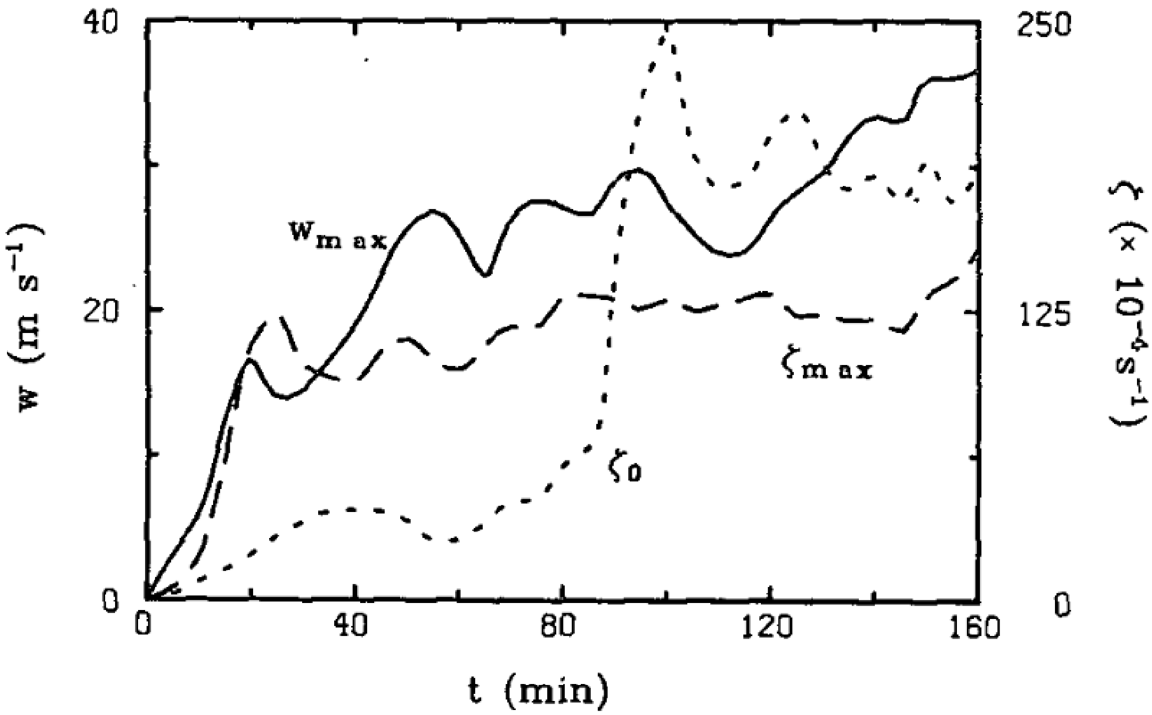

Figure 2.13: Maximum vertical velocity (solid line), maximum vertical vorticity at the middle levels (dashed line), and maximum vertical vorticity at the lowest grid level (dotted line) vs. time. (Adapted from Hartigan et al. 2021.)

CHAPTER 3: DATA AND METHODS

3.1 Introduction

The primary objective of this study is to use an idealized framework to investigate the response of simulated supercells within varying background environments consistent with a stationary frontal boundary. These simulations will allow us to deduce the role of the sharp gradients in the environment associated with stationary boundaries play in modulating storm structure, inflow environment, intensity, and longevity. Idealized numerical modeling allows us to observe how a simulated storm and its environment will evolve in a controlled manner. This will permit us to investigate how a storm from a common environment evolves in both the presence of a stationary boundary and lack thereof. This chapter is split into four additional sections to discuss our modeling and data collecting techniques. Section 3.2 explains why the specific numerical model was chosen for this study. Section 3.3 discusses the chosen configurations used to set up our modeling runs. Section 3.4 introduces the methods we used to introduce a stationary boundary to the background environment of a simulated supercell thunderstorm. Section 3.5 explains how the temporal variability of supercell/boundary interactions was implemented in the numerical model.

3.2 Model Selection

All of the simulations within this study were performed using Cloud Model 1 version 21.1 (CM1; Bryan and Fritsch 2002), a three-dimensional, non-hydrostatic, non-linear, time-dependent numerical model designed for idealized studies of a wide variety of atmospheric processes and phenomena. The idealized nature of CM1 is key for this study due to our ability to simplify the modeling environment by choosing configurations that restrict the degree of realism but capture the most important physical processes. More specifically, the idealized methods allow for the isolation of cause-and-effect relationships of boundary-associated variations in the near-storm environment without the addition of other processes in the Earth system (e.g., radiation, friction, Coriolis accelerations).

The method of base-state substitution (BSS; Letkewicz et al. 2013), applied continuously every time step (Davenport et al. 2019) was used within CM1 to simulate a changing background environment as a supercell thunderstorm crosses a stationary boundary. BSS allows for the temporal modification of the base-state model environment while maintaining any storm-induced perturbations, akin to a storm encountering a new representative inflow environment at a rate related to its storm motion. This method has been used in many research studies to generate better quality simulations of a supercell in a changing environment (e.g., French and Parker 2014; Coffer and Parker 2015; Wipf and French 2015; Davenport et al. 2019; Hartigan et al. 2021). The implementation of base-state substitution into CM1 will allow for a more precise look into the dynamics of a supercell thunderstorm interacting with a stationary boundary.

3.3 Model Configuration

All user-defined model configurations are provided in Table 3.1. A model domain of 250 km x 250 km was chosen with a uniform horizontal grid spacing of 250 m. The vertical extent of the domain reached 20 km, with a stretched vertical grid in the lowest 6 km, starting at 100 m spacing near the model surface to 500 m aloft. Rayleigh damping was applied above 15 km to limit the reflection of any gravity waves from the top of the domain back toward the surface. Free-slip boundary conditions were applied at the bottom of the domain, and all the lateral boundaries were open-radiative. Sub-grid turbulence was parameterized based on the turbulent kinetic energy scheme of Deardorff (1980), with no surface physics or effects of friction included. A constant large time step of 1.0 s was chosen to maintain model stability.

Each simulation was integrated for 4 hours, with output files being written every five minutes of integration time in light of storage limitations. Precipitation microphysics were governed by the Morrison double-moment scheme, including both hail and graupel. Convective initiation (CI) occurred via updraft nudging (Naylor and Gilmore 2012) to mimic frontal forcing, a common initiation method for supercells interacting with stationary boundaries. Nudging is applied over a 10 x 10 x 2 km^3 region located toward the center of the domain and acts to force a 15 ms^{-1} updraft for the first 15 minutes of integration before being turned off.

3.4 Stationary Boundary Environments

To ensure that the experiments and results were reasonably rooted in reality, a representative boundary environment from one specific case on May 29, 2011 near the Kansas/Nebraska border was selected from the Magee and Davenport (2020) dataset of supercells near stationary boundaries. This event had a supercell thunderstorm present near a clear stationary frontal inversion (Fig. 3.1), with little convection other than the supercell to ensure that model soundings generated from RUC were not convectively contaminated and were not modified by other nearby convection. The supercell of interest formed on the warm side of the stationary boundary propagated parallel to the boundary, staying on the warm side for the duration of its lifecycle. Although there were no tornado reports, there were several severe wind and hail reports associated with this supercell. The severe weather produced from this storm, along with the clear stationary boundary presence, made it an excellent case to use in idealized simulations.

To determine environments representative of each side of the stationary boundary for this event, archived WSR-88D radar data from the National Center for Environmental Information (NCEI) Weather and Climate Toolkit was used in conjunction with the National Oceanic and Atmospheric Administration (NOAA) Weather Prediction Center surface analysis archives to plot the supercell positions in relation to the stationary boundary. Using this data, inflow points of the supercell were chosen on the warm and cool sides of the boundary, along with a near-boundary environment. Once the latitude and longitude points on either side of the stationary boundary were selected, a vertical profile of the environment was generated using the 0-h analysis from the Rapid Update Cycle (RUC) (Benjamin et al. 2004, 2016). While there are inherent biases and errors with model data (e.g., Thompson et al. 2003; Coniglio 2012; Cohen et al. 2015), the significant spatiotemporal frequency of model data availability in comparison to observed rawinsondes (collected twice a day at select locations across the country) is strongly preferred to quantify environmental changes for the purposes of this study. Each environmental profile was generated based on this RUC data and was converted into skew-T, log-P format (Figs. 3.2 - 3.4).

3.5 Model Experiments

To understand the role of environmental variability on supercell evolution near a stationary boundary, we first conducted experiments where the background environment was fixed over time. This included running 3 control simulations: one using only the warm-side environment, one using only the cold-side environment, and one using only the boundary environment (Figs. 3.2 - 3.4). Next, to account for the effects of the stationary boundary, several experiments were conducted by implementing the base-state substitution technique within CM1

(BSS; Letkewicz 2013). This method altered the horizontally-homogeneous base-state environment continuously at each time step (as in Davenport et al. 2019) while maintaining the storm-induced perturbations. The broad progression of each BSS experiment was as follows. First, a supercell thunderstorm was initiated and allowed to mature in a horizontally-homogeneous environment (occurring over the first 60 min of the simulation). Once the storm matured, BSS was initiated and evolved the background environment in a manner consistent with progressing from a warm-side environment to a cool-side environment across the stationary boundary or vice-versa. In other words, each BSS experiment either began with the supercell initiating in the warm-side environment and transitioning into the boundary environment followed by the cold-side environment, or had the supercell initiating in the cold-side environment and transitioning into the boundary environment followed by the warm-side environment.

The angle at which a supercell interacts with a boundary has been demonstrated to be important for subsequent intensification and tornadogenesis (e.g., Atkins et al. 1999; Magee and Davenport 2020). Thus, to better understand the extent to which these benefits are the result of the circulation itself versus more "residence time" in the region of, for example, enhanced SRH on the cool side of a boundary, we systematically varied the timing of BSS to represent different types of supercell-boundary interactions (Table 3.2). Short transition times between environments (15 minutes) were implemented to simulate a rapid crossing of the boundary at an acute angle. Longer transition times (30, 45, or 60 minutes) were implemented to represent increasingly parallel interaction angles with the boundary. Additionally, the implemented transition times between the environments were varied. For example, one simulation could have all three environmental transition times be 15 minutes in length, while another simulation could have two environmental transition times be 15 minutes and the other environmental transition time be 30 minutes. Changing the interaction times is very important in understanding how the duration of these interactions can affect a supercell's morphology. The example above is just one way of varying the time, but it can be changed in numerous other ways to test other aspects of supercell/boundary interactions. Although the supercell in the observed case did not cross the boundary, it is still useful due to its proximity to the boundary and lack of convection in the surrounding environment.

To more easily discuss each individual experiment, nicknames were given based on the amount of time it took to implement each respective environment. For instance, if a simulation with a supercell originating on the warm side of the boundary took 15 minutes to transition from the warm side environment to the boundary environment, the nickname would begin with a "15". Next, if that same simulation had the supercell stay on the boundary for 15 minutes, another "15" would be added onto the nickname. Finally, if the same supercell took another 15 minutes to transition into the cold-side environment, a final "15" would be added to the nickname. The nickname for this experiment would end up being "15/15/15".

Table 3.1: A list of all relevant CM1 namelist parameters relevant to the universal configuration of our simulations. Any parameters not listed on the table remain at their default settings.

Namelist Parameter Description	***Chosen Value(s)***
Number of grid points in x, y, & z directions	*1000, 1000, 48*
Horizontal grid spacing in the x, y, & z directions (Note: dz is an approximate average due to stretching)	*250, 250, 100 m*
Large time step	*1.0 s*
Maximum integration time	*14400.0 s*
Frequency of 3D model output	*300.0 s*
CM1 Set-up to determine how turbulence is handled	*1 (Large Eddy Simulation)*
Adaptive time step flag	*0 (off)*
Sub grid-scale turbulence model for Large Eddy Simulation	*1 (TKE Scheme)*
Option for Rayleigh Damping Zone at the top of domain	*1 (On)*
Microphysics Scheme	*5 (Morrison Double-Moment Scheme)*
Include Coriolis Accelerations?	*0 (off)*
Equation set for moist microphysics	*2 (Energy & Mass conserving equation set which accounts for heat capacity of hydrometers)*
West, East, North, and South Lateral Boundary Conditions	*2 (Open-Radiative)*
Bottom & Top Boundary Conditions for wind	*1 (Free-Slip)*
Convective Initiation Option	*12 (Updraft Nudging)*
Base of the Rayleigh Damping Zone	*15000 m*
Include Atmospheric Radiation?	*0 (no)*
Vertical grid spacing & vertical grid stretching parameters	*1 (Wilhelmson & Chen), 20000, 0* *6000, 100, 500 m*

Table 3.2: A list of all base-state substitution experiments ran, along with the time that each environment was fully implemented. The warm-to-cold and cold-to-warm simulations are represented in this table through the same experiment name due to their equivalence in time.

Experiment	***Time for Warm/Cold-Side Environment to be Fully Implemented***	***Time for Boundary Environment to be Fully Implemented***	***Time for Warm/Cold-Side Environment to be Fully Implemented***
15/15/15	*3600.0 s*	*5400.0 s*	*6300.0 s*
15/30/15	*3600.0 s*	*6300.0 s*	*7200.0 s*
15/45/15	*3600.0 s*	*7200.0 s*	*8100.0 s*
15/60/15	*3600.0 s*	*8100.0 s*	*9000.0 s*

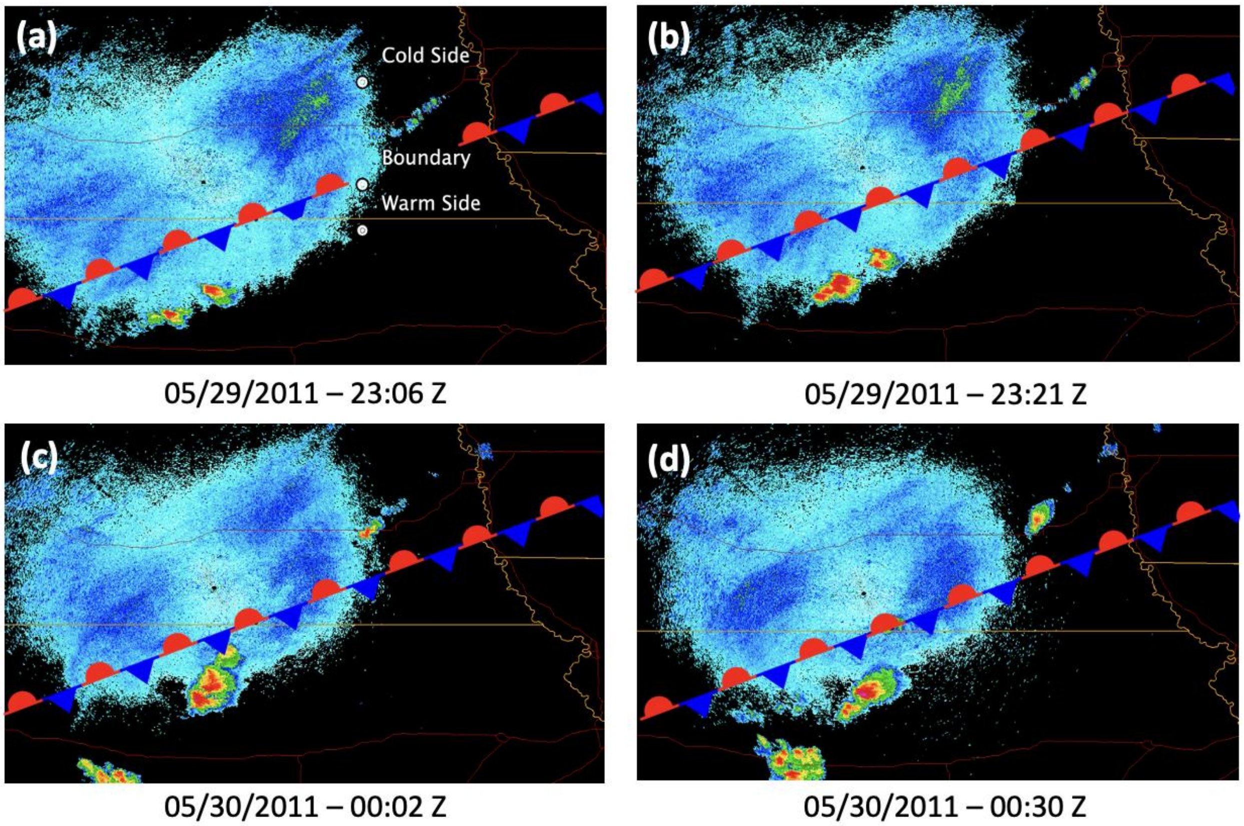

Figure 3.1: Radar snapshots of the 29 May 2011 supercell shown with an approximate position of the stationary boundary and the approximate positions of the sounding points (a).

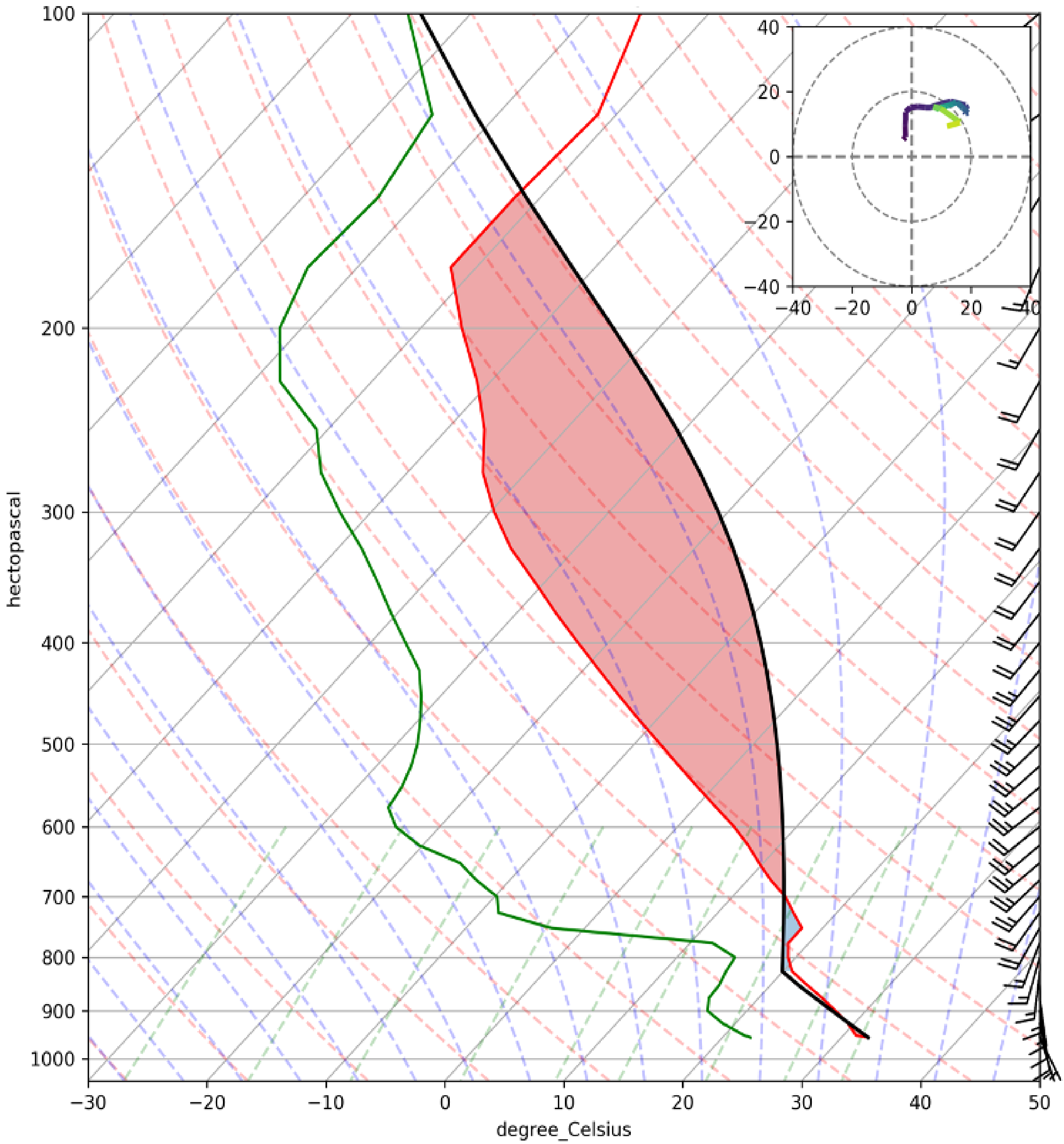

Figure 3.2: Skew-T, log-P diagram of the chosen warm-side inflow point.

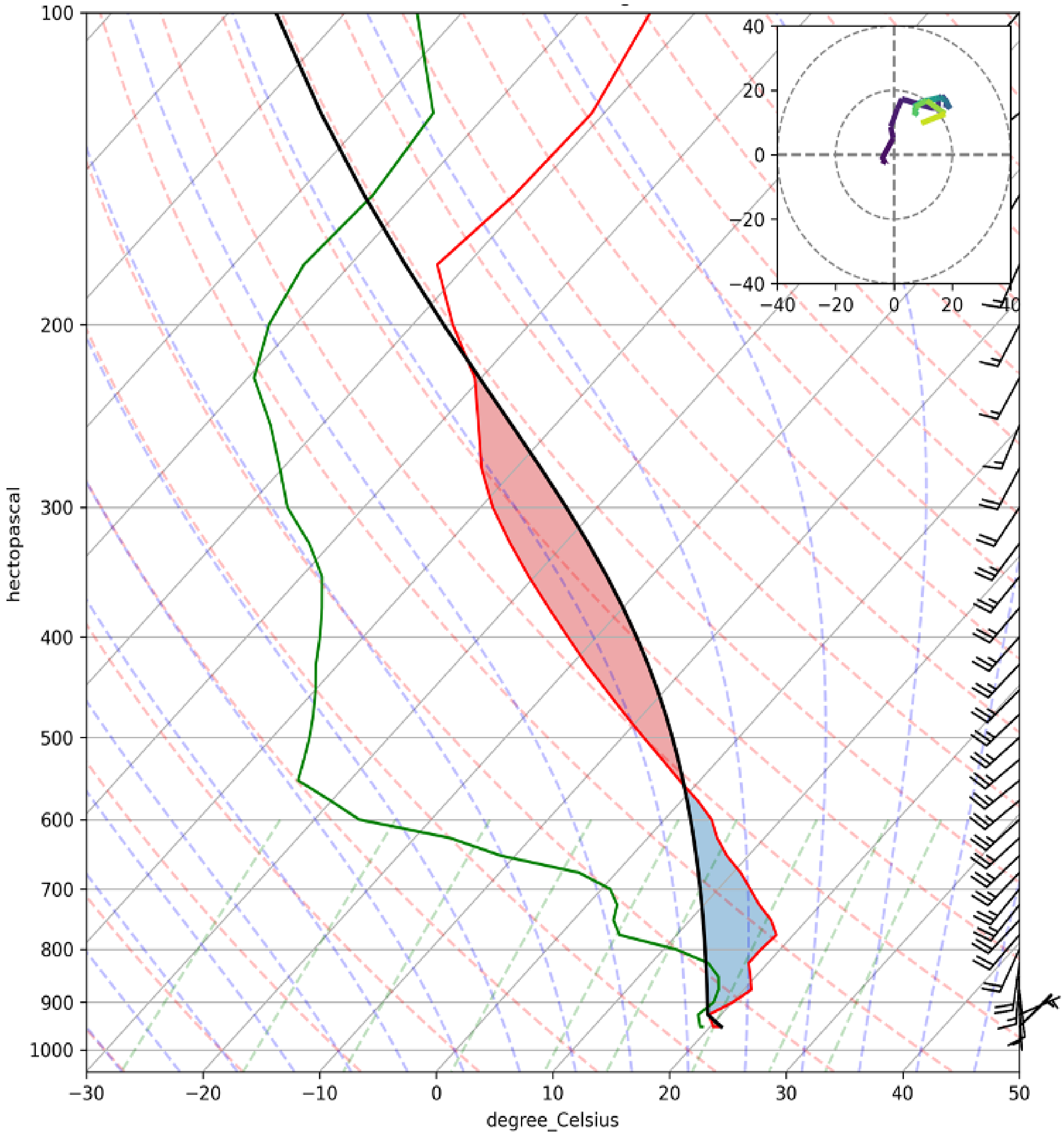

Figure 3.3: Skew-T, log-P diagram of the chosen cold-side inflow point.

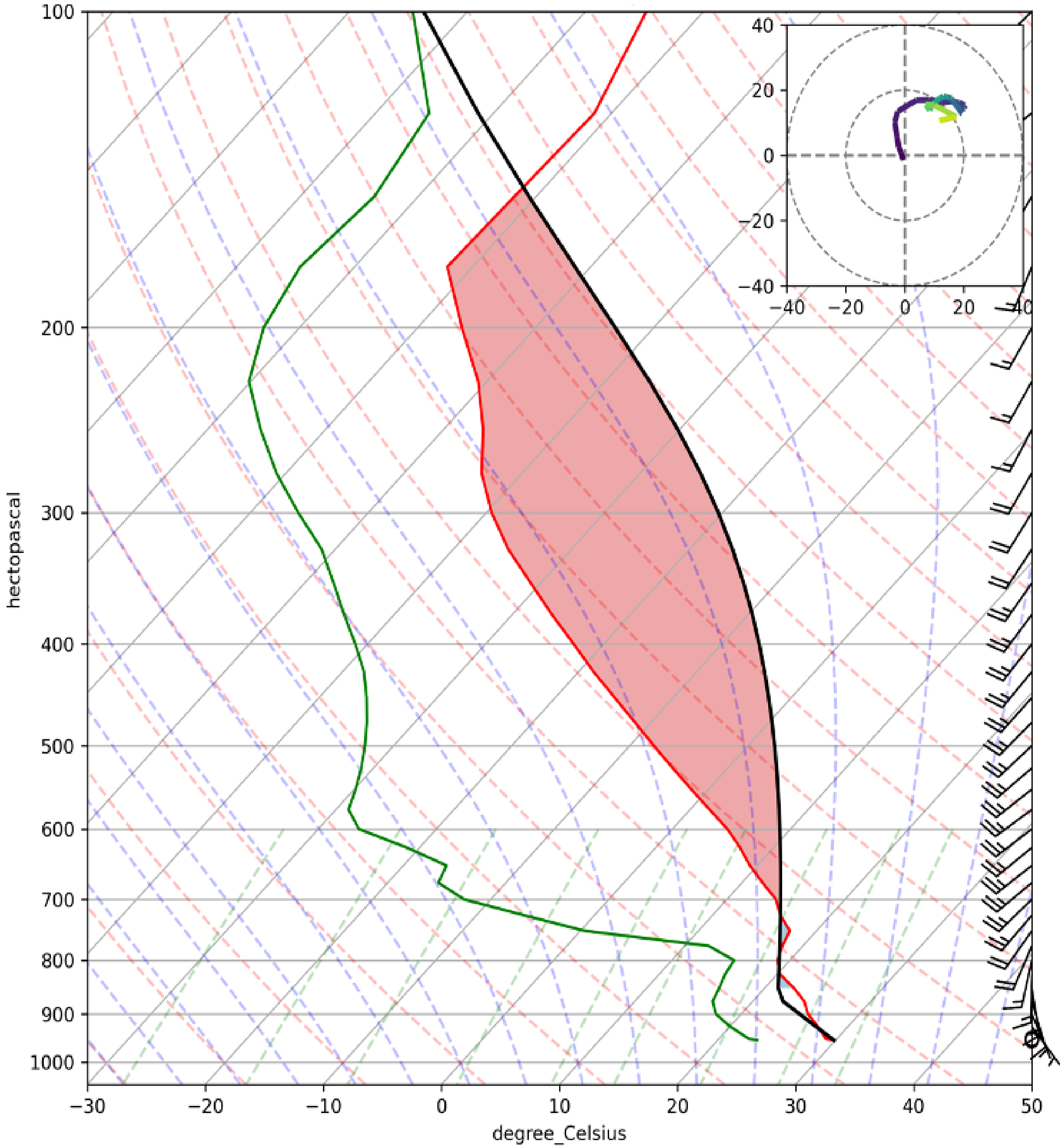

Figure 3.4: Skew-T, log-P diagram of the chosen stationary boundary inflow point.

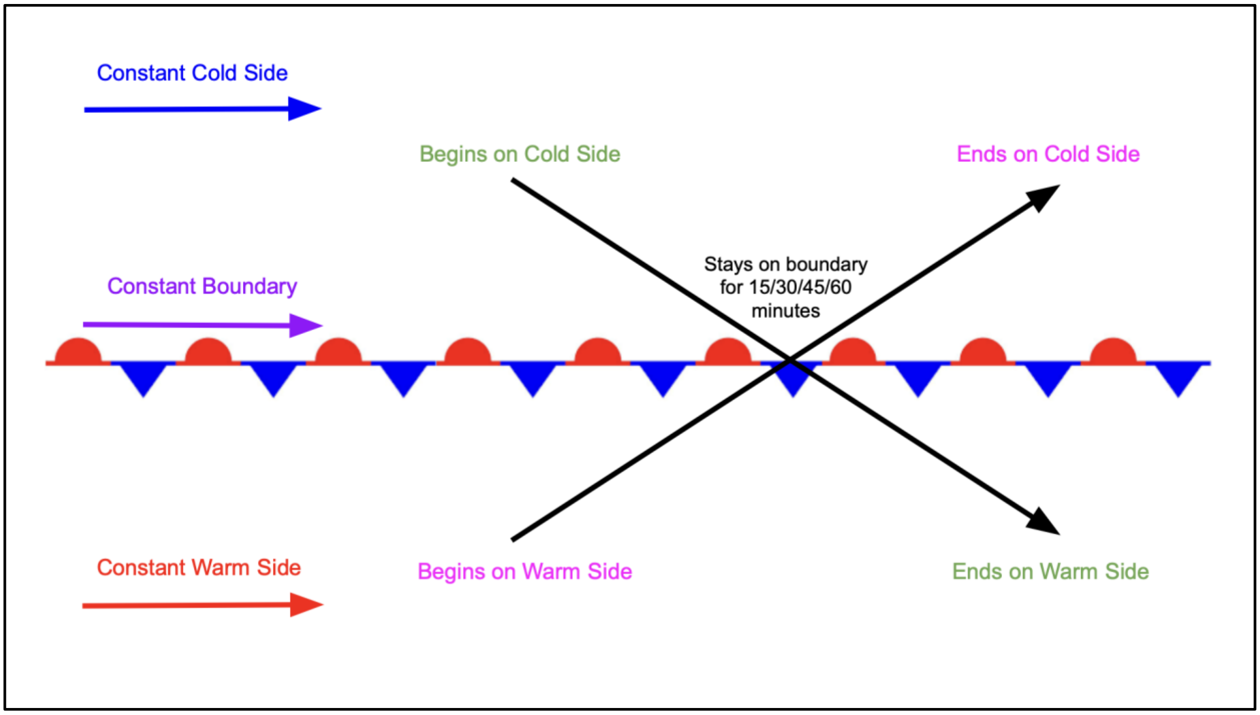

Figure 3.5: Conceptual schematic showing how simulations are run in relation to their position near the stationary boundary.

CHAPTER 4: RESULTS

4.1 Introduction

The following chapter elaborates on the results from each set of idealized experiments. The main goal of these experiments was to provide additional insight into the interactions between stationary boundaries and the mesoscale environment in regulating supercell intensity and behavior. Section 4.2 focuses on the control simulations used for this experiment, where a constant warm side, cold side, or boundary environment is used throughout the entire simulation. Next, simulations run using BSS will be discussed to see how the implementation of a boundary environment affects a supercell's morphology. This discussion will be organized so that we first observe simulations of a supercell lingering on a stationary boundary at varying times. To accomplish this, the "15/X/15" simulations will be the focus of section 4.3. Note that the "X" implies we will be changing the second environmental implementation time in these simulations (15, 30, 45, and 60 minutes), while keeping the first and third times constant at 15 minutes. Section 4.3.1 will focus on the "15/X/15" simulations where the supercell originates on the warm side of the stationary boundary environment and eventually moves into the cold-side environment (Warm-to-Cold). Section 4.3.2 will focus on the same type of simulations as section 4.3.1, but with a supercell that originates on the cold side of the stationary boundary environment and eventually moves into the warm-side environment (Cold-to-Warm).

4.2 Control Simulations

Our controls consist of three different simulations: one with a constant cold-side environment, one with a constant warm-side environment, and one with a constant boundary environment (Figs. 3.2 - 3.4). It is important to see how a supercell thunderstorm evolves in these constant base-state environments before observing how a varying background environment affects its structure, intensity, and evolution. Figure 4.1 shows the evolution of each control environment's supercell within the first 90 minutes of the simulations. Based on snapshots of storm evolution, it is evident that the boundary environment supports supercellular structure the most out of the three control environments. While the cold-side environment also supports a fairly strong storm, Fig. 4.2 demonstrates how this storm dissipates after 150 minutes. The warm-side supercell also dissipates after 150 minutes, only leaving the boundary environment supercell remaining at this time. This evolutionary difference among the control simulations is likely a function of the varying near-surface (i.e., 0-1 km) and slightly deeper low-level (i.e. 0-3 km) parameters (Table 4.1). Notably, the warm-side environment is thermodynamically and kinematically favorable for supercells, but the large amount of dry air aloft can lead to too much entrainment and a weaker storm (Fig. 3.2; e.g., James and Markowski 2010; Davenport and Parker 2015b). The cold-side environment has a strong low-level inversion (Fig. 3.3), which must be overcome to support supercell maintenance, either through robust mechanical (i.e., from a physical boundary) or dynamical (i.e., from a supercell updraft) forcing (e.g., Nowotarski and Markowski 2011; MacIntosh and Parker 2017). In contrast, out of the three background environments tested, the boundary control environment had the highest SBCAPE and MUCAPE values, as well as the highest SRH values. These enhanced severe-storm parameters in the boundary environment seemed to support stronger supercellular convection, especially later in the simulation. While there is still a lot of dry air aloft in the boundary environment, it has more kinematic support (via large SRH values; Table 4.1) than the warm-side environment. This leads to more dynamical updraft support and, overall, a longer-lived supercell.

In terms of overall intensity, the highest vertical velocities were present in the warm-side and boundary simulations (Figs. 4.4 - 4.5). The cold-side simulation (Fig. 4.3) also had fairly high vertical velocities, but not at the same magnitude as the other two simulations. This is most likely due to the lower CAPE values found in the cold-side environment, along with higher CIN values (Table 4.1). The boundary simulation had the most robust vertical structure out of the three controls, as evident in Fig. 4.5, where the vertical velocity in the boundary simulation is quasi-steady throughout the three-hour period shown. The higher vertical velocities also begin around 8 km in the boundary simulation, which is lower in the atmosphere than both the warm- and cold-side simulations. Additionally, a stronger and quasi-steady lower level updraft is present, while in the warm-side and cold-side simulations, the updraft weakens from the surface upwards over time (Figs. 4.3-4.4).

Figures 4.5 - 4.7 show the maximum vertical vorticity throughout all levels of the three control simulations. The boundary simulation has the highest maximum and most widespread vertical vorticity out of the controls, with intermittent periods of strong near-surface vertical vorticity, suggestive of potential tornado-like vortices (Fig. 4.8). The warm-side simulation initially contained similarly intense vertical vorticity as the boundary simulation, but this was evident only within the first 45 minutes (Fig. 4.7). The cold-side simulation had noticeably lower maximum vertical vorticity values than the other two simulations (Fig. 4.6), with its maximum values reaching about half of what the other two control simulations reached. These variations in vorticity among the control simulations can be attributed to differences in environments; in particular, the boundary environment contained high CAPE, as well as substantial low-level shear and SRH (Table 4.1), sufficient for dynamically and thermodynamically supporting a rotating updraft. In contrast, the drier warm-side environment and the weaker CAPE in the cold-side simulations in combination with (compared to the boundary environment) less robust low-level shear and SRH would be less supportive of strong rotation. .

4.3 15/X/15 Simulations

The following section discusses the spatiotemporal evolution of all simulations with varying times spent in the boundary environment. Importantly, these experiments test the effects of environmental changes associated with a boundary *without* the accompanying boundary circulation. All simulations within this section contained rapid shifts from the initial background environment to the boundary environment (15 min) and an equally rapid shift away from the boundary environment (15 min). The key parameter tested herein is the length of time spent within the boundary environment, which is designed to replicate the behavior of a supercell traveling quickly across the boundary at a larger angle (i.e., the 15/15/15 experiment) versus a supercell traveling approximately parallel to the boundary at a smaller angle (i.e., the 15/60/15 experiment; cf. Fig. 3.8). We will begin by focusing on the Warm-to-Cold simulations with varying times spent in the boundary environment, and then move onto the Cold-to-Warm simulations.

4.3.1 Warm-to-Cold Simulations

One major theme with the warm-to-cold simulations (Fig. 4.9) is the apparent development of model instability (i.e., anomalous convection throughout the domain) after the boundary environment is introduced (Fig. 4.10). Following a deeper analysis and additional experimentation, this “instability” is in fact a physical phenomenon resulting from the transition in the near-surface winds between the warm-side environment and the boundary environment. Specifically, the warm-side environment contains low-level southeasterly flow, while the cold-side environment contains northeasterly winds (Figs. 3.2 and 3.4). The impact of this low-level wind shift is evident in Fig. 4.11; when BSS modifies the kinematic environment, convergence is enhanced in the cold pool due to stronger northerly flow, resulting in the development of new convection that eventually grows upscale and interferes with the original supercell. However, when only the thermodynamic environment is modified via BSS, this enhanced convergence is not present, and new convection does not develop.

Thus, it is clear that the development of additional convection when using BSS to transition from the warm-side to the cold-side environment is rooted in the physical change in the wind profile, one that is necessarily tied to the transition to the boundary environment. However, the additional convection is also problematic, as it interferes with the original supercell. Workarounds for this issue were attempted. The primary fix tested was varying the amount of time spent transitioning from the warm to boundary environment; this timing was lengthened from 15 min to either 30, 45, or 60 min so that convergence would not be enhanced as quickly. Figure 4.12 shows four new simulations run with longer transition times between the warm-side environment and the boundary environment. Unfortunately, the same result occurs, but is delayed depending on how long the transition takes. This shows that lengthening the transition time between these two environments does not prevent the generation of convection; instead, it is simply delayed. Additional experimentation for addressing this issue is left to future work.

Given the above challenges of applying BSS in the warm-to-cold simulations, the height-time charts of maximum vertical velocity and vorticity for each simulation were not as informative with regards to the goal of this study as originally desired (Figs. 4.13 - 4.20). The first two hours of each simulation are represented in each height-time chart, and it is apparent that the additional convection affected all of the simulations in a similar fashion. The first 60 minutes of each simulation, before BSS began, was identical, as expected. Once BSS began and the warm-side environment began to switch to the boundary environment, the primary supercell began to rapidly dissipate. After the 60 minute mark for each simulation, there is very little vertical velocity/vertical vorticity left in the main supercell. Looking at Figs. 4.13 - 4.16, the first hour of the simulation shows a supercell with a very strong updraft in the upper levels. This updraft remains steady in size and magnitude while the supercell is in the warm-side environment. The same pattern can be seen for the vertical vorticity in Figs. 4.17 - 4.20. There are two clear vertical vorticity maxima at ~16 km within the first hour of each simulation. Once the warm-side environment switches to the boundary environment, these maxima disappear and the vertical vorticity within the main supercell quickly dissipates. Future work will consider how to account for such impacts of modifying the wind profile while still understanding the role of boundary circulations and environmental changes.

4.3.2 Cold-to-Warm Simulations

Supercells originating in the cold-side environment have visible structural differences compared to those originating in the warm-side environment. In contrast to the previous set of experiments, using BSS to transition from the cold-side environment to the warm-side environment did not result in a similar development of extensive convection owing to the low-level wind shift. Thus, these experiments can be more informative of the impact boundary-associated environmental variability without the boundary circulation.

Figures 4.21 and 4.22 show the evolution of all four simulations from 30 minutes to 150 minutes. Consistent with the control simulation (Figs. 4.1 - 4.2), the supercell generated in the cold-side environment was not as robust, owing to the stable low-level environment. However, while the control simulation produced a small supercell that was maintained for a couple of hours, implementing BSS by transitioning to the boundary environment did not lead to an increasingly strong supercell; instead, the storm eventually dissipated in each experiment (Figs. 4.21-4.22). Interestingly, as *more* time was spent in the boundary environment, the supercells became less and less organized. Notably, there was not a clear cold pool at any point in the simulation, suggesting there was weak low-level forcing for parcels into the main updraft. Furthermore, this in combination with the mid-level warming acting to reduce elevated instability and the increasingly large amounts of dry air in the mid levels likely encouraged additional entrainment into the updraft, which weakened the overall structure of the supercell (Fig. 4.31).

Figures 4.23 - 4.26 depict height-time charts of the maximum vertical velocity for the cold-to-warm simulations. As expected, the vertical velocity profiles of each simulation are identical within the first 60 minutes – before BSS has begun. The noticeable differences between each simulation occur once the boundary environment is introduced. One common theme in the maximum vertical velocity charts is that the supercells that spent less time in the boundary environment maintained the strongest updrafts within the two-hour period that's shown. The 15/15/15 cold-to-warm simulation's vertical velocity (Fig. 4.23) shows an updraft that consistently reaches 60 m s^{-1}. Once the residence time on the boundary is increased, the maximum vertical velocities do not go above 50 m s^{-1}. In the other three simulations (Figs. 4.24 - 4.26), the maximum vertical velocity after the first hour does not reach the same magnitude as in the first hour. The supercells' updrafts begin to dissipate fairly quickly with a longer boundary residence time.

Figures 4.27 - 4.30 show the maximum vertical vorticity for the cold-to-warm simulations. The trends seen in these figures are very similar to those observed in the maximum vertical velocity figures. The maximum vertical vorticity seen within the first 60 minutes of each simulation dissipates rather quickly after the boundary environment is introduced. This deterioration of vorticity happens sooner with a longer boundary residence time.

From the above results, it is worth noting that the environmental transition from the cold-side to the boundary and warm-side environments did not result in a longer-lived supercell. Unlike the constant boundary control simulation, the simulations with an environmental transition did not have a longer-lived storm; instead, the supercell weakened and dissipated. This suggests that the boundary circulation is an important contributor to the maintenance and severe weather production when a supercell thunderstorm is interacting with it. However the generality of this finding is uncertain. In this particular case, features of the environment may also be important, such as the warming mid-levels as well as the dry mid-level air present in the warm and boundary sides of the boundary (Figs. 4.31-4.32), which may have contributed to the dissipation of the supercells. The noticeable lack of an organized cold pool in these cases is another environmental feature that led to the dissipation of the supercells. Since these simulations began in the cold-side environment, they were not able to develop a proper cold pool before moving into the boundary and warm-side environments. The intrusion of dry air in the mid-levels along with the absence of a cold pool likely promoted the dissipation of the simulated supercells. It would be worthwhile to continue exploring the sensitivity of this finding about the central importance of the boundary circulation to other storm environments.

Table 4.1: Select sounding parameters from the constant warm-side, cold-side, and boundary soundings (see Figs. 3.2 - 3.4). These values were calculated using the MetPy package in Python.

	MU CAPE (J/kg)	**MU CIN (J/kg)**	**SB CAPE (J/kg)**	**SBCIN (J/kg)**	**D CAP E (J/kg)**	**0-1 km Shear (m/s)**	**0-3 km Shear (m/s)**	**0-1 km SRH (m^2/s^2)**	**0-3 km SRH (m^2/s^2)**
Warm Side	5794.5	-0.2	5794.5	-0.2	1986.9	10.09	23.60	175.95	300.36
Cold Side	2817.1	-121.3	1405.5	-405.0	1676.4	17.55	27.34	328.15	481.27
Boundary	5921.0	-9.4	5921.0	-9.4	1929.7	14.47	26.88	287.93	548.33

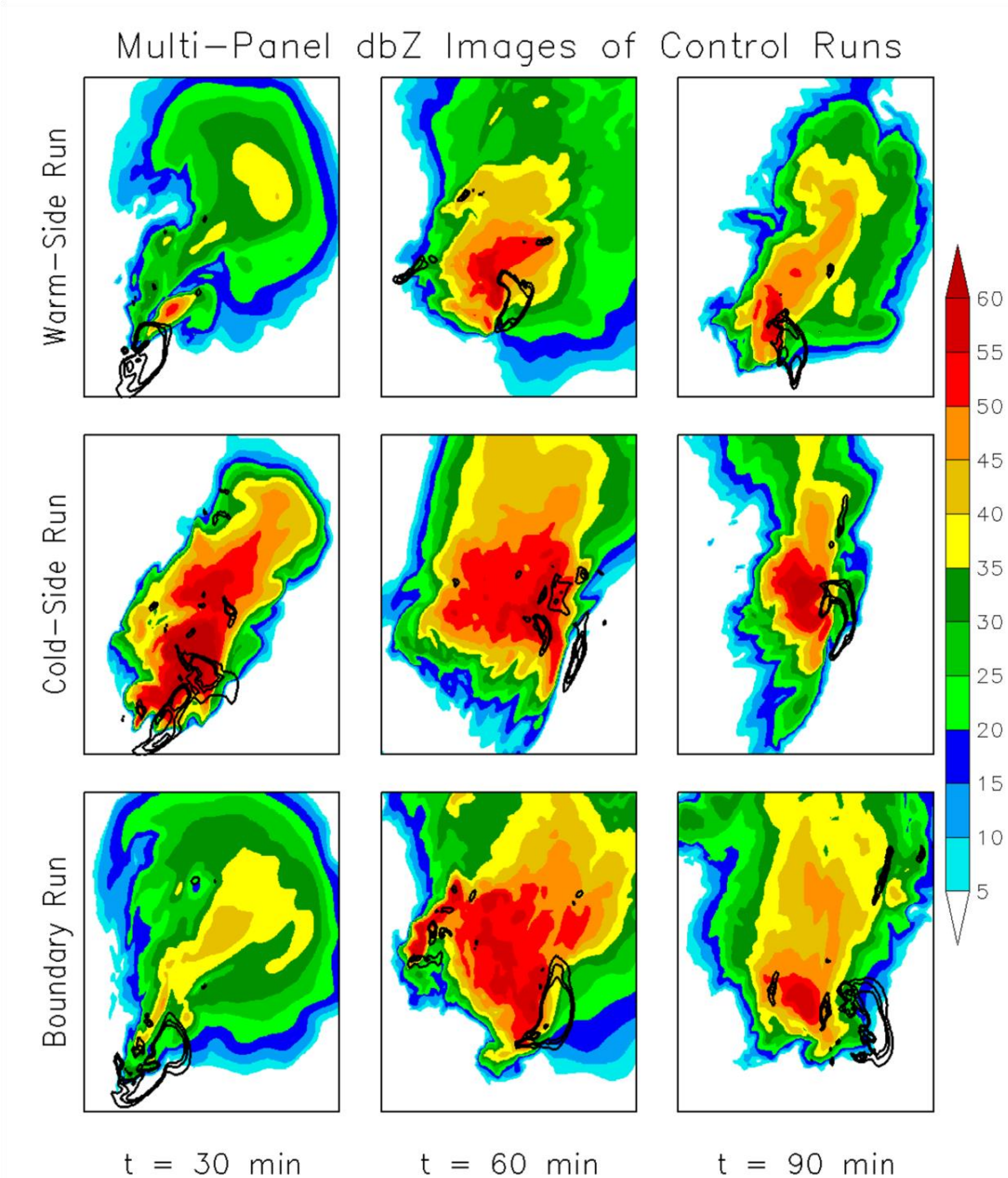

Figure 4.1: Simulated radar reflectivity (shaded) and updraft helicity (contoured; 200, 400, & 600 $m^2 s^{-2}$) shown at three different times in the cold-side, warm-side, and boundary control simulations.

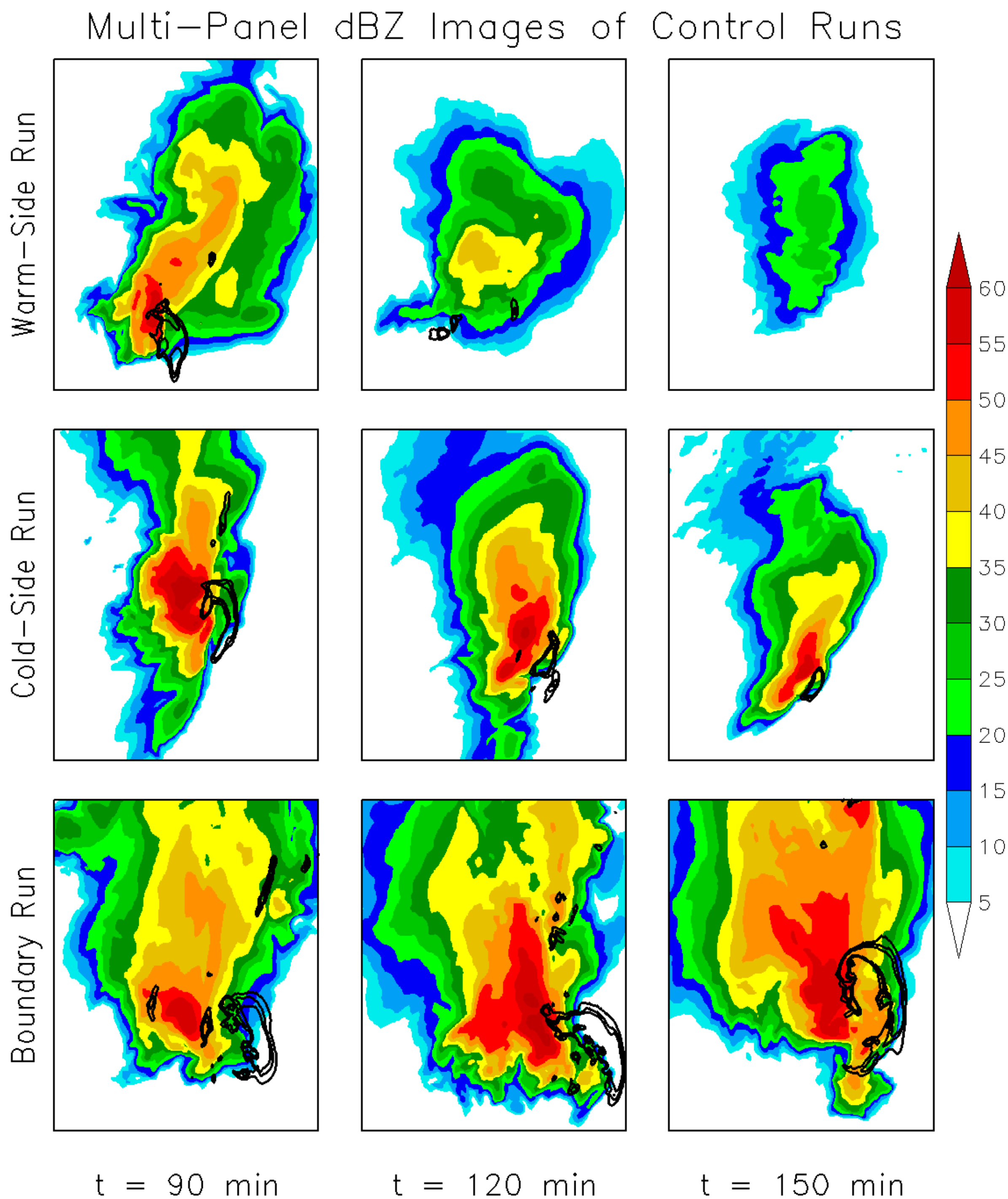

Figure 4.2: Simulated radar reflectivity (shaded) and updraft helicity (contoured; 200, 400, & 600 m^2 s^{-2}) shown at three more times in the cold-side, warm-side, and boundary control simulations.

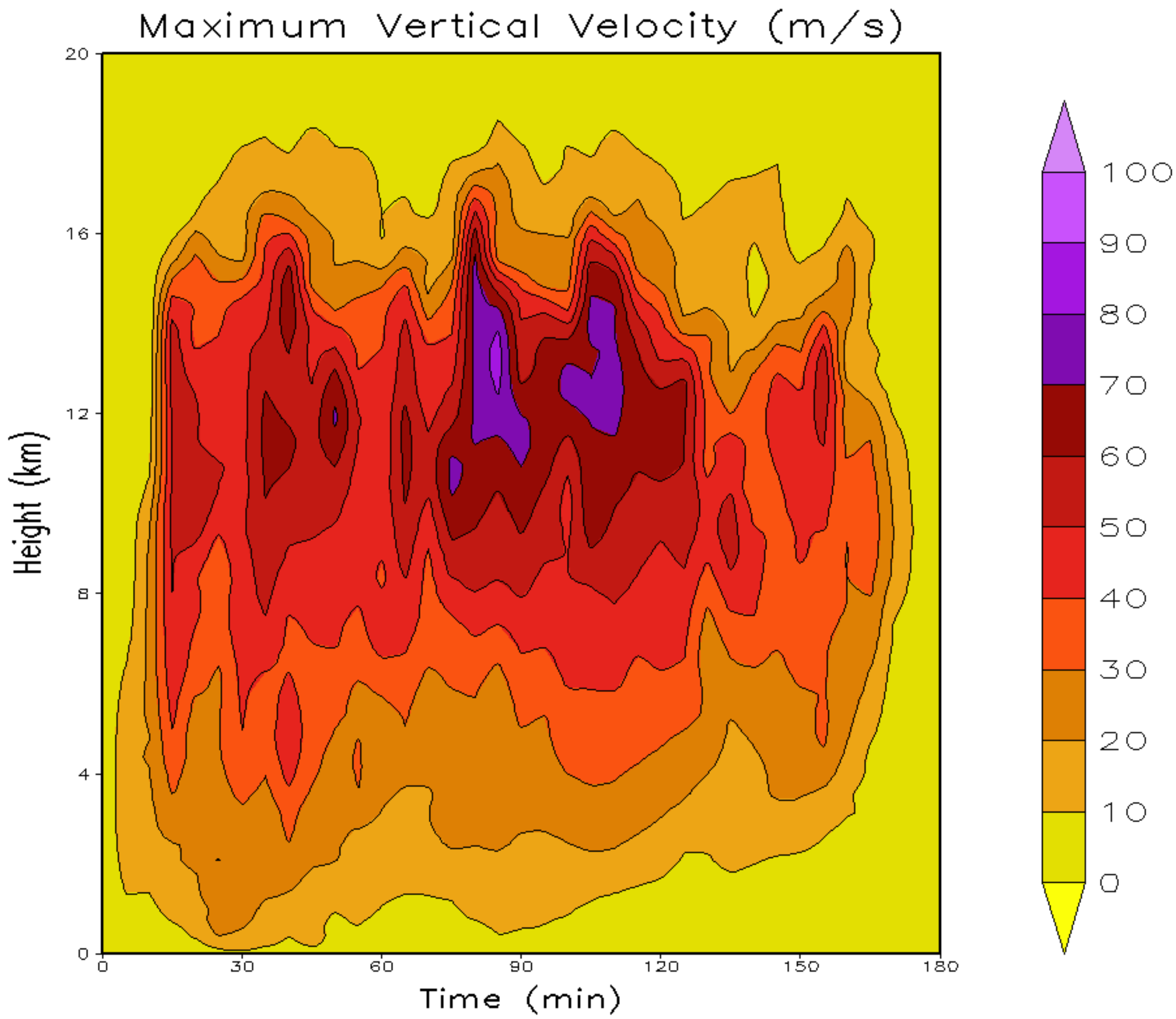

Figure 4.3: Time-height plot of maximum vertical velocity (shaded and contoured every 10 ms^{-1}) for the constant cold side simulation. The *x* axis represents simulated or observed time, while the *y* axis represents height in km.

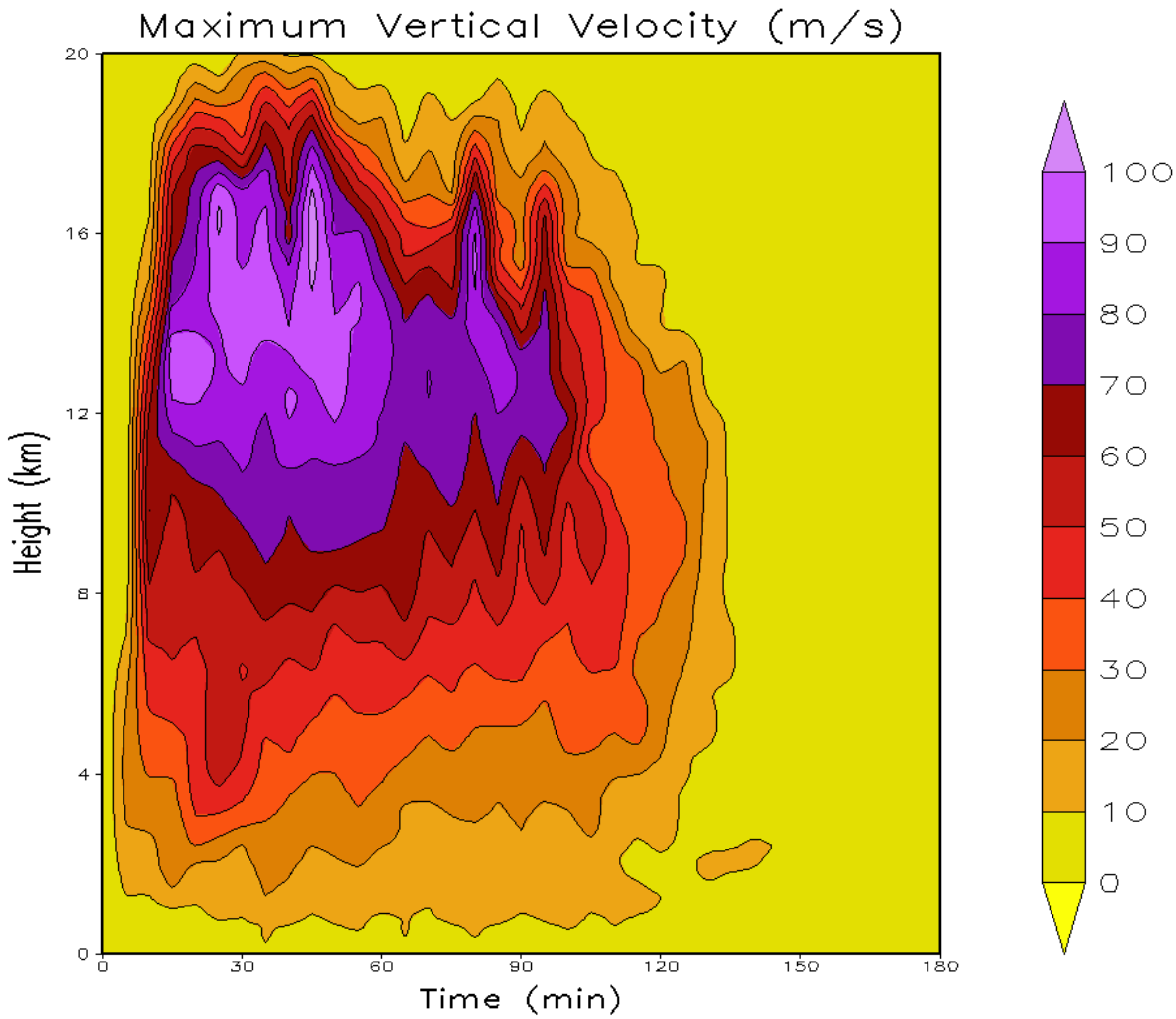

Figure 4.4: Time-height plot of maximum vertical velocity (shaded and contoured every 10 ms^{-1}) for the constant warm side simulation. The *x* axis represents simulated or observed time, while the *y* axis represents height in km.

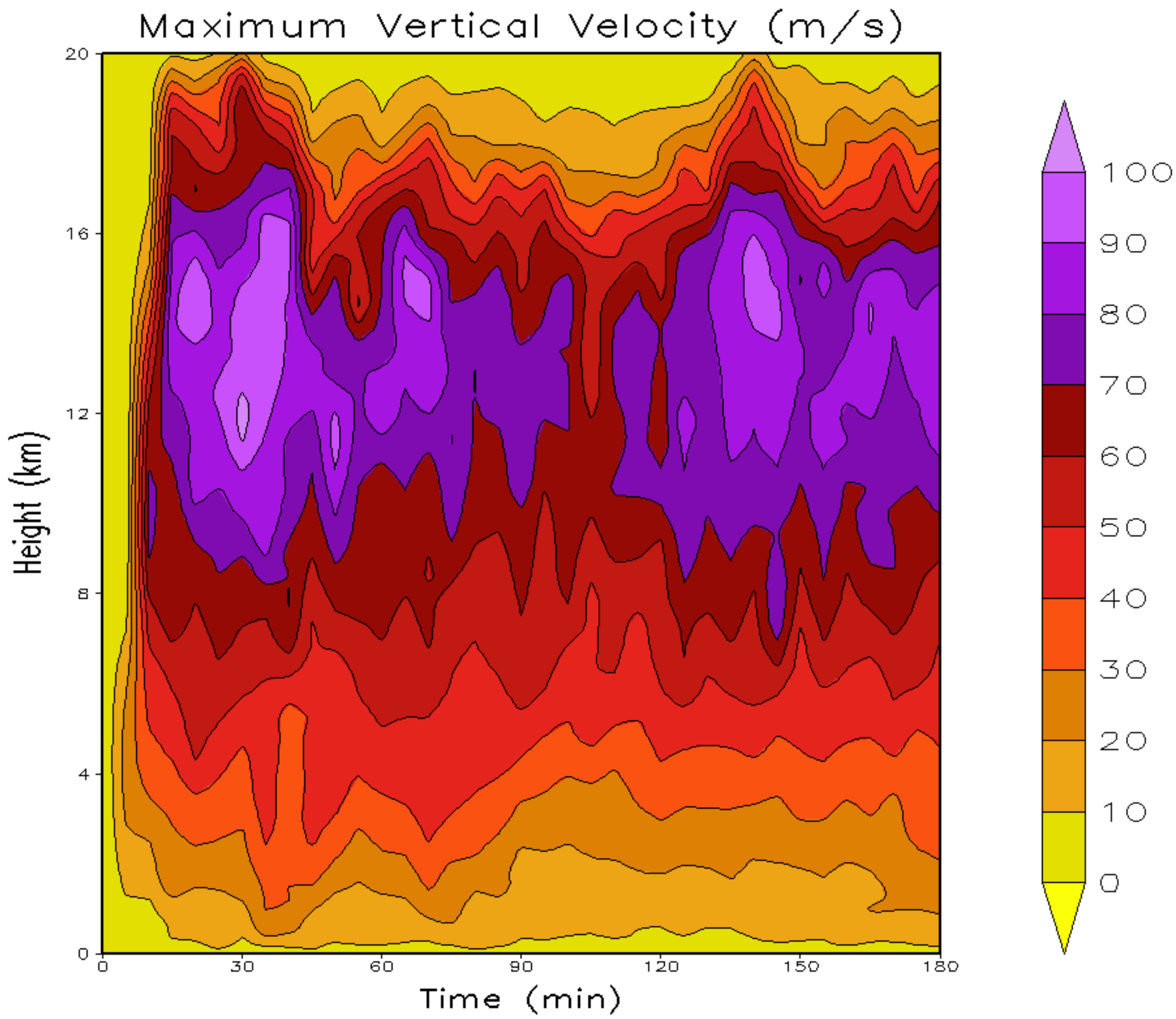

Figure 4.5: Time-height plot of maximum vertical velocity (shaded and contoured every 10 ms^{-1}) for the constant boundary simulation. The *x* axis represents simulated or observed time, while the *y* axis represents height in km.

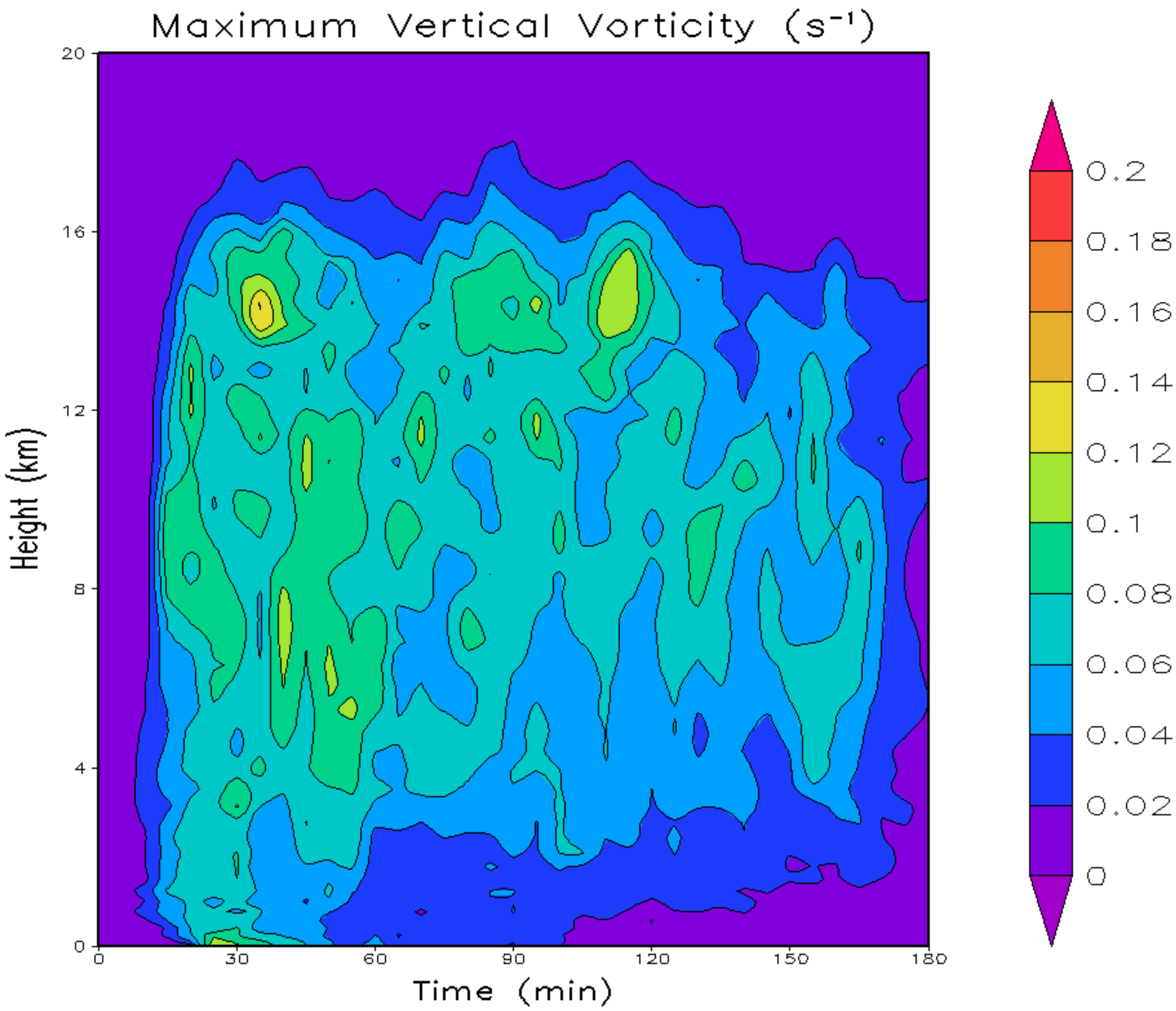

Figure 4.6: Time-height plot of maximum vertical vorticity (shaded and contoured every 0.02 s^{-1}) for the constant cold side simulation. The *x* axis represents simulated or observed time, while the *y* axis represents height in km.

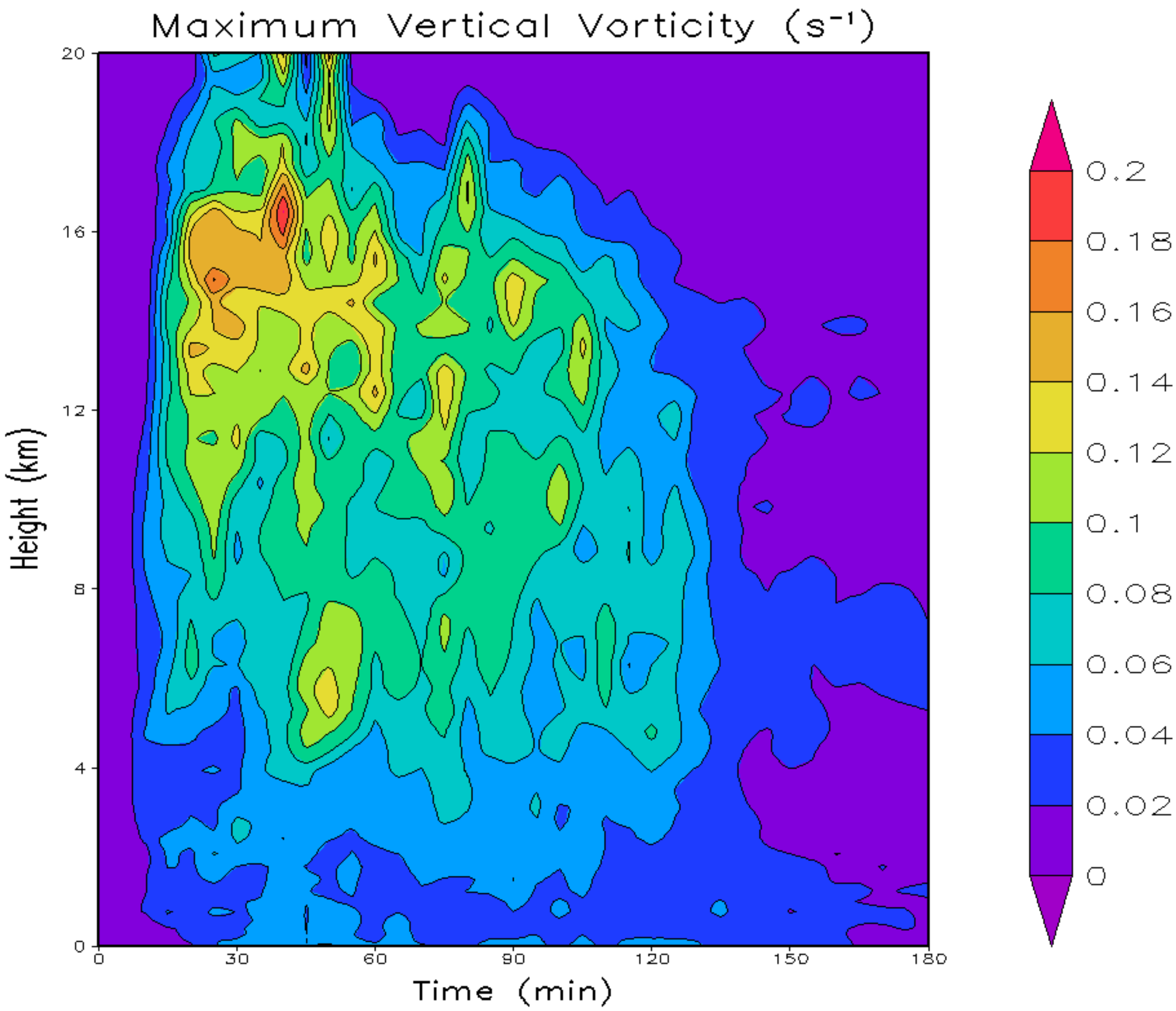

Figure 4.7: Time-height plot of maximum vertical vorticity (shaded and contoured every 0.02 s^{-1}) for the constant warm side simulation. The *x* axis represents simulated or observed time, while the *y* axis represents height in km.

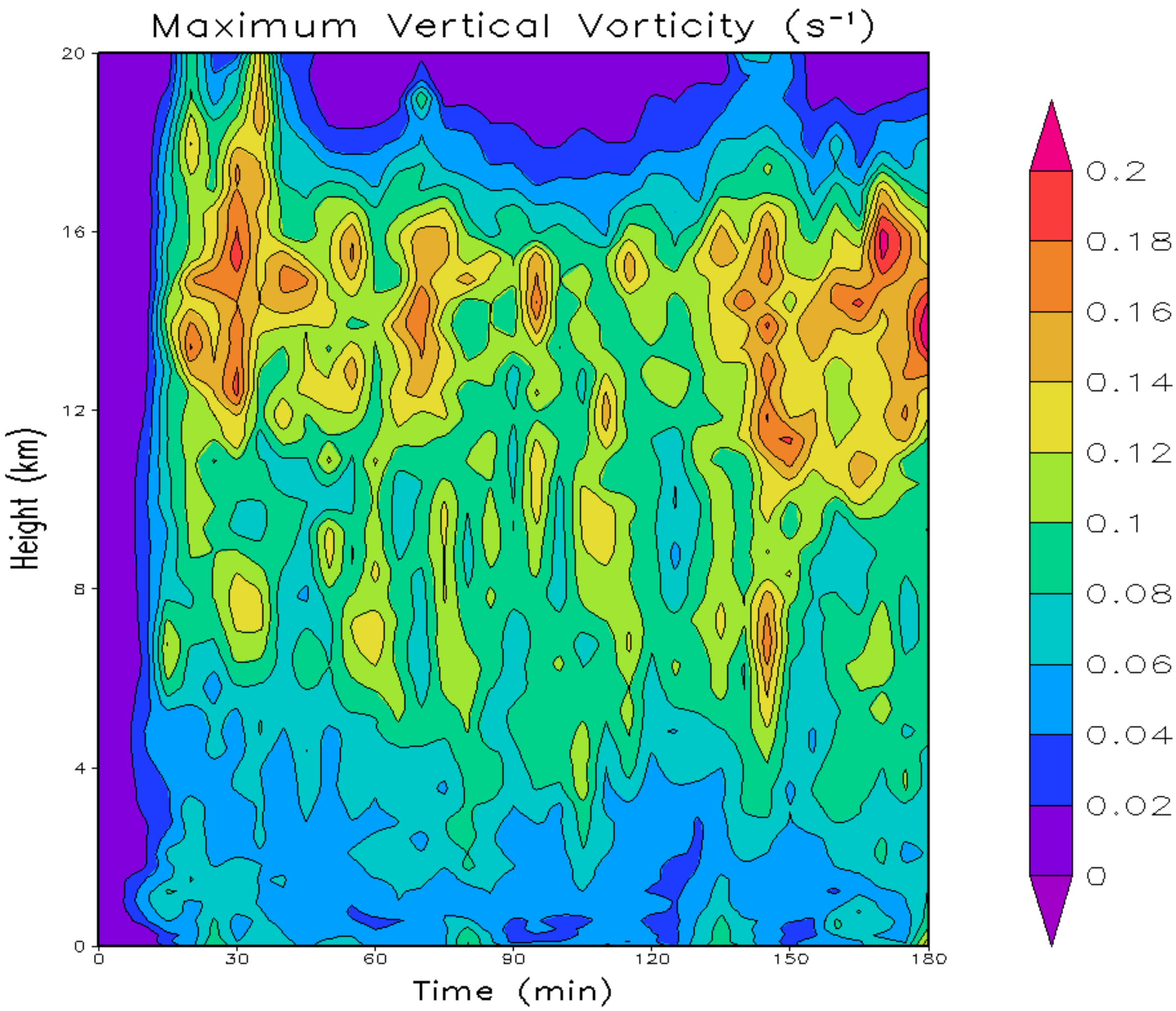

Figure 4.8: Time-height plot of maximum vertical vorticity (shaded and contoured every 0.02 s^{-1}) for the constant boundary simulation. The *x* axis represents simulated or observed time, while the *y* axis represents height in km.

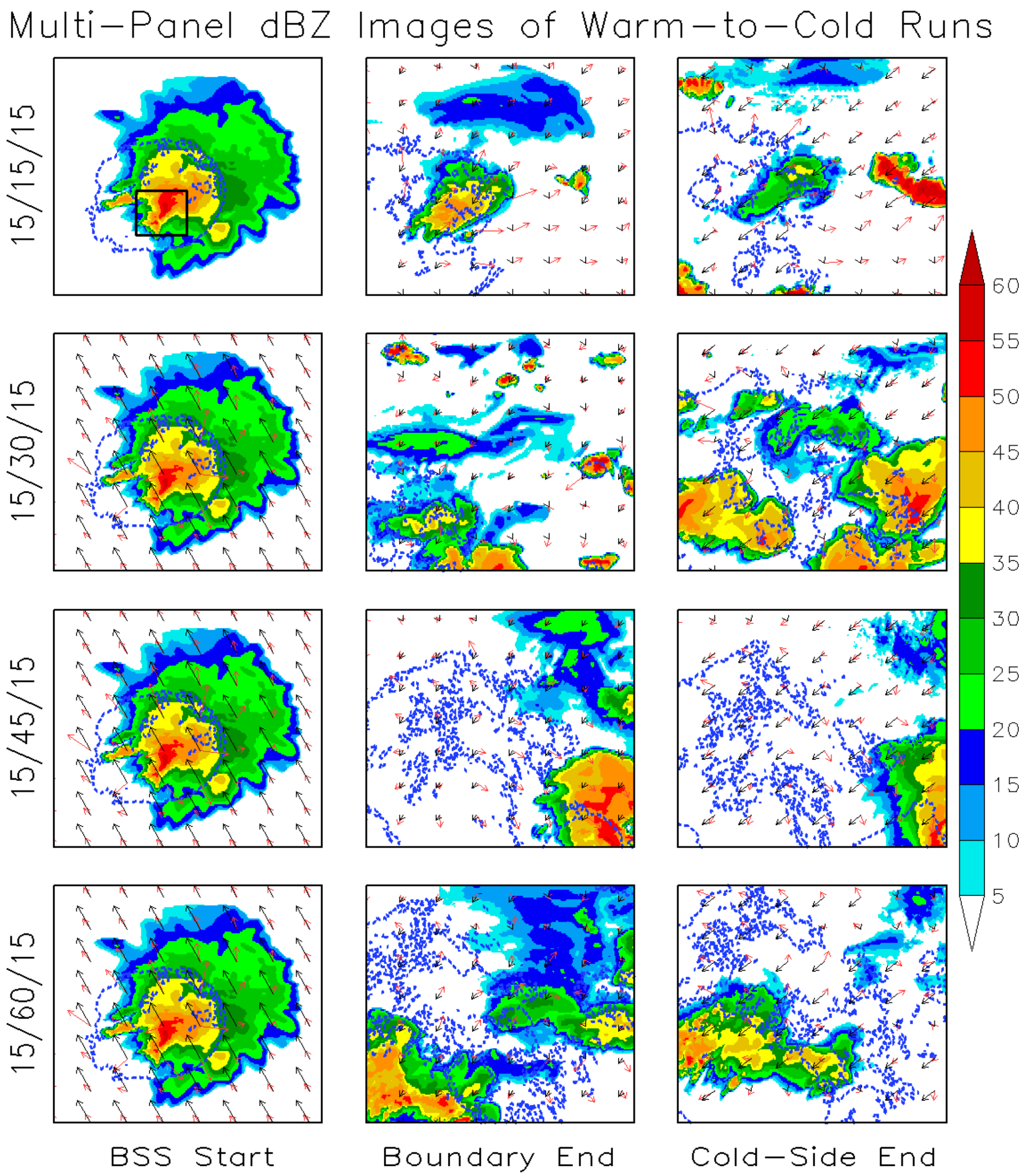

Figure 4.9: Simulated radar reflectivity (shaded), potential temperature perturbation (contoured, -1 K), base-state winds (black vectors), and total winds (red vectors) of the 15/X/15 warm-to-cold side simulations. The first column shows the reflectivity at the start of BSS. The second column shows the reflectivity at the end of the constant boundary environment. The third column shows the reflectivity when the cold-side environment has been fully implemented. The black box in the upper-left panel shows the area where the maximum vertical velocity and vorticity was taken at all levels for Figs. 4.13 - 4.20.

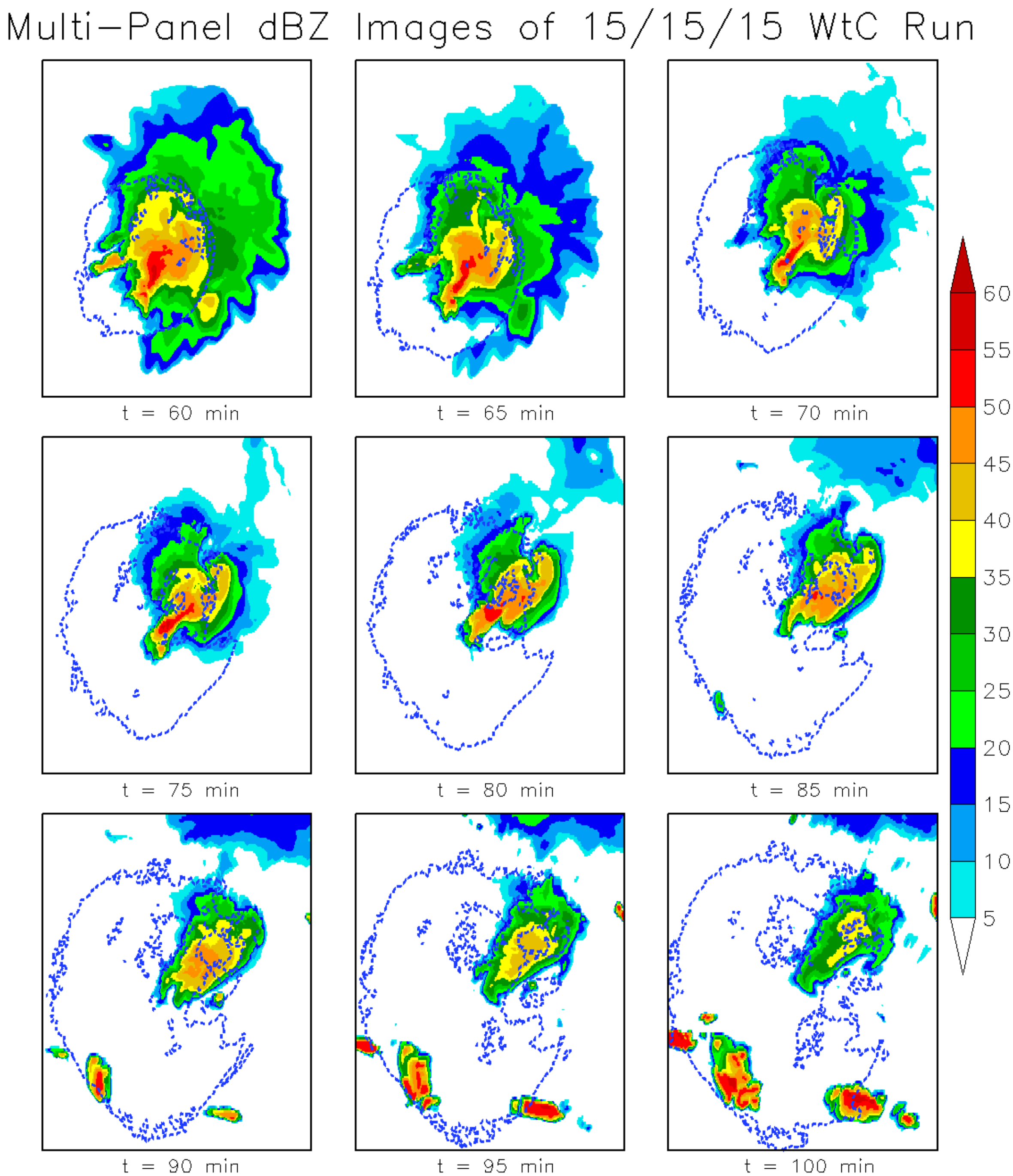

Figure 4.10: Simulated radar reflectivity (shaded) and potential temperature perturbation (contoured, -1 K) of the 15/15/15 warm-to cold side simulation – demonstrating the appearance of the anomalous convection after the boundary environment is introduced.

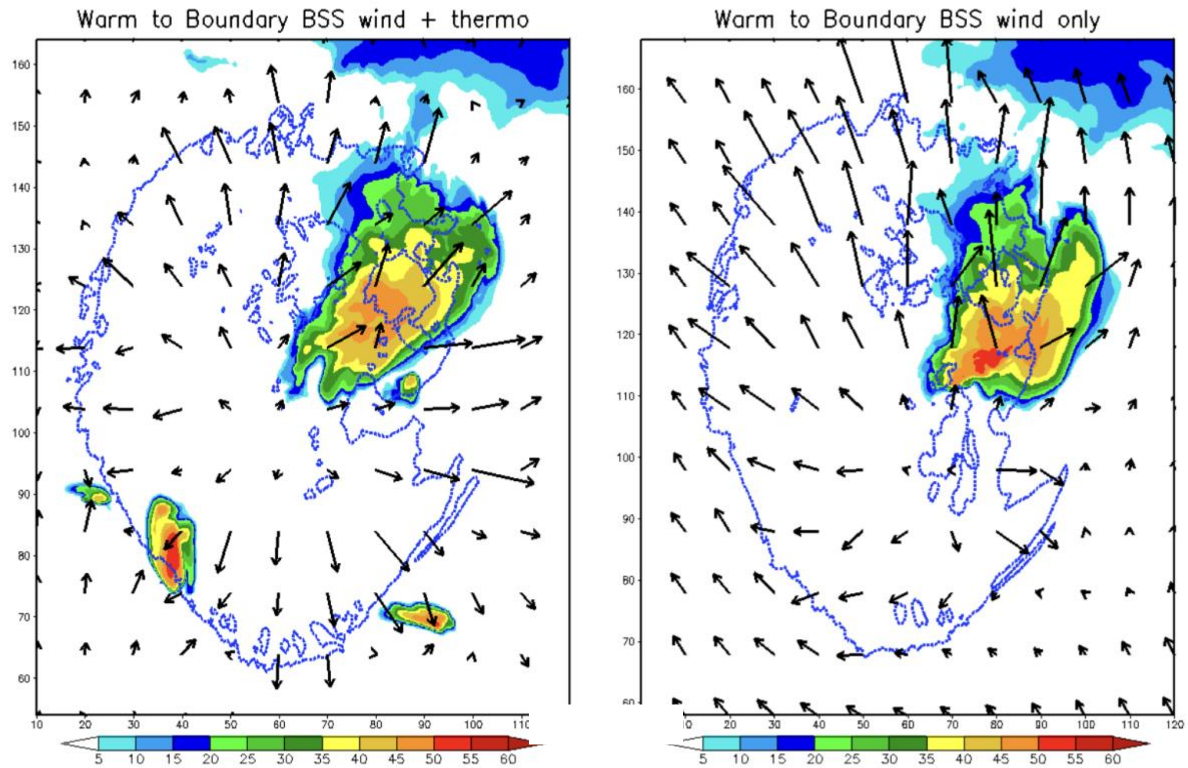

Figure 4.11: Simulated radar reflectivity (shaded), potential temperature perturbation (contoured, -1 K), and total winds (vectors) of the 15/15/15 warm-to-cold simulation at 90 minutes.

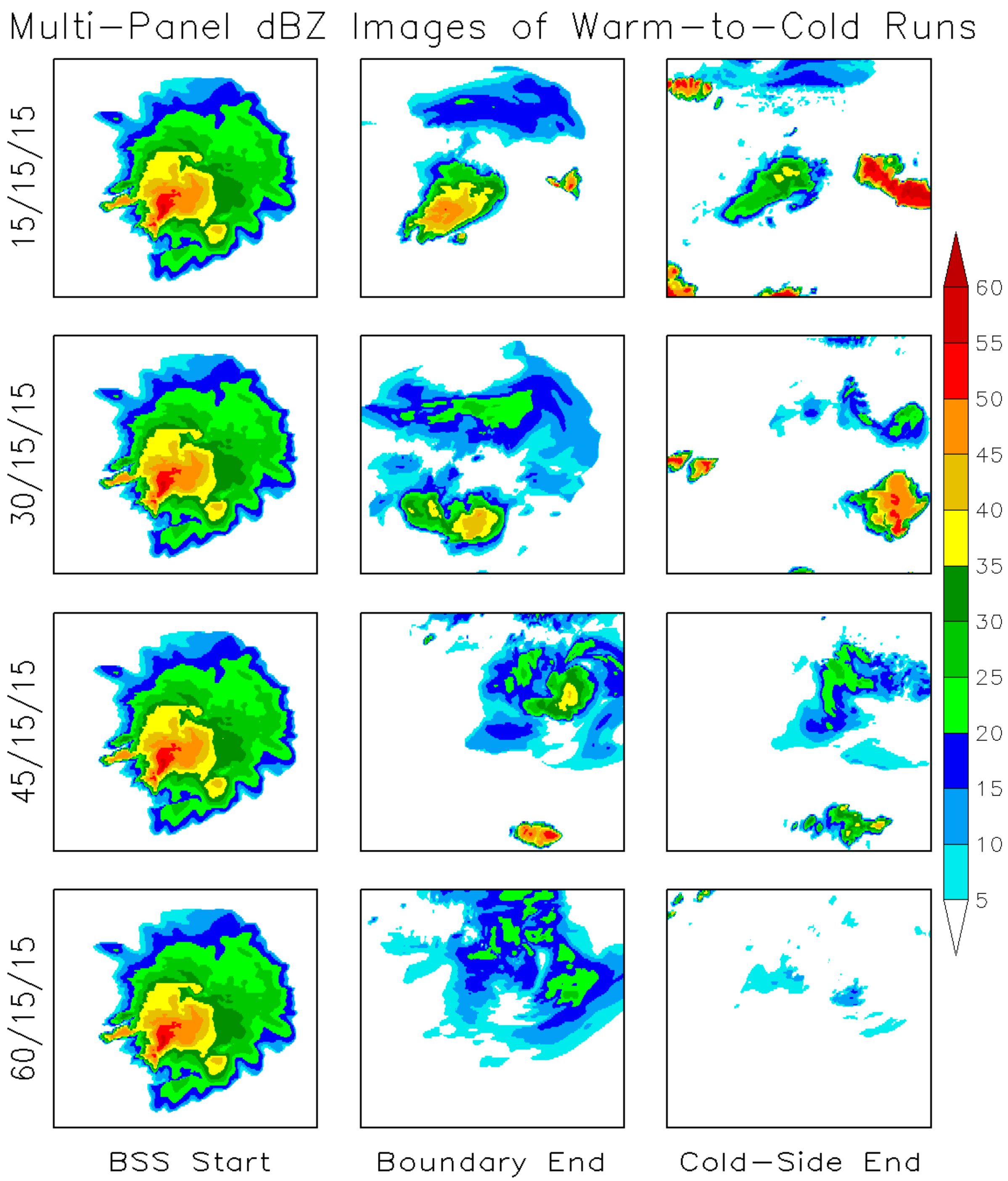

Figure 4.12: Simulated radar reflectivity (shaded) of the X/15/15 warm-to-cold side simulations. The first column shows the reflectivity at the start of BSS. The second column shows the reflectivity at the end of the constant boundary environment. The third column shows the reflectivity when the cold-side environment has been fully implemented.

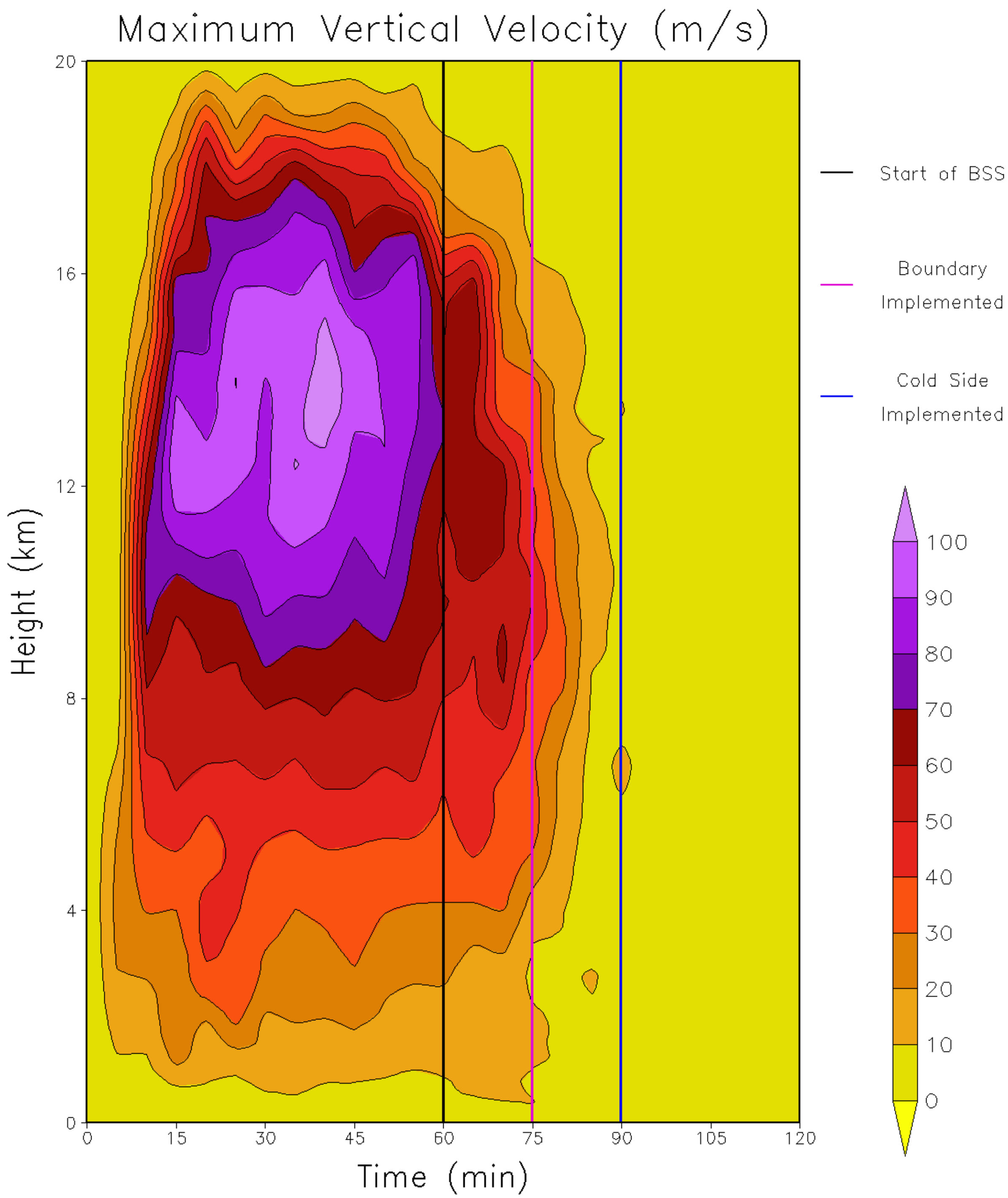

Figure 4.13: Time-height plot of maximum vertical velocity (shaded and contoured every 10 ms^{-1}) for the 15/15/15 warm-to-cold side simulation. The *x* axis represents simulated or observed time, while the *y* axis represents height in km.

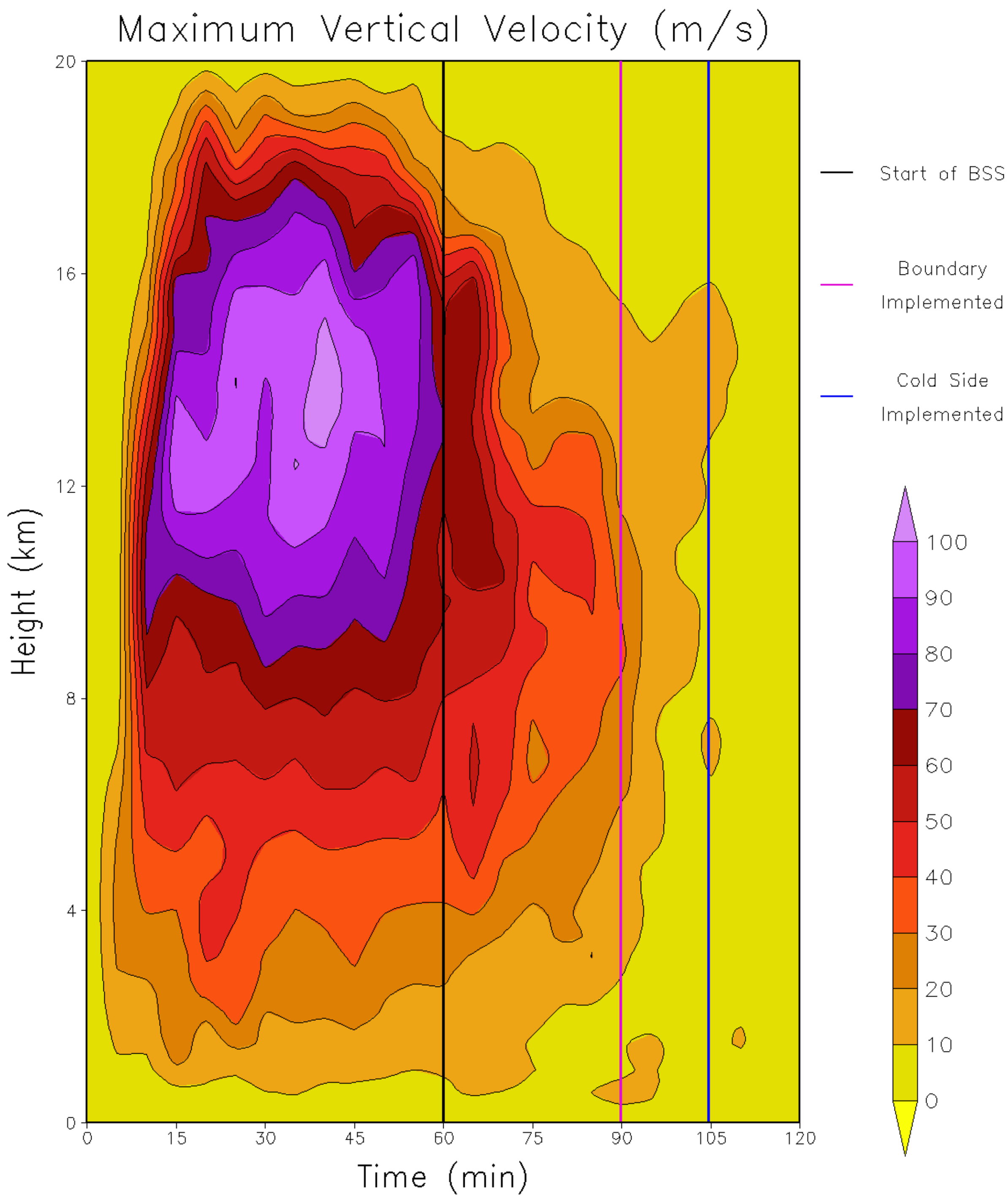

Figure 4.14: Time-height plot of maximum vertical velocity (shaded and contoured every 10 ms^{-1}) for the 15/30/15 warm-to-cold side simulation. The *x* axis represents simulated or observed time, while the *y* axis represents height in km.

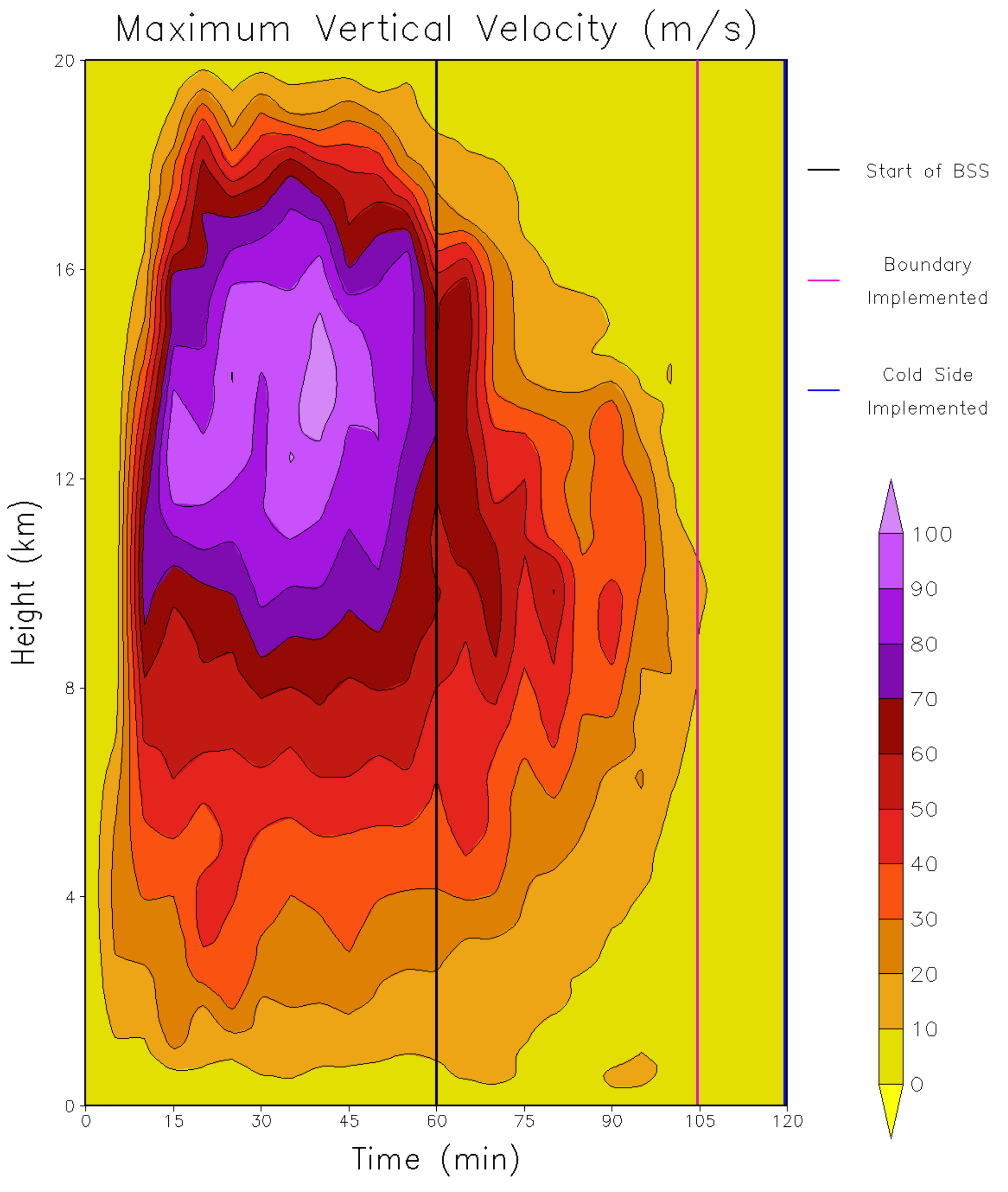

Figure 4.15: Time-height plot of maximum vertical velocity (shaded and contoured every 10 ms^{-1}) for the 15/45/15 warm-to-cold side simulation. The *x* axis represents simulated or observed time, while the *y* axis represents height in km.

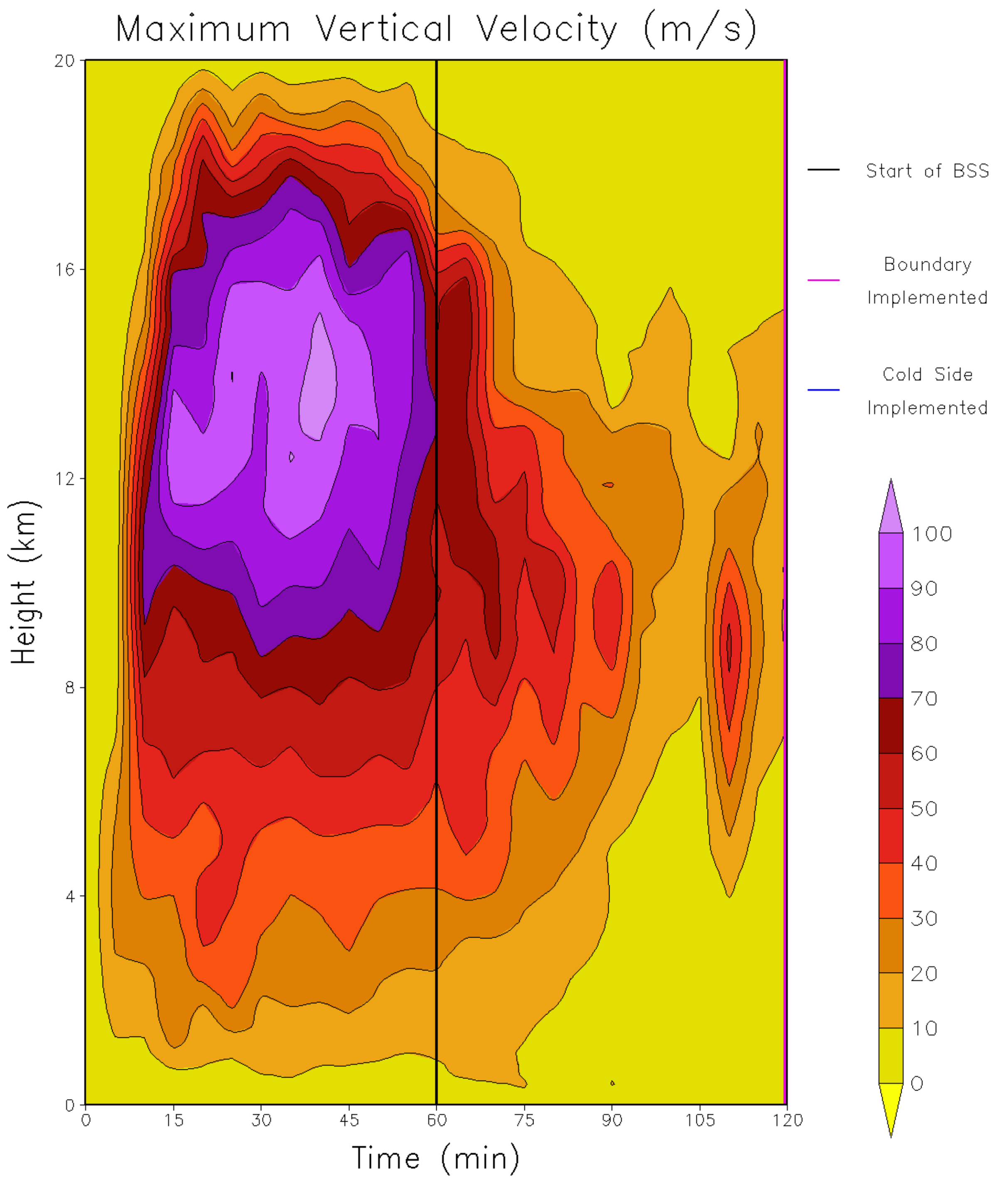

Figure 4.16: Time-height plot of maximum vertical velocity (shaded and contoured every 10 ms^{-1}) for the 15/60/15 warm-to-cold side simulation. The *x* axis represents simulated or observed time, while the *y* axis represents height in km. The “cold side implemented” line occurs off the graph.

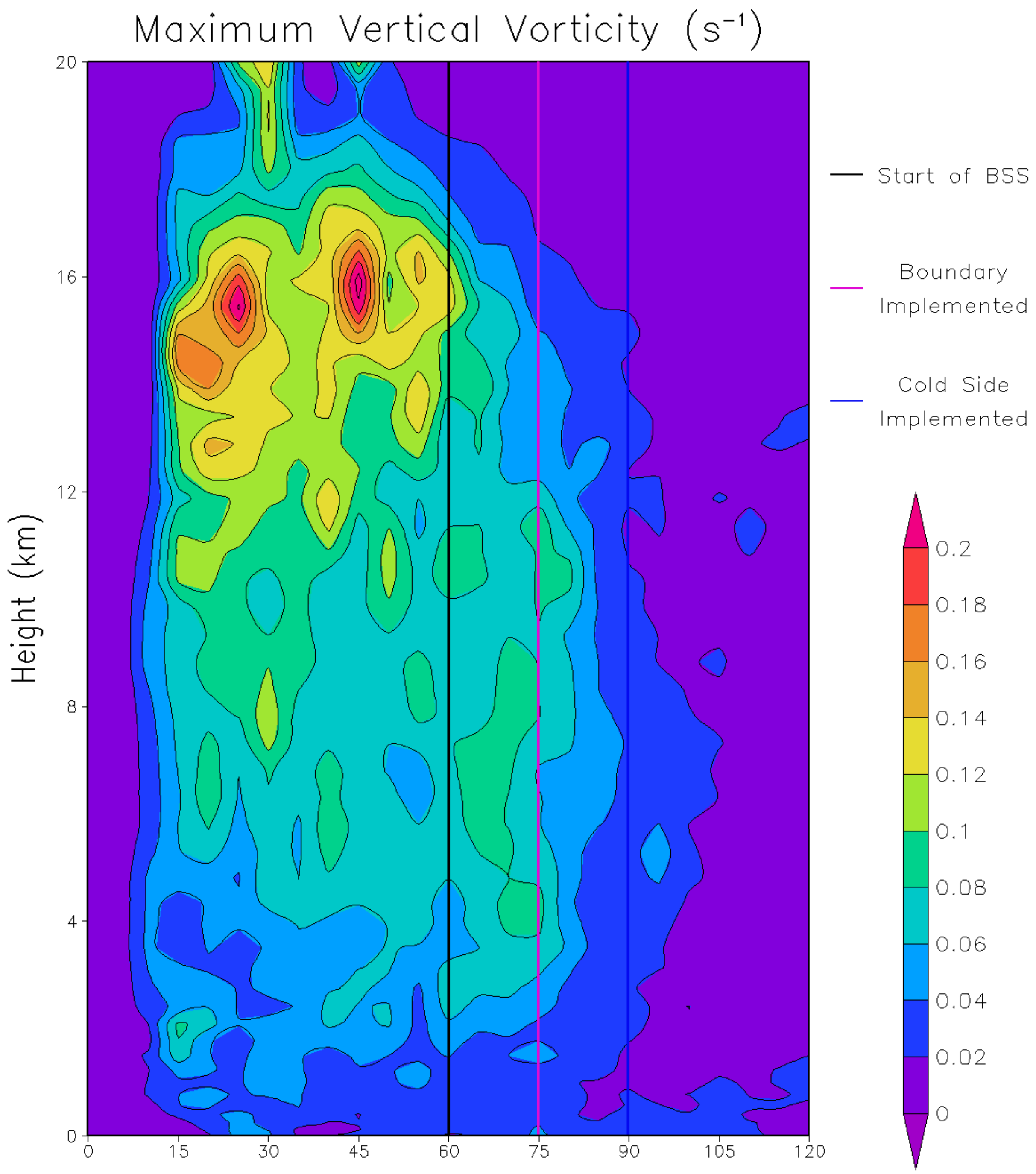

Figure 4.17: Time-height plot of maximum vertical vorticity (shaded and contoured every 0.02 s^{-1}) for the 15/15/15 warm-to-cold side simulation. The *x* axis represents simulated or observed time, while the *y* axis represents height in km. The constant boundary environment is located between the "Boundary Implemented" and "Cold Side Start" lines.

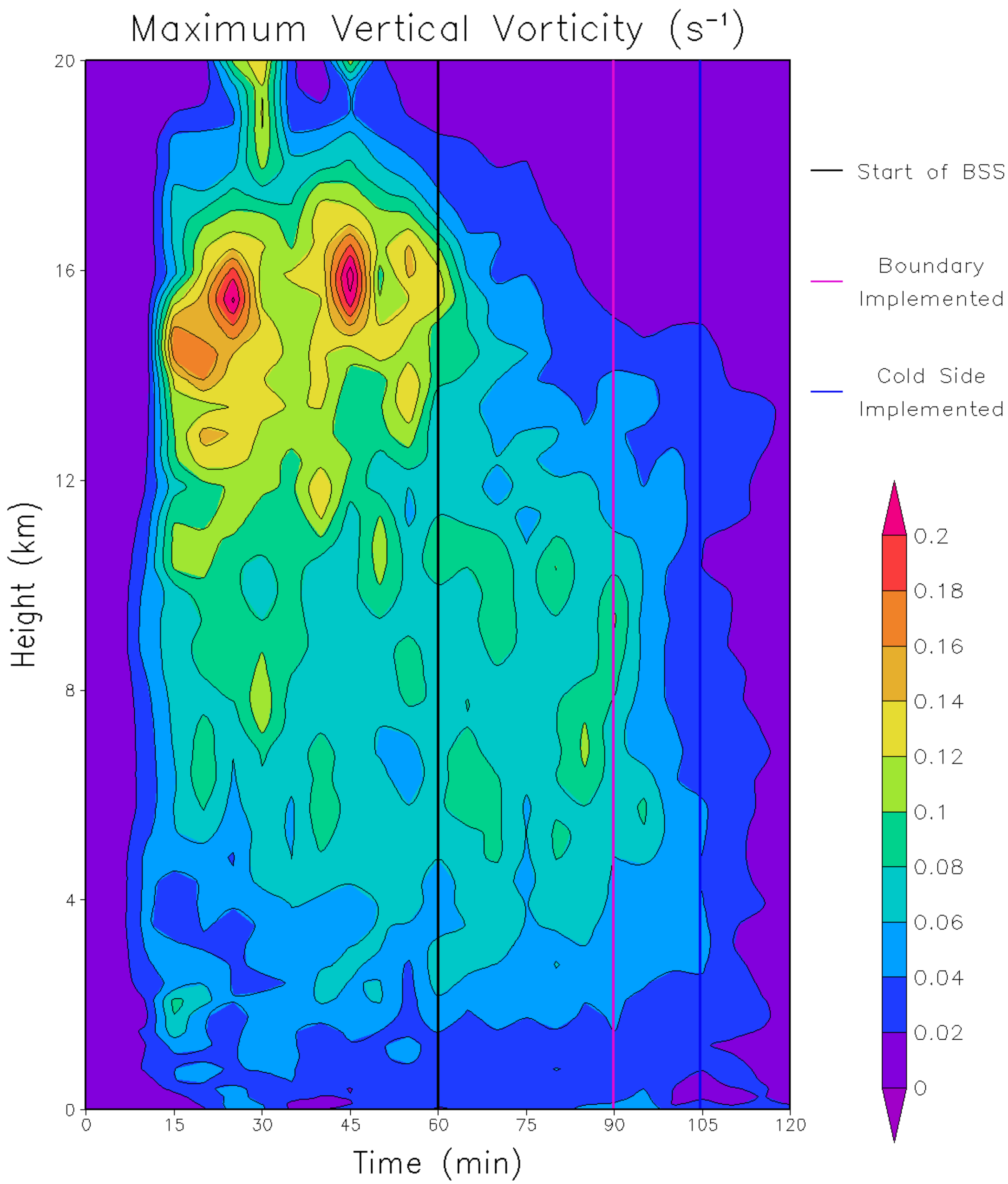

Figure 4.18: Time-height plot of maximum vertical vorticity (shaded and contoured every 0.02 s^{-1}) for the 15/30/15 warm-to-cold side simulation. The *x* axis represents simulated or observed time, while the *y* axis represents height in km.

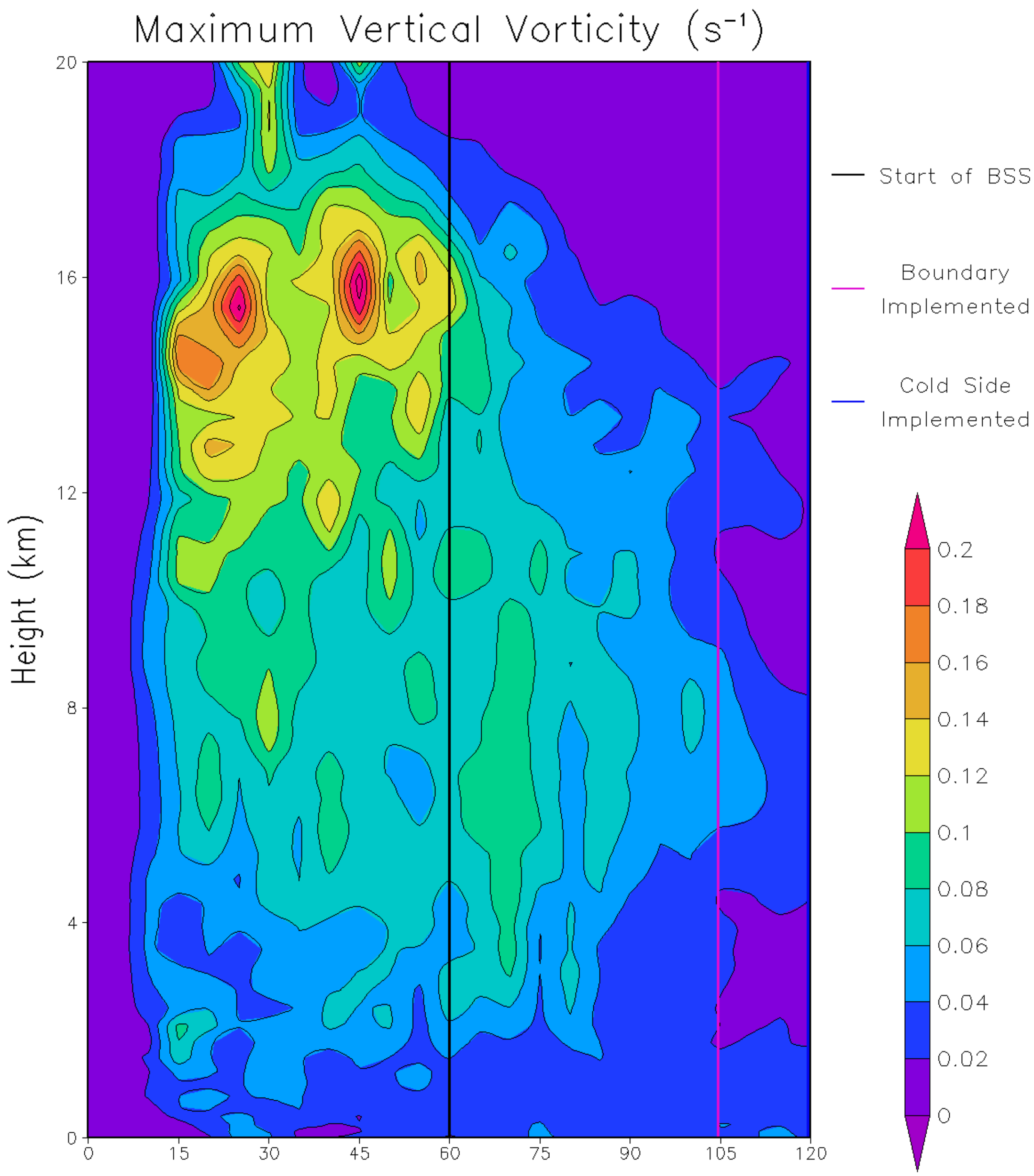

Figure 4.19: Time-height plot of maximum vertical vorticity (shaded and contoured every 0.02 s^{-1}) for the 15/45/15 warm-to-cold side simulation. The *x* axis represents simulated or observed time, while the *y* axis represents height in km.

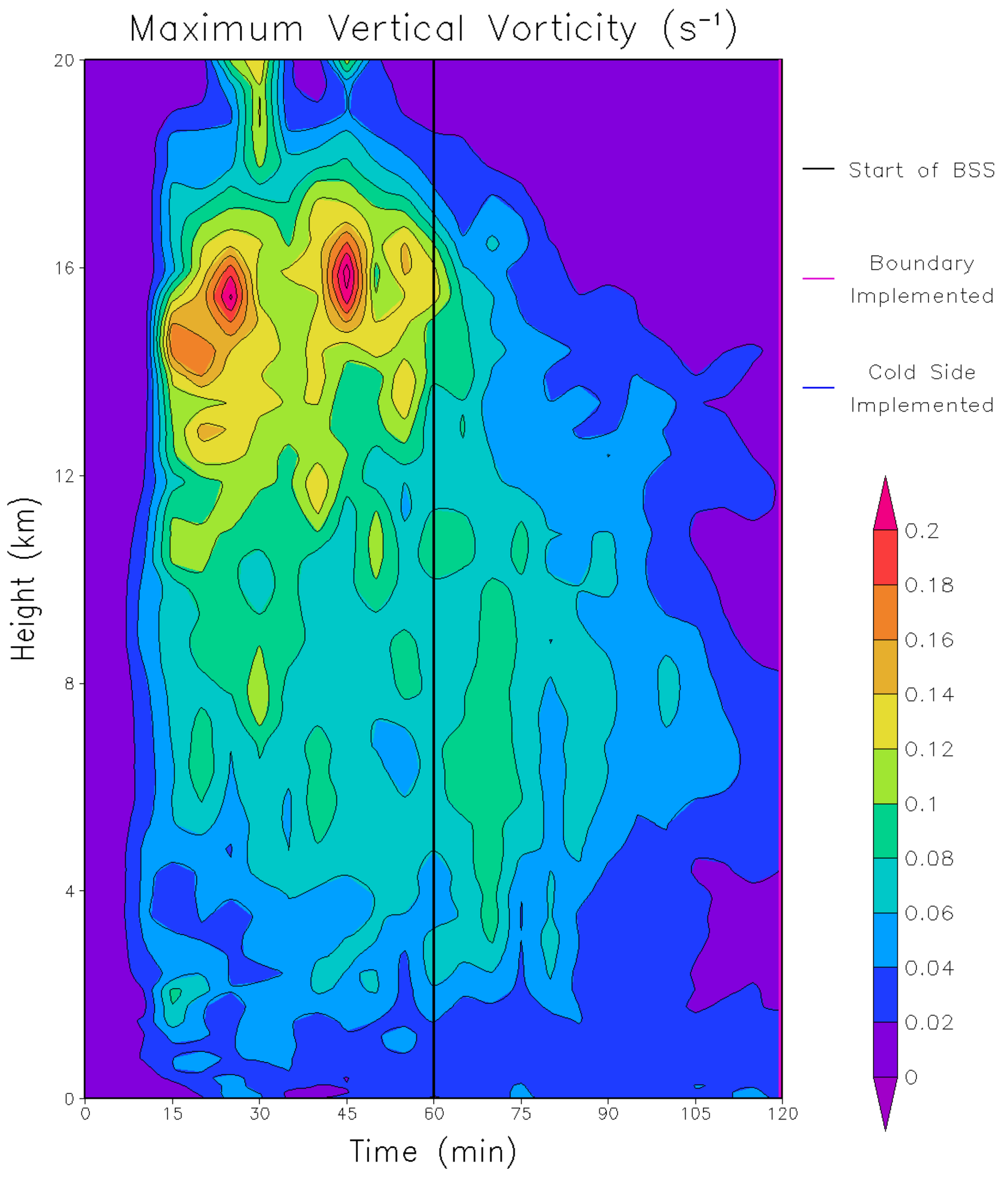

Figure 4.20: Time-height plot of maximum vertical vorticity (shaded and contoured every 0.02 s^{-1}) for the 15/60/15 warm-to-cold side simulation. The *x* axis represents simulated or observed time, while the *y* axis represents height in km. The "cold side implemented" line occurs off the graph.

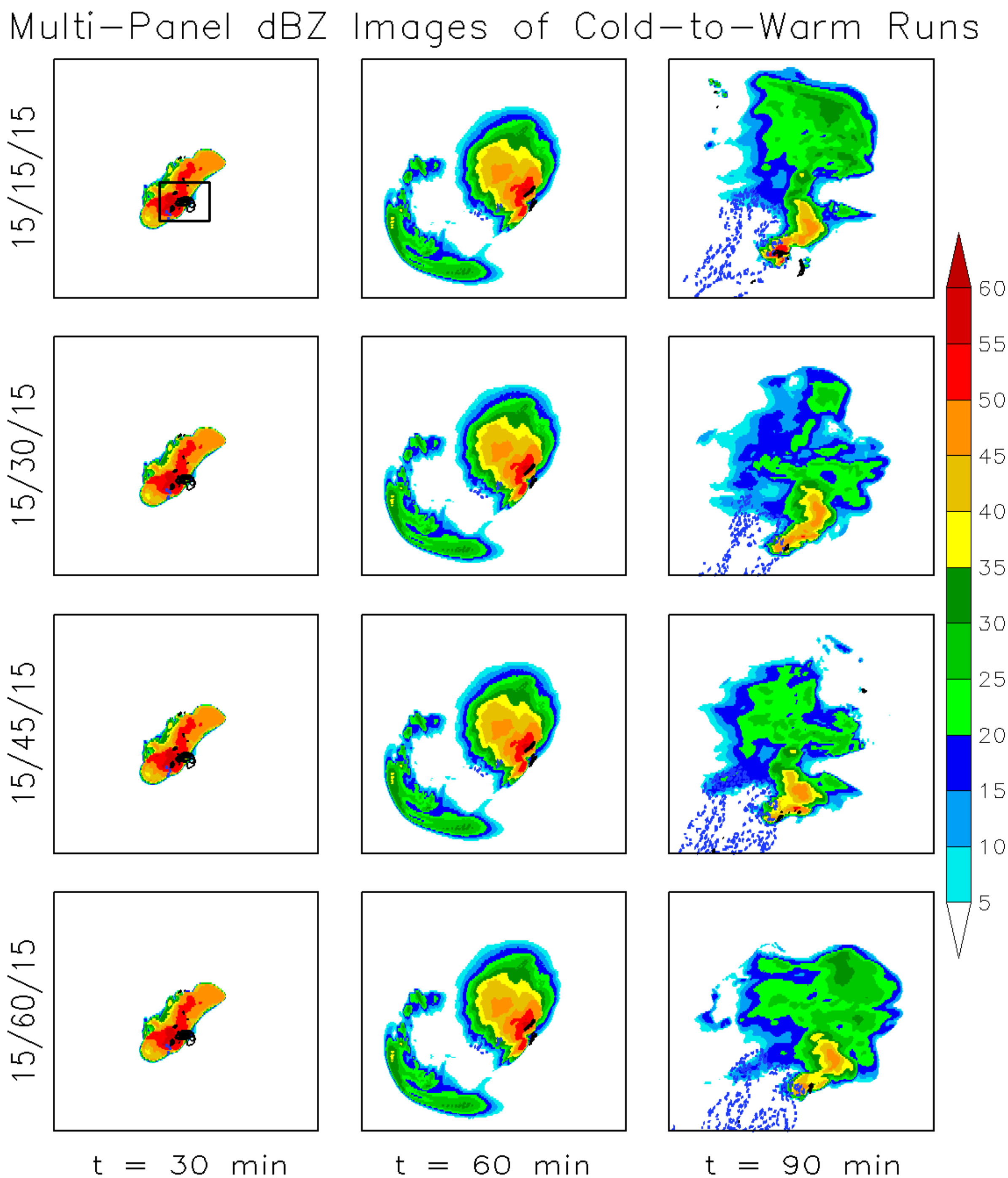

Figure 4.21: Simulated radar reflectivity (shaded), potential temperature perturbation (contoured; -1 K), and updraft helicity (contoured; 200, 400, & 600 $m^2 s^{-2}$) of the 15/X/15 cold-to-warm side simulations at three different times. The black box in the upper-left panel shows the area where the maximum velocity and vorticity was taken at all levels for Figs. 4.23 - 4.30.

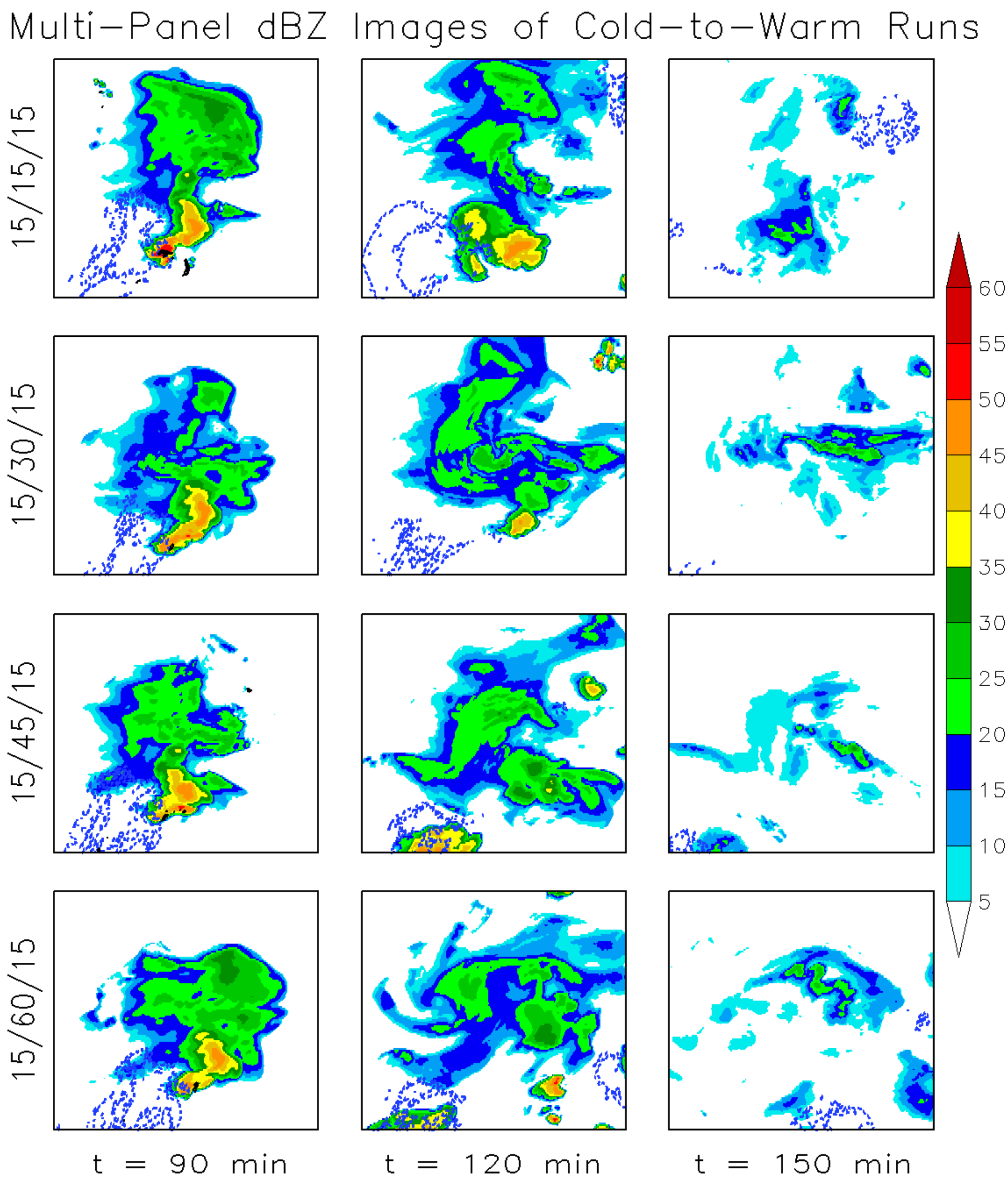

Figure 4.22: Simulated radar reflectivity (shaded), potential temperature perturbation (contoured; -1 K), and updraft helicity (contoured; 200, 400, & 600 $m^2\ s^{-2}$) of the 15/X/15 cold-to-warm side simulations at three different times.

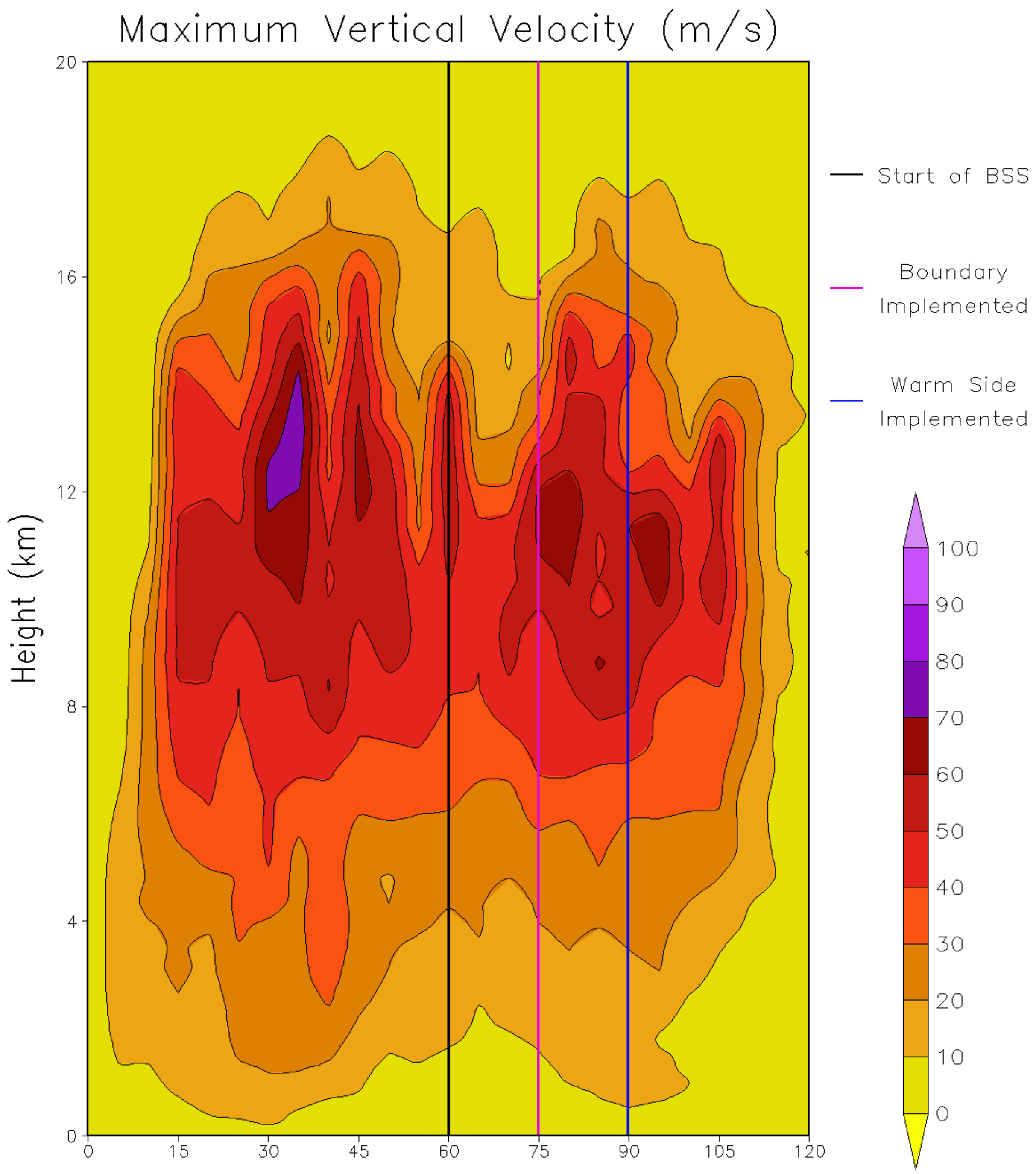

Figure 4.23: Time-height plot of maximum vertical velocity (shaded and contoured every 10 ms^{-1}) for the 15/15/15 cold-to-warm side simulation. The *x* axis represents simulated or observed time, while the *y* axis represents height in km.

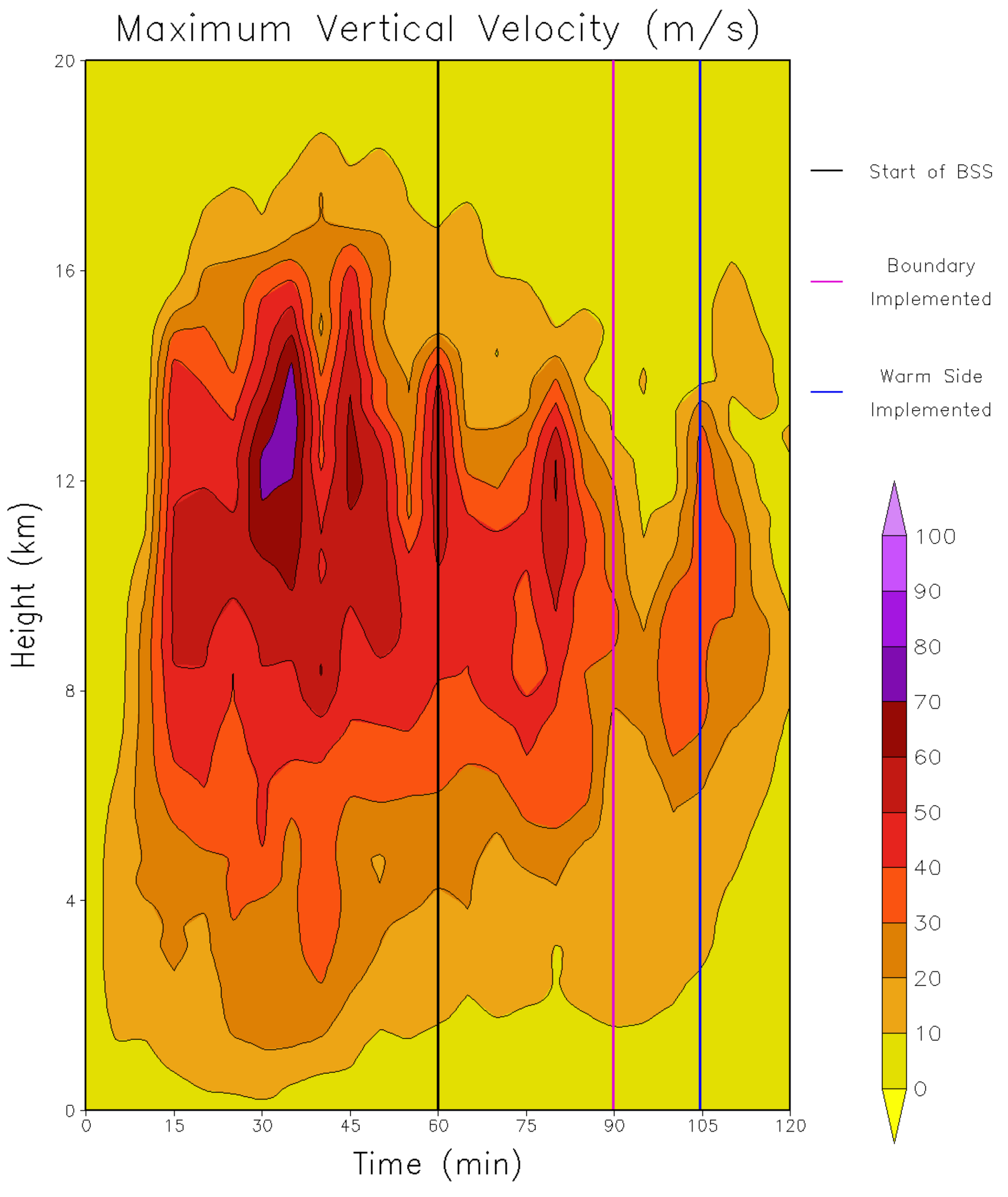

Figure 4.24: Time-height plot of maximum vertical velocity (shaded and contoured every 10 ms^{-1}) for the 15/30/15 cold-to-warm side simulation. The *x* axis represents simulated or observed time, while the *y* axis represents height in km.

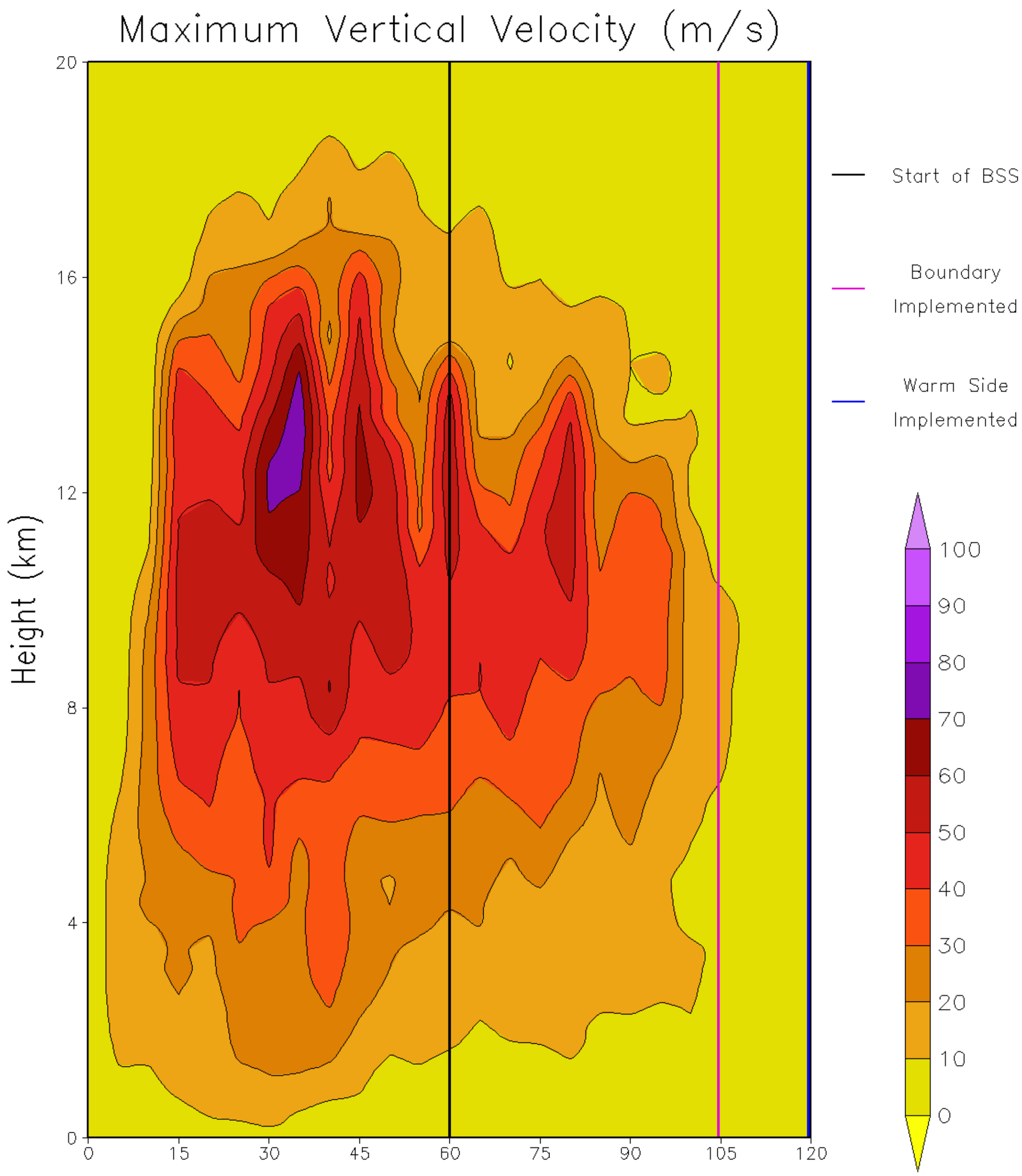

Figure 4.25: Time-height plot of maximum vertical velocity (shaded and contoured every 10 ms^{-1}) for the 15/45/15 cold-to-warm side simulation. The *x* axis represents simulated or observed time, while the *y* axis represents height in km.

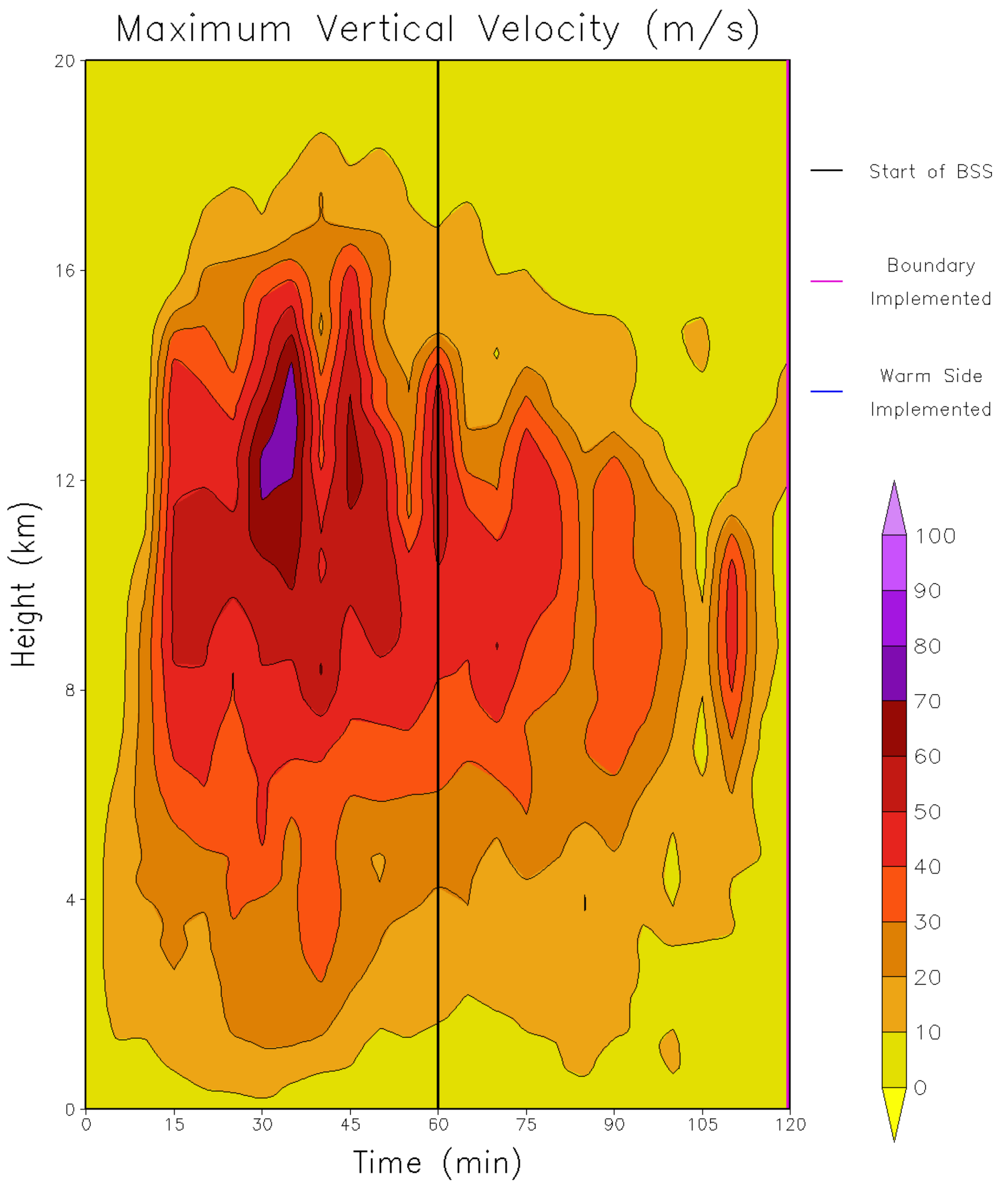

Figure 4.26: Time-height plot of maximum vertical velocity (shaded and contoured every 10 ms^{-1}) for the 15/60/15 cold-to-warm side simulation. The *x* axis represents simulated or observed time, while the *y* axis represents height in km. The "warm side implemented" line occurs off the graph.

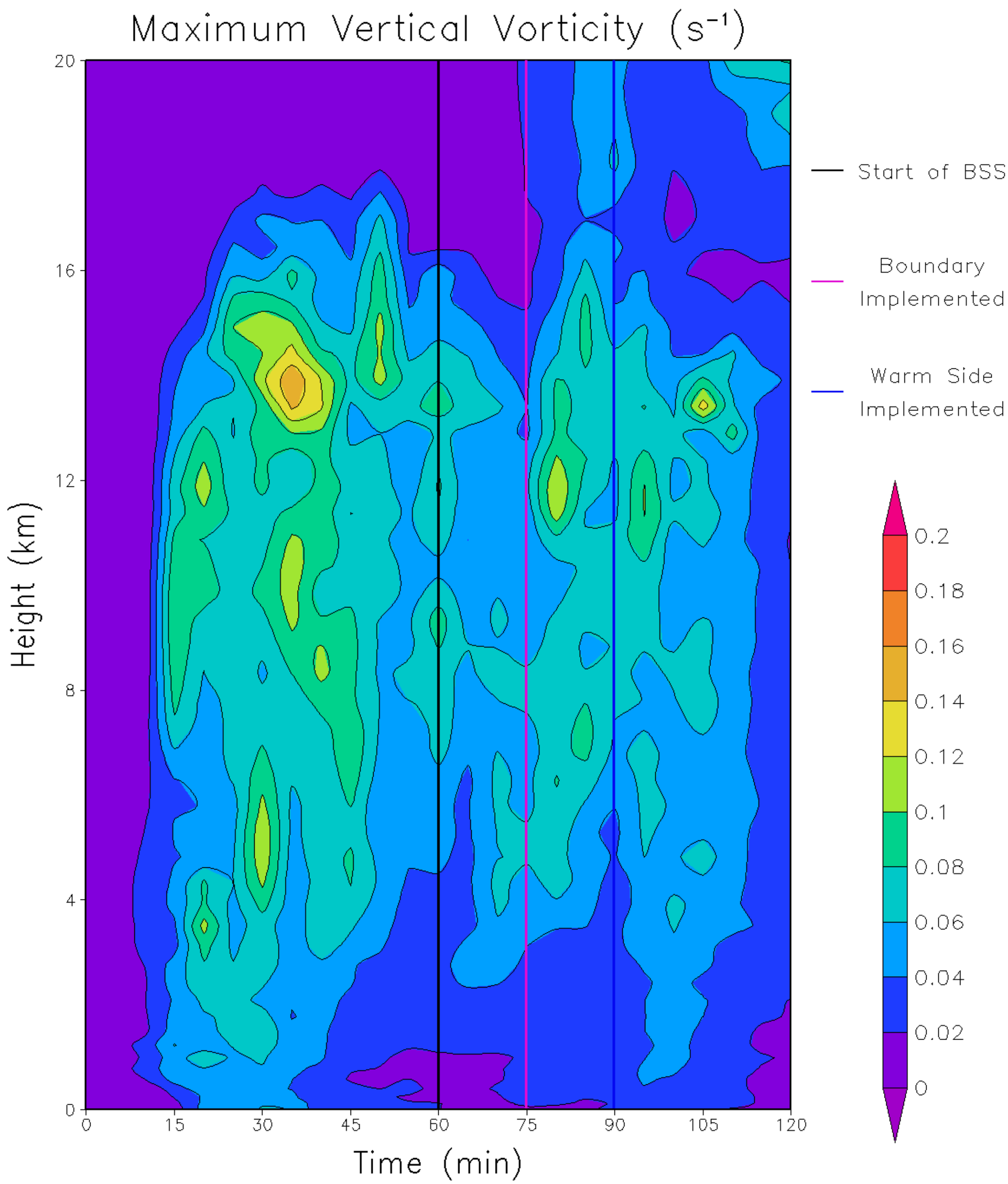

Figure 4.27: Time-height plot of maximum vertical vorticity (shaded and contoured every 0.02 s^{-1}) for the 15/15/15 cold-to-warm side simulation. The *x* axis represents simulated or observed time, while the *y* axis represents height in km.

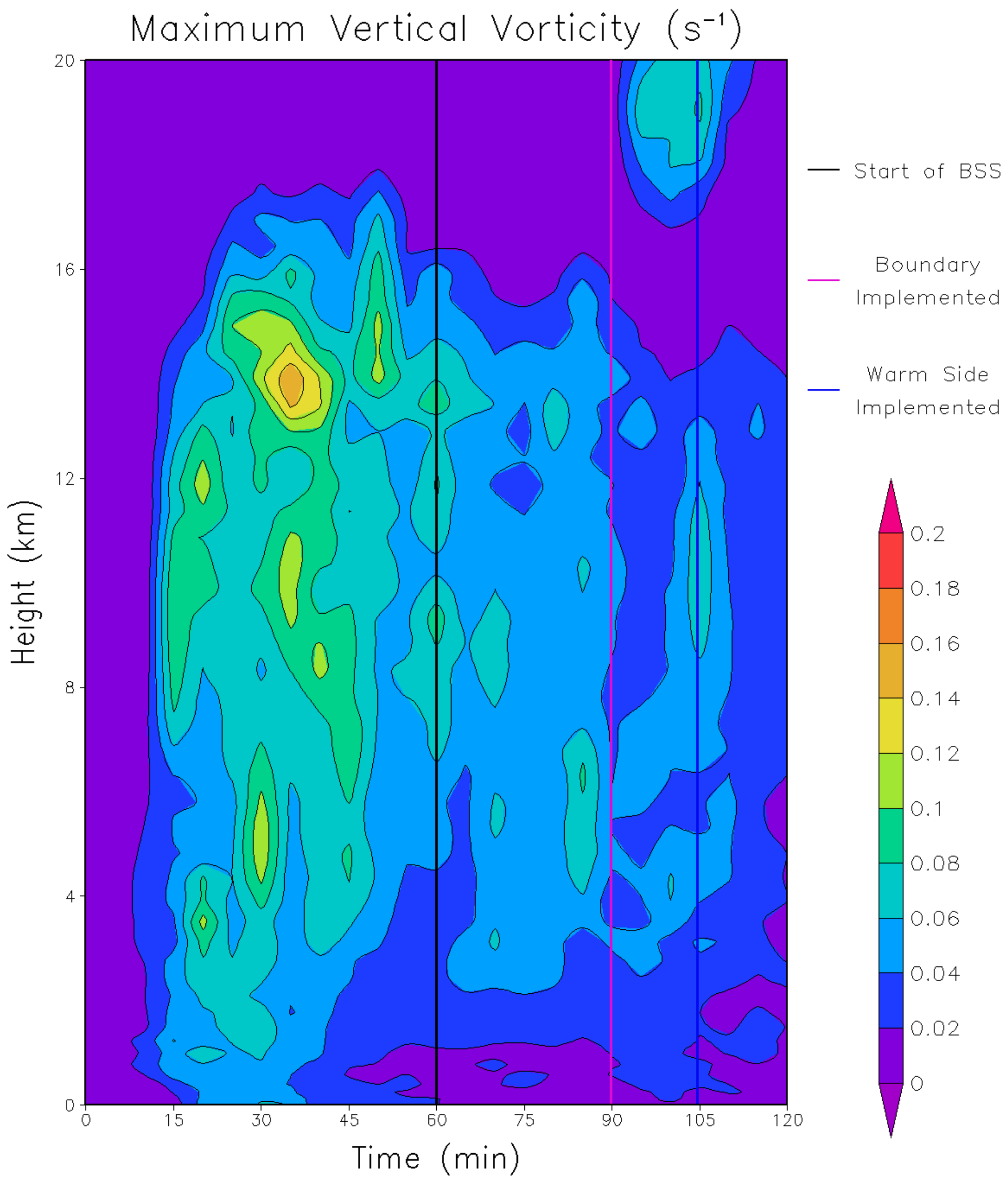

Figure 4.28: Time-height plot of maximum vertical vorticity (shaded and contoured every 0.02 s^{-1}) for the 15/30/15 cold-to-warm side simulation. The *x* axis represents simulated or observed time, while the *y* axis represents height in km.

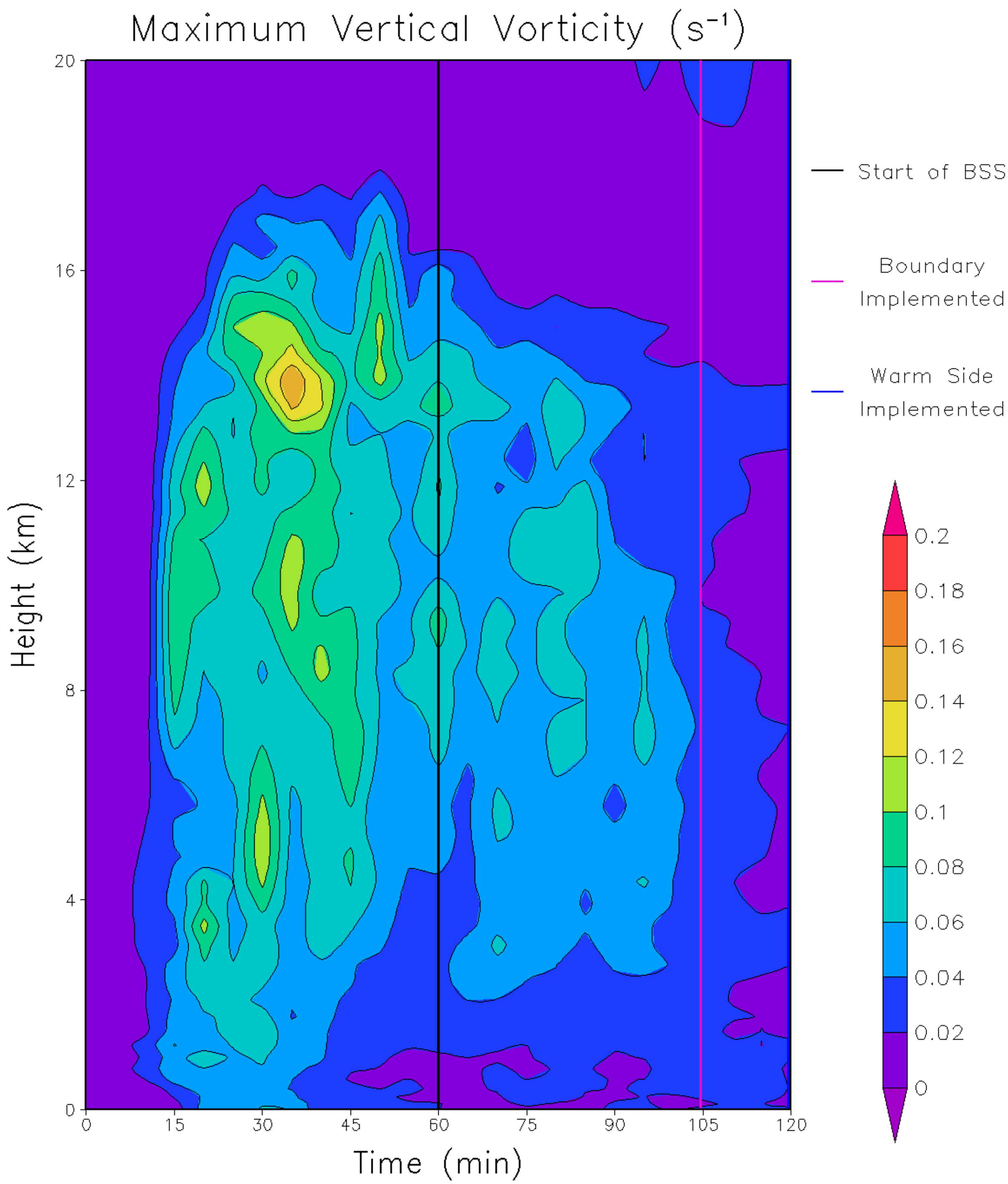

Figure 4.29: Time-height plot of maximum vertical vorticity (shaded and contoured every 0.02 s^{-1}) for the 15/45/15 cold-to-warm side simulation. The *x* axis represents simulated or observed time, while the *y* axis represents height in km.

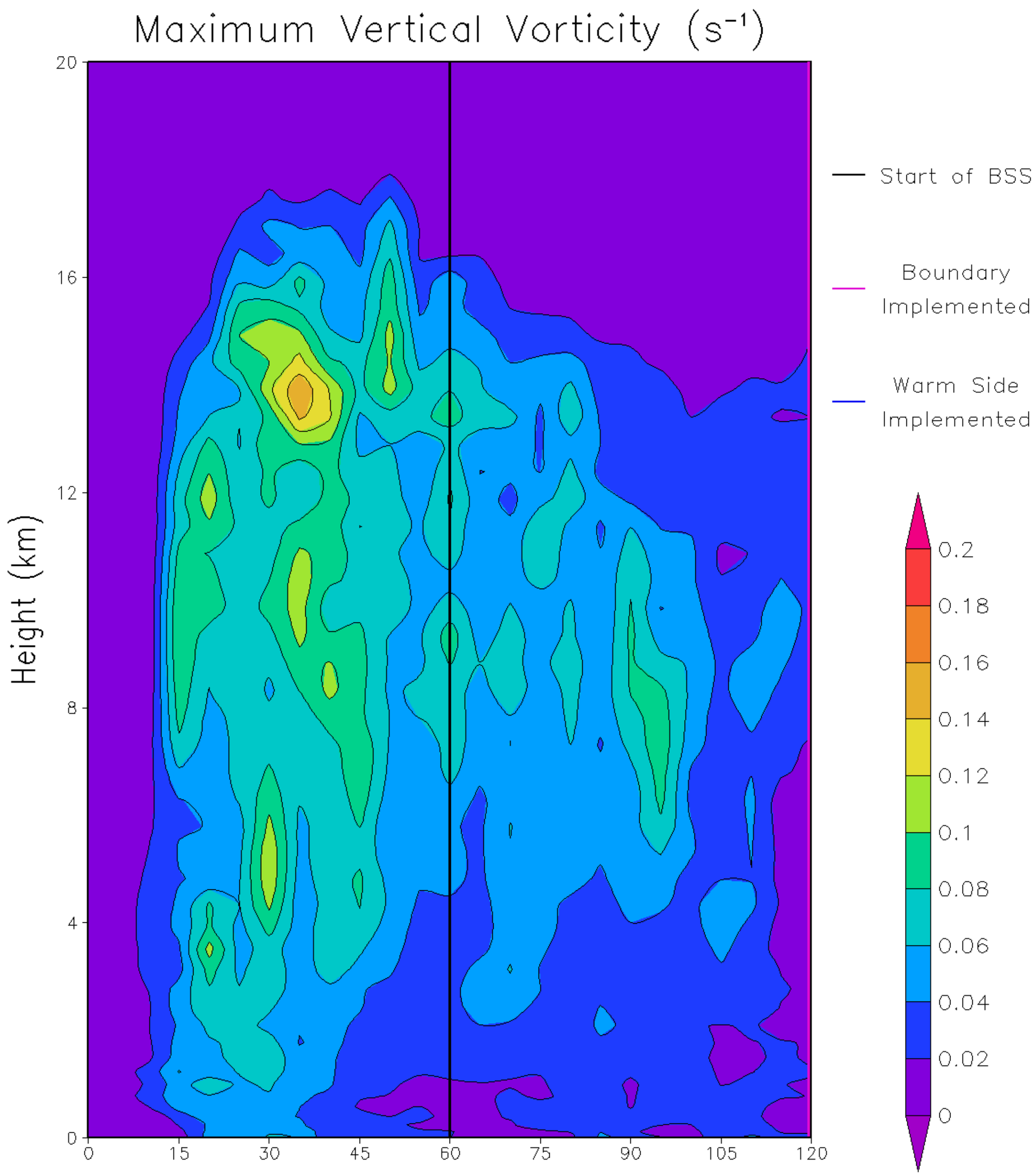

Figure 4.30: Time-height plot of maximum vertical vorticity (shaded and contoured every 0.02 s^{-1}) for the 15/60/15 cold-to-warm side simulation. The *x* axis represents simulated or observed time, while the *y* axis represents height in km. The “warm side implemented” line occurs off the graph.

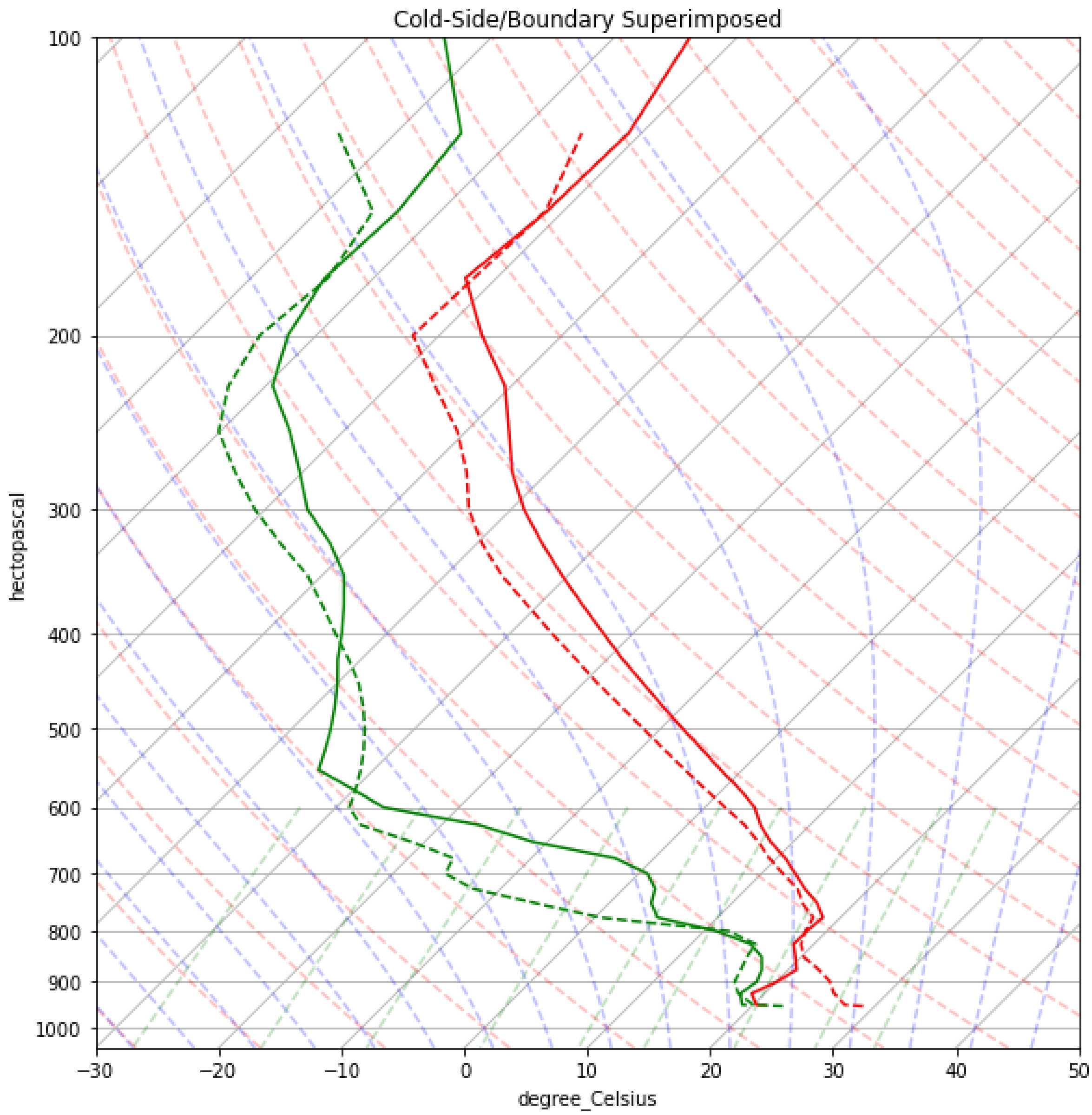

Fig. 4.31: Skew-T, log-P diagram depicting the control cold-side environment (solid lines) and control boundary environment (dashed lines) superimposed on one another.

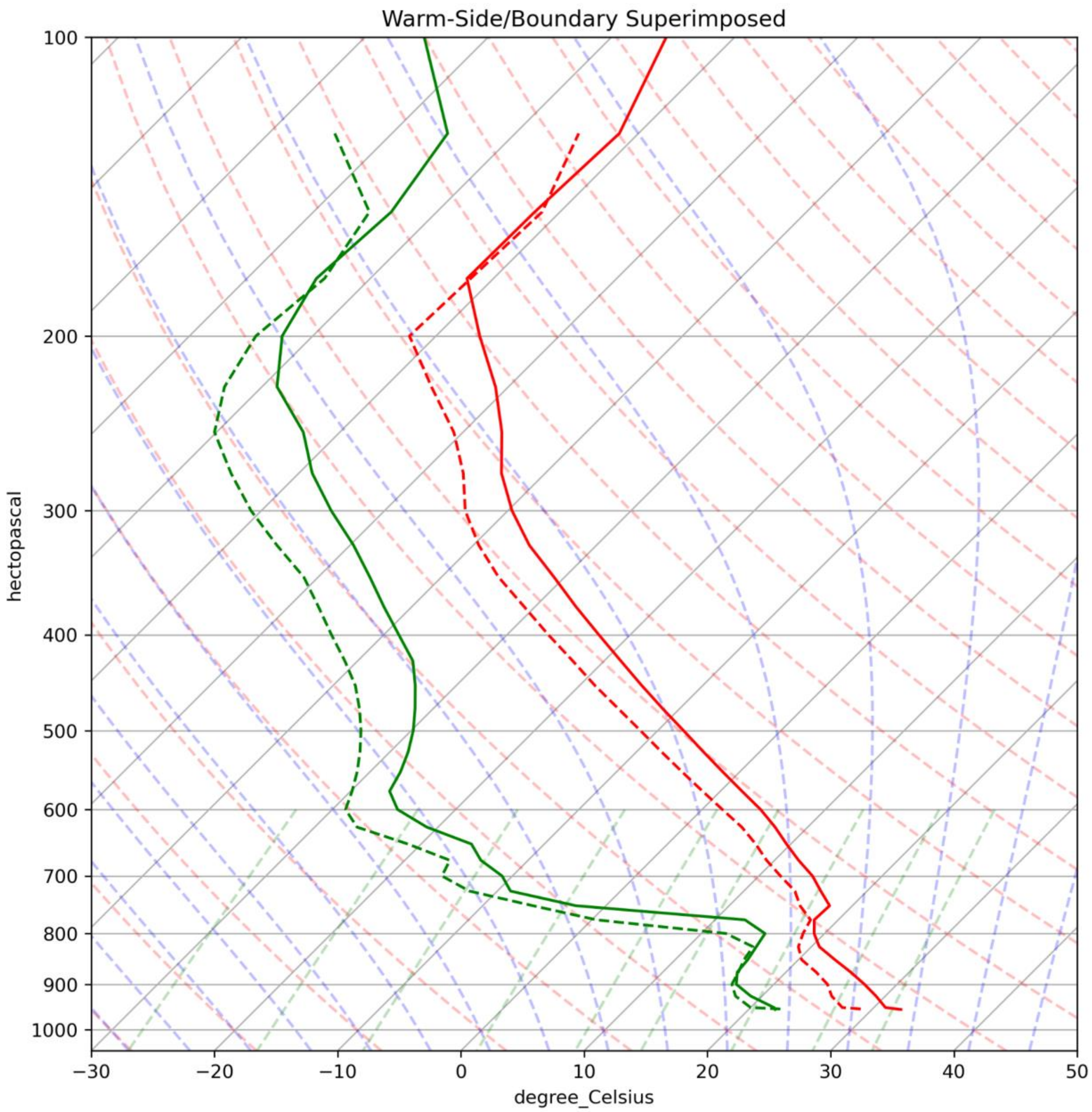

Fig. 4.32: Skew-T, log-P diagram depicting the control warm-side environment (solid lines) and control boundary environment (dashed lines) superimposed on one another.

CHAPTER 5: SUMMARY AND FUTURE WORK

5.1 Summary

The study described herein used an idealized, cloud-resolving numerical model (CM1; Bryan and Fritsch 2002) to explore the sensitivity of supercell thunderstorms within a background environment varying in a controlled manner analogous to interaction with a stationary surface boundary. The goal of this study was to improve our understanding of supercell-boundary interactions through idealized simulations, focusing on the role of spatial gradients in the environment (without the accompanying effects of a boundary circulation) and those contributions to supercell evolution.

Three different background environments from an observed event on 29 May 2011 were tested: one representing the warm side of the boundary, one representing the boundary itself, and another representing the cold side of the boundary (Figs. 3.2 - 3.4). Simulations were run with these constant background environments to serve as controls. Next, experiments with varying background environments were tested using BSS to temporally change the base-state environment; these experiments were designed to mimic a supercell crossing a boundary after it was initialized in the warm or cold side environment (Fig. 3.5). The time that the supercell spent in the constant boundary environment varied between each simulation to identify the impact of boundary dwell time on supercell evolution. The three control simulations established storm behavior in constant, unchanging background environments. Substantial variations in storm intensity and evolution were observed. Specifically, the boundary simulation was the only control simulation to maintain a supercellular structure after 150 minutes (Fig. 4.2). In contrast, the supercells simulated within the warm- and cold-side environments both began dissipating before the 150-minute mark (Fig. 4.1). These differing evolutions were attributed to the characteristics of the background environments. Notably, the boundary environment contained the highest CAPE values, as well as substantial low-level shear and SRH (Table 4.1), all of which promote robust dynamical support for a strong updraft and mesocyclone (e.g., Fig. 4.5). While the warm-side environment had the least amount of SB and MUCIN, it contained the weakest low-level shear and helicity, and also contained substantial mid-level dry air (Fig. 3.2). The cold-side environment contained stable low-levels (Fig. 3.3) that would require substantial dynamical forcing to maintain a strong updraft (e.g., Nowotarski and Markowski 2011).

Given the above simulated evolution in constant environments, the BSS experiments were anticipated to be informative of supercell evolution as the background environment changed over time in a manner consistent with interaction with a stationary boundary. However, the warm-to-cold BSS simulations were difficult to interpret due to the development of convection after the boundary environment was introduced (Fig. 4.9). This widespread convection was found to be a result of the low-level environmental wind shift associated with the boundary (Fig. 4.11). Unfortunately, even a slower transition in the wind profile produced the same result; thus, future work will need to further explore this issue and determine how to introduce such environmental transitions without the development of other convection.

The cold-to-warm simulations were more useful with regards to the study goal due to a lack of widespread convection associated with BSS. Notably, instead of the simulated supercell intensifying as a result of the transition towards the boundary environment (with more favorable thermodynamic and kinematic parameters; Table 4.1), these simulations instead produced dissipating supercells (Figs. 4.21-4.22). In fact, when more time was spent in the boundary environment, the supercells became less and less organized. This was hypothesized to be a result of the specific features of the thermodynamic profile, as well as the lack of a surface cold pool.

The transition from the cold-side to boundary environment resulted in increasingly dry mid-level air, as well as warming mid-levels (Fig. 4.31), which would enhance entrainment into the updraft while also reducing buoyancy. Furthermore, without a clear cold pool present, there was weak low-level forcing for parcels to be lifted into the updraft. Overall, this indicates that the circulation associated with the boundary is paramount for supporting a maintained and/or enhanced supercell during interaction, as opposed to enhanced shear or SRH that is typically present. Even so, application of these results to other contexts should be done with caution. The results from these simulations may not hold if other environments were tested.

5.2 Future Work

The work completed thus far has focused on changing the length of time spent in the boundary environment, which is designed to approximate varying supercell approach angles (Fig. 3.5). The results gathered from the varying boundary time simulations have been useful in examining how a supercell (from a single event on 29 May 2011) reacts to being on a boundary for different amounts of time. Thus, it would be instructive to test additional events and environments to determine the representativeness of our findings. Additionally, further testing the sensitivity of the length of time the supercell spends in either the warm-side or cold-side environment, given that these environments produced supercells of varying longevity and intensity (Figs. 4.1, 4.2, 4.9, 4.21 and 4.22), would also be informative. Testing this sensitivity could also provide more insight on the appearance of convection in the warm-to-cold simulations when switching from the warm-side to the boundary environment. Another possible way to test varying environments is by focusing on the height of the boundary and how that affects a supercell's structure. This study used one even with a constant height for its boundary environment, but testing multiple heights could yield much different results in terms of supercell structure and longevity. Additionally, a deeper analysis of the current simulations is warranted to better understand the physical mechanisms producing the various supercell evolutionary paths, such as examining the cold pool intensity and evolution, as well as other metrics of the mesocyclone, such as mesocyclone depth, volume, or updraft helicity areas. Including parcel trajectory analyses would also be helpful in identifying how lifting changes as the environment changes. Also, focusing more on low-level mesocyclone and tornado-like vortices would help tie into previous observed boundary studies. Lastly, determining how to address the development of widespread convection in the warm-to-cold BSS simulations due to the shift in low-level winds associated with the boundary would be useful for applying this study to other realistic scenarios.

REFERENCES

Atkins, N. T., M. L. Weisman, and L. J. Wicker, 1999: The influence of preexisting boundaries on supercell evolution. Mon. Wea. Rev., 127, 2910–2927, doi:10.1175/1520-0493(1999)127,2910: TIOPBO.2.0.CO;2.

Axon, K. 2022: Using Remote and in situ Observations from TORUS to Investigate a Preexisting Airmass Boundary and its Influence on a Tornadic Supercell on 28 May 2019. Master's Thesis. University of Nebraska-Lincoln

Barnes, S. L. 1978. Oklahoma thunder-storms on 29-30 April 1970. Part I : Morphology of a tornadic storm. Mon. Weather Rev. 106: 673-84

Benjamin, S., T. Smirnova, J. Brown, G. Grell, and R. Bleck, 2004: Mesoscale weather prediction with the RUC hybrid isentropic-terrain-following coordinate model. *Mon. Wea. Rev.*, **132**, 473–494, https://doi.org/10.1175/1520-0493(2004)132<0473:MWPWTR>2.0.CO;2.

Benjamin, S., and Coauthors, 2016: A North American hourly assimilation and model forecast cycle: The Rapid Refresh. *Mon. Wea. Rev.*, **144**, 1669–1694, https://doi.org/10.1175/MWR-D-15-0242.1.

Blanchard, D. O., 2008: Interactions between a Supercell and a Quasi-Stationary Frontal Boundary. *Mon. Wea. Rev.*, **136**, 5199–5210, https://doi.org/10.1175/2008MWR2437.1.

Bluestein, H. B., and M. H. Jain, 1985: Formation of mesoscale lines of precipitation: Severe squall lines in Oklahoma during the spring. *J. Atmos. Sci.*, **42**, 1711–1732.

Bryan, G. H., and J. M. Fritsch, 2002: A benchmark simulation for moist nonhydrostatic numerical models. Mon. Wea. Rev., 130, 2917-2928.

Burgess, D. W. 1976. Single Doppler radar vortex recognition. Part I : mesocyclone signatures. Preprints, Conf. Radar Meteo- rol., 17th, pp. 97-103. Boston : Am. Meteorol. Soc.

Coffer, B. E., and M. D. Parker, 2015: Impacts of Increasing Low-Level Shear on Supercells during the Early Evening Transition. *Mon. Wea. Rev.*, **143**, 1945–1969, https://doi.org/10.1175/MWR-D-14-00328.1.

Cohen, A., M. Coniglio, S. Cavallo, and H. Brooks, 2015: A review of planetary boundary layer parameterization schemes and their sensitivity in simulating southeastern U.S. cold season severe weather environments. *Wea. Forecasting*, **30**, 591–612, https://doi.org/10.1175/WAF-D-14-00105.1.

Coniglio, M., 2012: Verification of RUC 0–1-h forecasts and SPC mesoscale analyses using VORTEX2 environments. *Wea. Forecasting*, **27**, 667–683, https://doi.org/10.1175/WAF-D-11-00096.1.

Davenport, C. E., 2021: Environmental Evolution of Long-Lived Supercell Thunderstorms in the Great Plains. *Wea. Forecasting*, **36**, 2187–2209, https://doi.org/10.1175/WAF-D-21-0042.1.

Davenport, C., and M. Parker, 2015a: Impact of environmental heterogeneity on the dynamics of a dissipating supercell thunderstorm. *Mon. Wea. Rev.*, **143**, 4244–4277, https://doi.org/10.1175/MWR-D-15-0072.1.

Davenport, C., and M. Parker, 2015b: Observations of the 9 June 2009 dissipating supercell from VORTEX2. *Wea. Forecasting*, **30**, 368–388, https://doi.org/10.1175/WAF-D-14-00087.1.

Davenport, C. E., C. L. Ziegler, and M. I. Biggerstaff, 2019: Creating a More Realistic Idealized Supercell Thunderstorm Evolution via Incorporation of Base-State Environmental Variability. *Mon. Wea. Rev.*, **147**, 4177–4198, https://doi.org/10.1175/MWR-D-18-0447.1.

Davies-Jones, R. 1985: Dynamical Interaction between an Isolated Convective Cell and a Veering Environmental Wind. 14th Conference on Severe Local Storms, Indianapolis, IN, American Meteorological Society, Boston, 28 October-1 November 1985, 216-219

Fierro, A. O., M. S. Gilmore, E. R. Mansell, L. J. Wicker, and J. M. Straka, 2006: Electrification and Lightning in an Idealized Boundary-Crossing Supercell Simulation of 2 June 1995. *Mon. Wea. Rev.*, **134**, 3149–3172, https://doi.org/10.1175/MWR3231.1.

French, A. J., and M. D. Parker, 2014: Numerical Simulations of Bow Echo Formation Following a Squall Line–Supercell Merger. *Mon. Wea. Rev.*, **142**, 4791–4822, https://doi.org/10.1175/MWR-D-13-00356.1.

Gilmore, M. S., and L. J. Wicker, 1998: Supercells simulated in the 2 June 1995 West Texas Panhandle Environment. Preprints, 19th Conf. on Severe Local Storms, Minneapolis, MN, Amer. Me-teor. Soc., 242–245.

Gilmore, M. S., L. J. Wicker, E. R. Mansell, J. M. Straka, and E. N. Rasmussen, 2002: Idealized boundary-crossing supercell simulations of 2 June 1995. Preprints, 21st Conf. on Severe Local Storms, San Antonio, TX, Amer. Meteor. Soc., 251–254.

Gropp, M., and C. Davenport, 2018: The impact of the nocturnal transition on the lifetime and evolution of supercell thunderstorms in the Great Plains. *Wea. Forecasting*, **33**, 1045–1061, https://doi.org/10.1175/WAF-D-17-0150.1.

Hartigan, J., R. Warren, J. Soderholm, and H. Richter, 2021: Simulated changes in storm morphology associated with a sea-breeze air mass. *Mon. Wea. Rev.*, **149**, 333–351, https://doi.org/10.1175/MWR-D-20-0069.1.

James, R. P., and P. M. Markowski, 2010: A Numerical Investigation of the Effects of Dry Air Aloft on Deep Convection. *Mon. Wea. Rev.*, **138**, 140–161, https://doi.org/10.1175/2009MWR3018.1.

Klees, A., Y. Richardson, P. Markowski, C. Weiss, J. Wurman, and K. Kosiba, 2016: Comparison of the tornadic and nontornadic supercells intercepted by VORTEX2 on 10 June 2010. *Mon. Wea. Rev.*, **144**, 3201–3231, https://doi.org/10.1175/MWR-D-15-0345.1.

Klemp, J. B., 1987: Dynamics of tornadic thunderstorms. Annu. Rev. Fluid Mech., 19, 369–402, doi:10.1146/ annurev.fl.19.010187.002101.

Klemp, J. B., and R. Rotunno, 1983: A study of the tornadic region within a supercell thunderstorm. J. Atmos. Sci., 40, 359–377.

Klemp, J. B., R. B. Wilhelmson, and P. S. Ray, 1981: Observed and Numerically Simulated Structure of a Mature Supercell Thunderstorm. *J. Atmos. Sci.*, **38**, 1558–1580, https://doi.org/10.1175/1520-0469(1981)038<1558:OANSSO>2.0.CO;2.

Kropfli, R. A., Miller, L. J. 1976. Kinematic structure and flux quantities in a con-vective storm from dual-Doppler radar observations. J. Atmos. Sci. 33 : 520-29

Laflin, J. M., and A. L. Houston, 2012: A modeling study of supercell development in the presence of a preexisting airmass boundary. *Electron. J. Severe Storms Meteor.*, **7** (1), https://ejssm.org/archives/wp-content/uploads/2021/09/vol7-1.pdf.

Lemon, L. R., Doswell, C. A. III. 1979. Severe thunderstorm evolution and meso- cyclone structure as related to tornado- genesis. Mon. Weather Rev. 107 : 1 1 84- 97

Letkewicz, C., A. French, and M. Parker, 2013: Base-state substitution: An idealized modeling technique for approximating environmental variability. *Mon. Wea. Rev.*, **141**, 3062–3086, https://doi.org/10.1175/MWR-D-12-00200.1.

Lyza, A. W., M. D. Flournoy, and E. N. Rasmussen, 2022: Observed Characteristics of the Tornadic Supercells of 27–28 April 2011 in the Southeast United States. *Mon. Wea. Rev.*, **150**, 2883–2910, https://doi.org/10.1175/MWR-D-21-0274.1.

MacIntosh, C. W., and M. D. Parker, 2017: The 6 May 2010 Elevated Supercell during VORTEX2. *Mon. Wea. Rev.*, **145**, 2635–2657, https://doi.org/10.1175/MWR-D-16-0329.1.

Maddox, R., L. Hoxit, and C. Chappell, 1980: A study of tornadic thunderstorm interactions with thermal boundaries. *Mon. Wea. Rev.*, **108**, 322–336, https://doi.org/10.1175/1520-0493(1980)108<0322:ASOTTI>2.0.CO;2.

Magee, K., and C. Davenport, 2020: An observational analysis quantifying the distance of supercell-boundary interactions in the Great Plains. *J. Oper. Meteor.*, **8**, 15–38, https://doi.org/10.15191/nwajom.2020.0802.

Mansell, E. R., D. R. MacGorman, C. L. Ziegler and J. M. Straka, 2002: Simulated three-dimensional branched lightning in a numerical thunderstorm model. J. Geophys. Res., 107, 4075, doi:10.1029/2000JD000244.

Mansell, E. R., D. R. MacGorman, C. L. Ziegler and J. M. Straka, 2005: Charge structure and lightning sensitivity in a simulated multicell thunderstorm. J. Geophys. Res., 110, D12101, doi:10.1029/2004JD005287.

Markowski, P. M., and Richardson, Y.P., 2009: Tornadogenesis: Our current understanding, forecasting considerations, and questions to guide future research, Atmospheric Research, Volume 93, Issues 1–3, Pages 3-10, ISSN 0169-8095, https://doi.org/10.1016/j.atmosres.2008.09.015.

Markowski, P., E. Rasmussen, and J. Straka, 1998a: The occurrence of tornadoes in supercells interacting with boundaries during VORTEX-95. *Wea. Forecasting*, **13**, 852–859, https://doi.org/10.1175/1520-0434(1998)013<0852:TOOTIS>2.0.CO;2.

Markowski, P., J. Straka, E. Rasmussen, and D. Blanchard, 1998b: Variability of storm-relative helicity during VORTEX. *Mon. Wea. Rev.*, **126**, 2959–2971, https://doi.org/10.1175/1520-0493(1998)126<2959:VOSRHD>2.0.CO;2.

Morton, R. B. 1966. Geophysical vortices. In Progress in Aeronautical Sciences, ed. D. Kiichmann, 7 : 145-94. Oxford/ London : Pergamon. 220 pp.

Nowotarski, C. J., P. M. Markowski, and Y. P. Richardson, 2011: The Characteristics of Numerically Simulated Supercell Storms Situated over Statically Stable Boundary Layers. *Mon. Wea. Rev.*, **139**, 3139–3162, https://doi.org/10.1175/MWR-D-10-05087.1.

Rasmussen, E. N., and S. A. Rutledge, 1993: Squall line evolution. Part I: Kinematic and reflectivity structure. J. Atmos. Sci., 50, 2584–2606.

Rasmussen, E., S. Richardson, J. Straka, and P. M. D. Blanchard, 2000: The association of significant tornadoes with a baroclinic boundary on 2 June 1995. *Mon. Wea. Rev.*, **128**, 174–191, https://doi.org/10.1175/1520-0493(2000)128<0174:TAOSTW>2.0.CO;2.

Rotunno, R., and J. B. Klemp, 1982: The influence of the shear- induced pressure gradient on thunderstorm motion. Mon. Wea. Rev., 110, 136–151, doi:10.1175/1520-0493(1982)110,0136: TIOTSI.2.0.CO;2.

Rotunno, R., and J. B. Klemp, 1985: On the rotation and propagation of simulated supercell storms. J. Atmos. Sci., 42, 271–292, doi:10.1175/ 1520-0469(1985)042,0271:OTRAPO.2.0.CO;2.

Rotunno, R., J. B. Klemp, and M. L. Weisman, 1988: A theory for strong, long- lived squall-lines. J. Atmos. Sci., 45, 463–485.

Schlesinger, R. E. 1975. A three-dimensional numerical model of an isolated deep con-vective cloud : preliminary results. J. Atmos. Sci. 32: 934-57

Scott, A. K. 2017: Simulating Boundary Crossing Supercells Using a Non-Hydrostatic Cloud Model. Master's Thesis. University of Oklahoma

Straka, J. M., and E. R. Mansell, 2005: A bulk microphysics parameterization with multiple ice precipitation categories. J. Appl. Meteor., 44, 445–466.

Thompson, R., R. Edwards, J. Hart, K. Elmore, and P. Markowski, 2003: Close proximity soundings within supercell environments obtained from the Rapid Update Cycle. *Wea. Forecasting*, **18**, 1243–1261, https://doi.org/10.1175/1520-0434(2003)018<1243:CPSWSE>2.0.CO;2.

Thorpe, A. J., Miller, M. J. 1978. Numerical simulations showing the role of the down-draught in cumulonimbus motion and splitting. Q. 1. R. Meteorol. Soc. 104 : 873-93

Wakimoto, R. M., and J. W. Wilson, 1989: Nonsupercell tornadoes. *Mon. Wea. Rev.*,**117,** 1113–1140.

Wilhelmson, R. B. 1974. The life cycle of a thunderstorm in three dimensions. J. Atmos. Sci. 31 : 1629-51

Wilhelmson, R. B., Klemp, J. B. 1978. A three-dimensional numerical simulation of splitting that leads to long-lived storms. J. Atmos. Sci. 35 : 1037-63

Ziegler, C. L., E. R. Mansell, J. M. Straka, D. R. MacGorman, and D. W. Burgess, 2010: The impact of spatial variations of low- level stability on the life cycle of a simulated supercell storm. Mon. Wea. Rev., 138, 1738–1766, doi:10.1175/2009MWR3010.1.